Monthly Scientific-Technical and Production Journal

The Paton WELDING JOURNAL

February 2002 # 2

English translation of the monthly «Avtomaticheskaya Svarka» journal published in Russian since 1948

The National Academy of Sciences of Ukraine
The E.O. Paton Electric Welding Institute of the NAS of Ukraine
International Association «Welding»

«The Paton Welding Journal» is published monthly by the International Association «Welding»

Promotion group:
V.N.Lipodaev, V.I.Lokteva
A.T.Zelnichenko (exec. director)
Translators:
S.A.Fomina, I.N.Kutianova, T.K.Vasilenko
Editor
N.A.Dmitrieva
Electron galley:
I.V.Petushkov, T.Yu.Snegireva

Editorial and advertising offices are located at PWI, International Association «Welding», 11, Bozhenko str., 03680, Kyiv, Ukraine
Tel.: (38044) 227 67 57
Fax: (38044) 268 04 86
E-mail: journal@paton.kiev.ua

State Registration Certificate KV 4790 of 09.01.2001

Subscriptions:
$460, 12 issues per year, postage and packaging included.
Back issues available

«The Paton Welding Journal» Website: http://www.nas.gov.ua/pwj

CONTENTS

SCIENTIFIC AND TECHNICAL

Kuchuk-Yatsenko S.I., Kharchenko G.K., Grigorenko G.M., Falchenko Yu.V., Taranova T.G., Gritskiv Ya.P., Zagadarchuk V.F. and **Grigorenko S.G.** Heterogeneity of pipe steel joints made by flash butt welding ... 2

Makhnenko V.I., Korolyova T.V. and **Lavrinets I.G.** Effect of microstructural transformations on redistribution of hydrogen in fusion welding of structural steels ... 6

Shchetinina V.I., Shchetinin S.V., Chapni N.I., Shcherbina A.V., Melnikov A.E. and **Golubkov S.P.** Effect of welding speed on welding current magnetic field ... 14

Poklyatsky A.G., Ishchenko A.Ya., Grinuyk A.A., Chajka A.A. and **Fedorchuk V.E.** Non-consumable electrode argon-arc welding of aluminium alloys with arc oscillations ... 18

Mikhajlovskaya E.S., Shulym V.F. and **Zagrebelny A.A.** Results of experiments on manual EBW In a manned space simulation test chamber ... 23

Dobrushin L.D., Fadeenko Yu.I. and **Petushkov V.G.** Special conditions for formation of joints in shock wave welding of metals ... 28

INDUSTRIAL

Paton B.E. and **Gordonny V.G.** Works of the E.O. Paton Electric Welding Institute of the NAS of Ukraine in the field of military tank construction ... 33

Blashchuk V.E. Erection assembly-welding of tubular structures of niobium alloys in the jig ... 40

Tyurin Yu.N., Zhadkevich M.L., Golovenko S.I. and **Chigrinova N.M.** Deposition of oxide coatings on surfaces of products of aluminium-based alloys ... 44

Nevidomsky V.A., Krasilnikov S.G., Panin A.D., Gulida V.P. and **Lychko I.I.** New machine for electroslag welding of large parts at JSC «NKMBF» ... 49

BRIEF INFORMATION

Zhadkevich M.L., Bondarev A.A., Zelenin V.I., Teplyuk V.M., Sidorenko S.I., Mokhort V.A., Nesterenko Yu.V. and **Zelenin O.V.** Technology of restoration of gas turbine blades ... 52

Nesterenko N.P. Optimization of characteristics of electroacoustic transducers for ultrasonic welding of thermoplastic composite materials ... 54

Borisov Yu.S., Sychev V.S., Shavlovsky E.N., Labunets V.F. and **Zolotareva E.P.** Tribological characteristics of composite carbide coatings ... 56

NEWS

Visit of the Minister of Foreign Affairs of the Republic of India to the E.O. Paton Electric Welding Institute of the NAS of Ukraine ... 59

Extraordinary and Plenipotentiary Ambassador of the USA to Ukraine is Introduced to the activity of STC «E.O. Paton Electric Welding Institute» ... 60

6th International Seminar «Numerical analysis of weldability» ... 62

Professor Detlef von Hofe is 60 ... 64

HETEROGENEITY OF PIPE STEEL JOINTS MADE BY FLASH BUTT WELDING

S.I. KUCHUK-YATSENKO, G.K. KHARCHENKO, G.M. GRIGORENKO, Yu.V. FALCHENKO, T.G. TARANOVA, Ya.P. GRITSKIV, V.F. ZAGADARCHUK and S.G. GRIGORENKO
The E.O. Paton Electric Welding Institute, NASU, Kyiv, Ukraine

Results of examination of physical, chemical and structural inhomogeneity of joints from low-alloyed low-carbon pipe steels made by the flash butt welding are presented. It is shown that changes in chemical composition and metal structure and also the decrease in its density is occurred in the butt at the area corresponding to the location of a light band. Ferritic band and joint line are revealed inside the dark band after appropriate heat treatment and etching.

Key words: *flash butt welding, pipe steel, metal density, decarburized zone, butt, light band, ferritic band, joint line*

The flash butt welding (FBW) is widely used in construction of pipelines of diameter from 100 to 1420 mm. The most part of pipelines used for transportation of gas and oil is constructed from pipes which are manufactured from low-alloy steels of 17G1S (C — 0.14–0.2; Si — 0.4–0.6; Mn — 1.0–1.4 wt.%), 09G2S (C — 0.09–0.1; Si — 0.4; Mn — 1.5 wt.%) types, and foreign steels of X60, X65 and X70 types in accordance with standard API5LX.

During FBW the joint is formed in a narrow near-contact metal layer where the intensive deformation in the joint zone is accompanied by the movement of the molten metal. As a result, the macro- and microstructure of butt metal is differed significantly from the structure of neighboring regions of HAZ. During welding of low-alloyed steels a layer of metal with a decreased mass fraction of carbon is formed. This is so-called light band (LB) of up to 1.5 mm width [1], which can be revealed in a macrosection at visual inspection of butt after etching (Figure 1). Existing inhomogeneity does not influence the characteristics of mechanical properties of welded joints during tensile and bending tests. In welding at optimum conditions these characteristics are close to similar characteristics of the parent metal. At impact bend test of notched specimens the impact strength is lower in metal of LB region than that of neighboring regions. The length of region with decreased ductile properties is coincided usually with LB width.

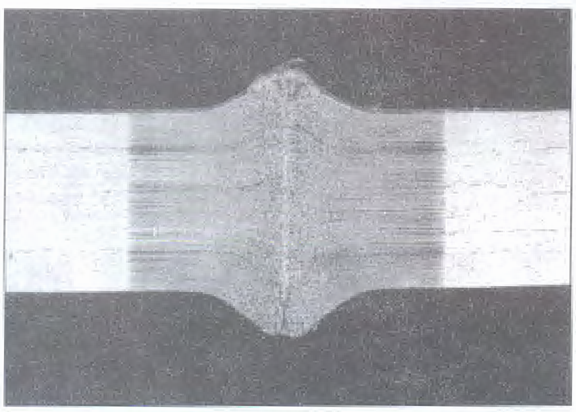

Figure 1. Macrostructure of light band in welded joint after etching

After heat treatment (normalizing or quenching with tempering) the microstructure of metal in butt is almost similar to the structure of the rest HAZ regions. The characteristics of the impact strength after heat treatment are also increased significantly. However, these values are lower than those in parent metal, obtained after heat treatment. This difference is expressed more clearly in testing specimens with a sharp notch at low temperatures.

The data obtained give all the ground to assume that the metal in FBW undergoes irreversible changes and, as a result, differs significantly from the parent metal.

It is known that the metal density depends on the microstructure, chemical composition and also on the plastic deformation to which steel was subjected in the process of treatment [2–5]. For example, the density of electrolytic iron, remelted in vacuum (0.02 % C) is 7.874, and after rolling — 7.900 g/cm^3.

It was determined in [6] using the method of electron fractography that in FBW of pipes from dissimilar steels and up to 6 mm wall thickness the micropores are observed at the surfaces of a trancrystalline fracture of the joints. It is assumed, that their formation in a decarburized zone is stipulated by a migration of vacancies to the regions with a strongly distorted crystalline lattice. The mechanisms of formation of micro- and macropores, and also cracks in crystalline bodies at their plastic deformation are described in detail in [7, 8]. It is known that the submicroscopic discontinuities are realized by a vacation mechanism in deformation in the region of premelting temperatures, and the microdefects are revealed most intensively in deformation of metals containing brittle inclusions of an elongated shape. The rolled metal structure is fractured during melt movement in the butt. According to [9] the action of upset force promotes the melt penetration into near-contact metal areas along the grain boundaries where microcracks can form as a result of a plastic deformation and cured in melt interaction with a solid metal.

Thus, it can be stated that the metal in butt is weakened in FBW. However, there are no quantitative estimation in change of metal density using the mentioned method in the known literature.

The aim of the present work is to study the physical, chemical and structural inhomogeneity of LB metal where the highest decrease in impact strength values is observed.

The investigations were performed on sample of 20 mm thick pipe steel X70 of controllable rolling. They were cut from plates of 200 mm width which were welded at optimum conditions [1]. Here, the structure of parent metal can be characterized as ferritic-pearlitic with a clearly expressed banding. All the investigations were carried out at a local region of the sample in width, corresponding to LB.

The contradictory of data, obtained by many authors [10–14] in evaluation of distribution of elements in the butt, is due to the fact that it is very difficult to determine precisely the content of elements in the narrow layer of LB. In the present work the spectral analysis was performed not in the section plane where the LB width was 0.8–1.2 mm, but in planes S_1 and S_2 located parallel to the butt (Figure 2). 4–5 mm thick plate was cut from the butt. The light band was located in the middle of the plate whose thickness was decreased gradually from both sides to the size of not less than 0.35 mm. Plates of smaller thickness were not manufactured because of a possible burn-out during spectral analysis. Before the spectral analysis the density of the cut plates was measured. The chemical composition of LB metal was also estimated by a successive removal of layers from one side of the butt. However, in this case the density of the joint zone metal was not determined.

To estimate the density a method of hydrostatic weighing was used. The content of carbon, silicon and manganese was determined using the spectral analysis in Spectrovac-1000 instrument of Baird Company. The Table presents the results of measurements of chemical composition and density of metal of the welded joint butt, made at optimum welding conditions. Analysing these data, it can be concluded that the maximum reduction of a mass fraction of carbon and values of density is observed in the middle of LB. There are conclusions in [1, 11, 12] about the presence of a decarburized layer in the butt. Data of works [13, 14] about the change in mass fraction of manganese and silicon were not confirmed.

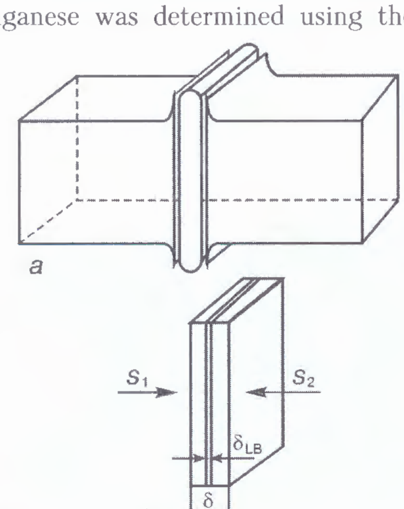

Figure 2. Scheme of cutting sample (*a*) and its general view (*b*): δ — thickness of plate cut from the butt; δ_{LB} — width of LB (0.8–1.2 mm); S_1, S_2 — planes of sample on which the analysis of chemical composition of metal was made

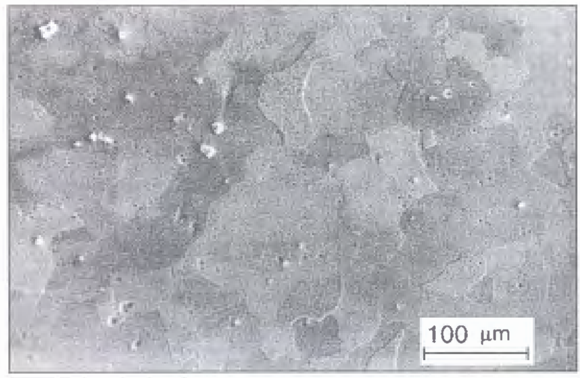

Figure 3. Microstructure of LB metal after ion etching (filming in electron microscope JSM-840) (×350)

Polished sections without etching and after chemical electrolytic and ion etching were examined in optical and scanning electron microscopes. The latter were examined in Lonsputter JFC-1100 unit of JEOL Company. It was stated that in welding at optimum conditions the micro- and macrodefects in the butts were not observed. The type of microstructure revealed by an ion etching (Figure 3) proves the formation of common grains in the LB region and the absence of interface of parts being welded. LB metal has the coarser-grain structure than the HAZ metal. The formation of the common grains in the butt proves the high quality of the welded joint [1, 15, 16].

In parallel with the above-mentioned physical (density) and chemical (composition) inhomogeneties of LB metal, the structural inhomogeneity is also observed. This is displayed more clearly after annealing of the joint with a subsequent slow cooling. In accordance with recommendations of works [15, 17, 18] the annealing of welded joints was made in the furnace at 950–1000 °C for 1–2 h with a subsequent cooling

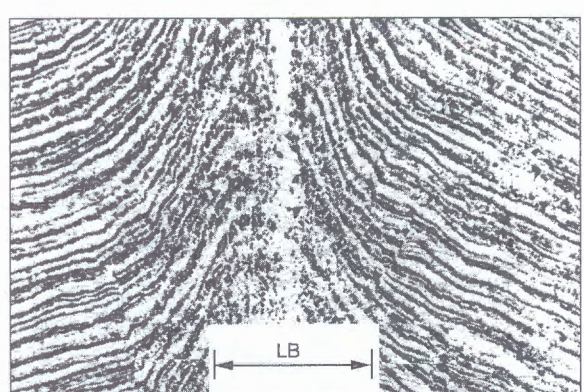

Figure 4. Macrostructure of as-annealed butt (×25)

Chemical composition and density of metal in butt

No. of experiment	Thickness of plate, δ, mm	Mass fraction of elements, %						Density, ρ, g/cm^3
		C		Mn		Si		
		S_1	S_2	S_1	S_2	S_1	S_2	
1	2.21	0.176	0.176	1.56	1.56	0.490	0.49	7.80
	0.77	0.111	0.170	1.55	1.56	0.490	0.49	7.73
	0.65	0.106	0.154	1.54	1.55	0.440	0.49	7.71
	0.50	0.103	0.150	1.49	1.41	0.460	0.51	7.69
	0.35	0.100	0.140	1.51	1.54	0.360	0.46	7.68
2	3.20	0.178	0.178	1.50	1.50	0.390	0.36	7.80
	0.88	0.141	0.170	1.47	1.51	0.350	0.36	7.76
	0.75	0.100	0.131	1.49	1.48	0.310	0.38	7.74
	0.35	0.090	0.110	1.49	1.51	0.300	0.35	7.73
3*	Parent metal	0.084	–	1.54	–	0.299	–	Not measur.
	0.6	0.080	–	1.56	–	0.303	–	Same
	0.4	0.079	–	1.55	–	0.303	–	»
	0.2	0.074	–	1.55	–	0.293	–	»
	0.1	0.067	–	1.52	–	0.290	–	»
	Middle of LB	0.060	–	1.49				»

*Content of elements was determined only from one side of butt.

of samples at 120–150 °C/h rate. After this cooling the conditions are created when the banded texture of steel in the butt is recovered. Figure 4 presents macrostructure of the welded joint after annealing. It is seen from the Figure that the banding in the butt was recovered and a ferritic band (FB) is distinguished. In welding at optimum conditions it has the 100–200 μm width. Figure shows also the location of LB of width of about 1.2 mm. It was stated that the width of FB increases in the direction of melt movement under the action of the electrodynamic force. As was described earlier [15, 18, 19], the formation of FB occurs in case of decarburization of the contact zone, and also at the presence of non-metallic inclusions (NMI) in the butt. It can be assumed that the melt movement in the butt stipulates the NMI orientation in the joint line (JL).

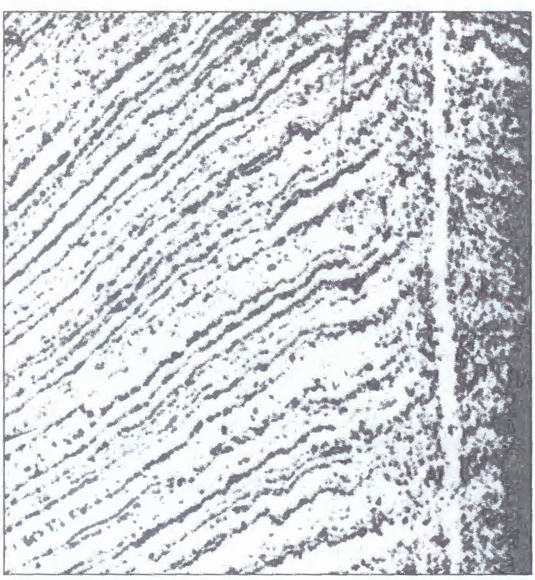

Figure 5. Macrostructure of butt after impact bend testing and annealing of the welded joint (×25)

The metallographic examinations and quantitative measurements of density give all grounds to assume that LB corresponds to the butt area in which the decrease in mass share of carbon and metal density is observed. This region will have always another etchability than the neighboring regions of HAZ independently of heat treatment. Depending on the method of etching this region can differ from the parent metal by more light or dark colour, but the coefficient of light reflection at this region will be different in any case as compared with neighboring regions. It is naturally, that the question is arisen whether the FB location is a hazardous place during testing sharp-notched samples at low temperatures. Figure 5 shows a typical type of structure of the sample after tests and appropriate heat treatment. The results of examination of a batch of samples showed that their fracture occurs in many cases out of FB. Undoubtedly, to study this problem more profoundly it is necessary to perform special experiments in future.

The next stage of our investigations was to test the procedure of revealing JL in the butt. It is known

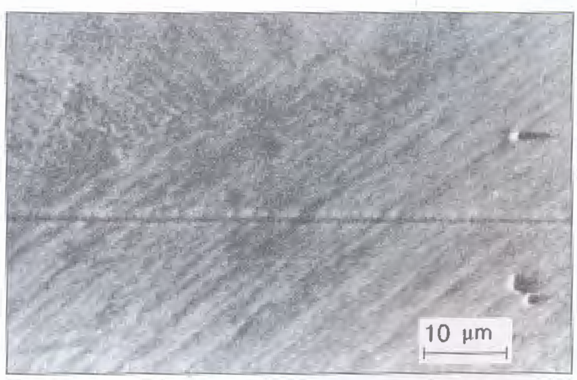

Figure 6. View of the joint line (filming in electron microscope JSM-840) (×1000)

that in welding at optimum conditions it was not managed to reveal it in the butt. Authors of [16] noted that in welded joints produced in upsetting being lower than optimum upsetting, JL can be detected on non-etched sections. It is observed in the butt in the form of a chain of oxides.

It is known that in pressure welding with heating in air the content of oxygen in LB metal is increased [1, 15, 17]. The increase of oxygen in LB as compared with parent metal was confirmed using a chemical etching, which is reacting even on the negligible changing of mass share of oxygen in the metal [14]. Authors of [1, 14, 16] assume that the presence of oxygen in LB can influence negatively on the ductility and toughness of the welded joint metal.

The absence of the cast structure in the butt at optimum parameters of upsetting is explained by the fact than the thin band of melt, being crystallized on grains of the hard metal, repeats its structure. Authors of the present work have developed the procedure of revealing the region in FB, saturated with oxygen, i.e. JL location. Samples of welded joints were annealed at 900–1000 °C, microsections were subjected to ion etching, and then the structure was examined.

According to [20, 21], during annealing NMI should be formed in JL of butt as a result of interaction of alloying elements of steel with oxygen. Figure 6 shows microstructure of butt with typical JL. However, at more than 2000 magnification it has a form of a chain of NMI round-shape particles of size of not more than 1 μm. It should be noted that at separate regions of the butt parallel to JL the NMI clusters are also observed. Analysis made by energy-dispersion spectrometer of Link Company at the scanning electron microscope showed that chemical composition of NMI includes mainly oxides of silicon, manganese and sulfides. It should be noted that after annealing a large amount of randomly located NMI of the same composition that in the JL metal was also revealed in the parent metal.

CONCLUSIONS

1. Great changes in chemical composition and structure of metal accompanied by decrease of its density occur at the butt region. This region has always another etchability than the neighboring regions of HAZ.

2. Decrease in mass shear of carbon as compared with parent metal is observed in the light band metal. The great change in content of other elements was not observed.

3. Ferritic band and joint line are revealed inside the light band after appropriate heat treatment.

1. Kuchuk-Yatsenko, S.I. (1992) *Flash-butt resistance welding*. Kyiv: Naukova Dumka.
2. Slavinsky, M.P. (1952) *Physico-chemical properties of elements*. Moscow: Metallurgizdat.
3. Livshits, V.T. (1959) *Physical properties of metals and alloys*. Moscow: Mashgiz.
4. Novikov, I.V., Goncharov, V.G., Obydalo, K.I. et al. (1978) Density and linear expansion factor of higher heat resistance tool steels. *Metally*, **5**, 73–75.
5. Kupriyanov, A.A., Filipov, S.I. (1968) Density and structural changes in iron and iron alloys with carbon. *Izv. Vuzov, Chern. Metallurgia*, **1**, 10–15.
6. Smirnova, E.K. (1979) *Electron microscope examination of defects formed in joints in pressure welding of steels and alloys*. Synopsis of Thesis for Cand. Sci. Degree. Moscow.
7. Cheremskoj, P.T., Slezov, V.V., Betekhtin, V.I. (1990) *Pores in solids*. Moscow: Energoatomizdat.
8. Geguzin, Ya.E. (1962) *Macroscopic defects in metals*. Moscow: Metallurgizdat.
9. Lebedev, V.K., Tabelev, V.D., Pismenny, A.S. (1983) Butt brazing of steel pipelines under pressure. *Avtomatich. Svarka*, **9**, 25–27.
10. Forostavets, B.A., Kirdo, I.V. (1970) Influence of high temperature strain of steel at presence of liquid phase on structure and properties of welded joints. *Ibid*., **6**, 14–17.
11. Zak, J., Rys, P. (1972) The origin of «Light area» in upset weld of rolled carbon steel. *Welding J*., **5**, 272–279.
12. Takamura, T., Shimomura, T., Suzuki, S. (1984) Formation mechanism of white line in butt welded joints by resistance heating. *J. Iron and Steel Inst. of Jap.*, **10**, 153–159.
13. Forostovets, B.A. (1968) Conditions of formation of light band in continuous flash-butt welding. *Avtomatich. Svarka*, **9**, 18–22.
14. Pujko, V.A., Zubareva, V.A., Blinkova, I.P. et al. (1983) Study of heterogeneity of flash-butt welded joints. In: *Voprosy Svarochn. Proizvodstva*. Chelyabinsk: ChPI.
15. Polosukhin, N.A. (1952) *Structure and strength of pressure-gas welded joints*. Moscow: Mashgiz.
16. Gelman, A.S. (1970) *Fundamentals of pressure welding*. Moscow: Mashinostroyeniye.
17. Bochvar, A.A. (1940) *Principles of heat treatment of alloys*. Moscow: Metallurgizdat.
18. Falkevich, A.S. (1952) Conditions of formation and properties of ferritic band in pressure methods of welding. *Avtogen. Delo*, **8**, 8–12.
19. Kuchuk-Yatsenko, S.I., Kharchenko, G.K., Falchenko, Yu.V. et al. (2000) Features of ferrite band formation in vacuum pressure welding of steel. *The Paton Welding J.*, **6**, 10–15.
20. Kofstad, P. (1969) *High-temperature oxidation of metals*. Moscow: Mir.
21. Malinochka, Ya.N., Shmelev, Yu.S., Olikhova, M.A. et al. (1981) Formation of oxides in hard steel in diffusion of oxygen in it. *Izv. AN SSSR, Metally*, **5**, 110–119.

EFFECT OF MICROSTRUCTURAL TRANSFORMATIONS ON REDISTRIBUTION OF HYDROGEN IN FUSION WELDING OF STRUCTURAL STEELS

V.I. MAKHNENKO[1], **T.V. KOROLYOVA**[1] and **I.G. LAVRINETS**[2]
[1]The E.O. Paton Electric Welding Institute, NASU, Kyiv, Ukraine
[2]R&PC «Korba», Bucha, Kyiv District, Ukraine

Kinetics of distribution of hydrogen in the HAZ metal formed in welding of a root butt joint in structural steel of the A-508 type was investigated by numerical methods. The effect of chemical composition of steel and kinetics of microstructural transformations in the melting zone during welding on a local distribution of hydrogen is shown.

Key words: *fusion welding, microstructural transformations, hydrogen concentration, reversible and irreversible traps*

The unfavourable role of hydrogen in cold (hydrogen) cracking in welding of low-alloy high-strength structural steels, sensitive to formation of quenching microstructures (martensite, low-temperature bainite) in the near-weld zone is well known [1–3, etc.] in the art.

There are many versions of explanation of the mechanism of the effect of hydrogen on formation of the said defect [1, 2, etc.], according to which the higher the hydrogen concentration of metal, the higher the probability of cold cracking, other conditions being equal. As cold cracks are a local phenomenon, it is just natural that their formation is determined by local hydrogen concentration C. The latter depends upon the mean hydrogen concentration in the weld zone. However, such dependence is far from being ambiguous. Existing experimental methods intended for quantitative estimation of hydrogen concentration in the weld zone [1–3] make it possible to judge only of the mean concentration in sufficiently large volumes of a welded joint metal (as compared with a local region of formation of a specific cold crack), which involves certain difficulties in quantitative estimation of the critical hydrogen content for specific welding conditions.

This circumstance determined the interest in application of calculation methods for evaluation of the kinetics of local hydrogen concentrations in the cross section of the weld. Several studies [4–7, etc.] were conducted in this area, where the issue is considered on the basis of certain assumptions. In particular, no allowance is made for the kinetics of microstructural transformations in the weld and HAZ metal. Meanwhile, many researchers [1–5, etc.] note that a non-simultaneous transformation of austenite in the weld and HAZ metal may have a fundamental effect on the local hydrogen concentration, which precedes formation of cold cracks.

Development of the calculation methods for prediction of microstructural changes in welding of steels, based on the time-temperature transformation (TTT) and Schaeffler diagrams [8–10, etc.], allows some upgrading of the existing calculation diagrams for estimation of a local distribution of hydrogen in welding of steels, the weld and near-weld microstructure of which is sensitive to the welding thermal cycle. This study is dedicated to consideration of this issue.

Mathematical model which describes kinetics of distribution of hydrogen across the welded joint (Figure 1), namely in region Ω confined by surface Γ, with time t, according to [4, 7], has the following form:

$$\operatorname{div}(KD\operatorname{grad}\Pi) - \overline{V}\operatorname{grad}K\Pi - Q_{\mathrm{H}} = \frac{\partial}{\partial t}(K\Pi), \tag{1}$$

$$x,\ y \in \Omega,\quad t = 0,$$
$$\Pi(x, y, 0) = \mathrm{H}_0(x, y)/K(x, y, 0) \tag{2}$$

and on surface Γ

$$\Pi(x, y, 0) = \sqrt{p_{\mathrm{H}}}, \tag{3}$$

where $\Pi(x, y, t)$ is the concentration potential, $\sqrt{\mathrm{MPa}}$; $\mathrm{H}(x, y, t)$ is the concentration of diffusible hydrogen at a point with coordinates (x, y) at time moment t, cm^3/100 g; p_{H} is the partial pressure of hydrogen; K is the coefficient of solubility of diffusible hydrogen related to the hydrogen concentration and its potential Π through the following expression:

$$\mathrm{H} = K\Pi, \tag{4}$$

i.e. $[K]$ = cm^3/100 g $\sqrt{0.1\ \mathrm{MPa}}$; D is the diffusion coefficient, cm^2/s; V is the convective transfer velocity vector, cm/s; and Q_{H} are the losses of diffusible hydrogen per unit time and volume, related to reversible and irreversible traps and chemical reactions, cm^3/(100 g·s). For the reversible and irreversible traps the Q_{H} value can be expressed as follows:

$$Q_{\mathrm{H}} = \mu\frac{\partial}{\partial t}\left(\beta\frac{100\ \mathrm{g}}{\gamma_m}\,\frac{\Pi^2}{0.1\ \mathrm{MPa}}\,\frac{293}{273+T}\right), \tag{5}$$

where β is the relative volume of the traps per unit volume of a material with density γ_m and temperature

T; for the reversible traps $\mu = 1$ and for the irreversible traps $\mu = 1$ at

$$\frac{\partial}{\partial t}\left(\beta \frac{100\ \text{g}}{\gamma_m} \frac{\Pi^2}{0.1\ \text{MPa}} \frac{293}{273 + T}\right) > 0,$$

otherwise $\mu = 0$. Often the same microdiscontinuities, depending upon the temperature, may play the role of reversible or irreversible traps, i.e. above a certain temperature T_{rev} the traps are reversibe, and below it they become irreversible. In this case the following expression is used:

$$\mu = 0 \text{ at } T < T_{\text{rev}} \text{ and}$$
$$\frac{\partial \beta}{\partial t} + \frac{2\beta}{\Pi}\frac{\partial \Pi}{\partial t} - \beta \frac{\partial T}{\partial t}\frac{1}{273 + T} < 0, \tag{6}$$
$$\mu = 1 \text{ in the rest of the cases.}$$

Here, the hydrogen content of the traps is determined from the following formula:

$$H_2(x, y, t) = \int_0^t Q_H^{\text{tr}}(x, y, t')dt', \quad 0 \le t' \le t. \tag{7}$$

Losses of diffusible hydrogen for chemical reactions in transport of the latter in the solid state are normally insignificant. Therefore, further on they will be ignored. In addition, to simplify the problem, the convective transport of hydrogen in the molten weld pool ($V = 0$ in (1)) will be ignored too. We believe this can be well compensated for by assigning the efficient diffusion coefficient within this zone at the corresponding temperatures.

With the described statement of the problem, allowance for the effect of microstructural transformations is made through the corresponding characteristics of a material — D, K and β, which are assumed to be not only the functions of temperature, but also the functions of a microstructural state of the material at a specific point with coordinates (x, y) at a moment of time t. Here we use the following dependencies:

$$D(x, y, t) = \sum_j D_j(T)\nu_j(x, y, t),$$
$$K(x, y, t) = \sum_j K_j(T)\nu_j(x, y, t), \tag{8}$$
$$\beta(x, y, t) = \sum_j \beta_j(T)\nu_j(x, y, t),$$

where ν_j is the share of the j-th microstructure in unit volume of the material at a moment of time t (j may have the following designations: a — austenite; f — ferrite, p — pearlite, b — bainite and m — martensite).

In a general case, it is necessary to have data on $D_j(T)$, $K_j(T)$ and $\beta_j(T)$. So far the information available on this issue is very scanty. It is possible to find some literature data on diffusion coefficients D_j and much less literature data on solubility coefficients $K_j(T)$ or $K_j(T)/K_0$, where K_0 is a certain constant factor.

Thus, based on [7], the following dependencies can be used for low-carbon steel:

$$D_j(T) = D_j^0 \exp\left[-\frac{E_j}{T + 273}\right],$$
$$\frac{K_j(T)}{K_0} = A_j + B_j(T - F_j) \text{ at } K_0 = 1\sqrt{0.1\text{MPa}}, \tag{9}$$

where for austenite: $D_a^0 = 0.015$ cm^2/s, $E_a = 5900$ K, $A_a = 10$, $B_a = 1/130$ 1/°C, $F_a = 1500$ °C at $1500 > T > 850$ °C, $A_a = 5$, $B_a = 0$ at $T < 850$ °C; for ferrite: $D_f^0 = 0.014$ cm^2/s, $E_f = 1600$ K at $800 > T > 200$ °C, $D_f^0 = 0.120$ cm^2/s, $E_f = 3900$ K at $T < 200$ °C, $A_f = 2$, $B_f = 1/650$ 1/°C, $F_f = 850$ °C at $850 > T > 200$ °C, $A_f = 2$, $B_f = 0.005$ 1/°C, $F_f = 0$ at $0 < T < 200$ °C.

In a liquid part of the weld pool at $T > 1500$ °C, according to [7], the following can assumed:

$$D = 0.1 \text{ cm}^2/\text{s}, \quad K/K_0 = 20. \tag{10}$$

In the first approximation the same data are used for pearlite, bainite and martensite as for ferrite (α-iron is the base).

As far as β is concerned, it is most appropriate to relate its value to a conditional microporosity of the material, caused by some defects of a crystalline structure. It is highly probable that the highest values of β correspond to a martensitic microstructure, which contains, as a rule, a maximum amount of the said defects. However, this issue requires special investigations, based on a combined use of experiments and calculations. It is very likely that a certain role in this case can be played by calculation algorithms, similar to that considered in this study.

The algorithm described provides for the appropriate kinetics of variations of temperatures in the welded joint zone and microstructures in the melting zone (MZ) and HAZ. In this study the temperature fields were determined using a numerical method, based on solution of the corresponding thermal conductivity problem for a material with variable (depending upon the temperature) thermal-physical properties, effective thermal conductivity within the molten metal and latent melting (solidification) heat [10]. The welding process conditions are set by energy parameters of electric arc welding: current I_w, arc voltage U_a, welding speed v_w, filler metal chemical composition and deposition efficiency α_d for given conditions, butt joint groove preparation geometry (Figure 1, see colour insert), initial temperature T_0 and coefficient α_h of heat exchange with the environment, following the Newton law.

The calculated effective heat input

$$q_h = \eta_h U_a \frac{I_w}{v_w} \text{ [J/cm]} \tag{11}$$

Table 1. Chemical composition of materials used

Material	*C*	*Mn*	*Si*	*Cr*	*Ni*	*Mo*	*Nb*	*Al*	*Ti*
A-508	0.162	1.35	0.296	0.196	0.7	0.504	0.006	0.047	0
Alloy I	0.14	0.4	0.12	0.2	–	–	–	–	–
Alloy II	0.03	1.6	0.5	17.0	12.0	0.5	–	–	–
Alloy III	0.03	0.1	0.15	30.0	60.0	0.01	0.02	0	0.33

(here η_h is the effective efficiency of heating for a given type of arc welding) is introduced together with filler metal and partially as a distributed heat source acting per unit length of the weld during a period of time t_0, i.e. the first part of the effective heat input of melting Q_{melt} is determined through the mean temperature of the introduced filler metal, T_{filler}, with allowance for the latent heat of melting, q_{lat}, as follows:

$$Q_{melt} = \frac{I\alpha_d}{3600 v_w \gamma_H} (T_{filler} c\gamma_l + q_{lat}) \ [\mathrm{J/cm}],$$

where $c\gamma_l$ is the volumetric heat capacity of a liquid filler metal. Accordingly, the second part is as follows:

$$Q_{dis} = q_h - Q_{melt} \ [\mathrm{J/cm}]. \tag{12}$$

Energy Q_{dis} is distributed in space x, y, z following the normal law, i.e., according to [11], it holds for unit volume

$$g(x, y, z) = \frac{Q_{dis} 6\sqrt{3 v_w}}{abc\pi\sqrt{\pi}} \times \\ \times \exp\left\{(-3\left[\left(\frac{x}{a}\right)^2 + \left(\frac{y}{b}\right)^2 + \left(\frac{z}{c}\right)^2\right]\right\}, \tag{13}$$

where a, b and c are the parameters of this distribution. Energy Q_{dis} may have other distributions as well. However, in view of the principle of a local effect, according to which an error for temperatures due to inadequacy of distribution dramatically decreases with an increase in distance from an instantaneous position of the source centre, it is worth to consider a very convenient approximate energy distribution, which is based on an assumption that energy Q_{dis} is introduced in the form of a volumetric heat source, uniformly distributed in volume of the deposited metal (or MZ), during time $t_0 = \tau_0 + B/v_{tr}$, where τ_0 is the constant related to characteristics of the welding arc and approximately equal to 0.5–1.0 s; B is the amplitude of transverse oscillations and v_{tr} is the transverse oscillations velocity. This distribution was validated in a number of studies [10, etc.], and the results are in good agreement with experimental data on temperatures and sizes of the MZ.

The share of the j-th microstructure ν_j in a unit volume depends upon the temperatures and chemical composition. Chemical composition of MZ is calculated from chemical composition of the filler metal, base material and material of previous passes melted in a given pass during multi-pass welding (see Figure 1), i.e. percentage of element X is as follows:

$$X = \frac{1}{F} \sum_q X_q F_q, \tag{14}$$

where F is the total area of the melting zone (see Figure 1); F_q is the q-th component of an area melted in a given pass (here q = I is the base material, II is the previous layer and III is the filler);

$$F_{III} = \frac{\alpha_d I_w}{3600 \gamma_m v_w}; \tag{15}$$

X_q is the percentage of element X in a section with surface area F_q.

The kinetics of microstructural transformations is determined from chemical composition of the MZ and HAZ metal using, as noted above, the corresponding Schaeffler diagrams for high-alloy welds and TTT diagrams for carbon and low-alloy steels [8, 9], or the corresponding parametric dependencies adequate to specific steel compositions. In this study the numerical investigations were conducted for butt joints in low-alloy steel of the A-508 type, the chemical composition of which is given in Table 1. Alloys, for which chemical composition of the pure deposited metal is also given in Table 1, were used as the filler metal.

Considered was the root weld of a butt joint (see Figure 1) made by arc welding under conditions which provided effective heat input q_h = 9146 J/cm for all the variants investigated, the deposition efficiency

Table 2. Mean chemical composition of the root weld melting zone

Variant No.	*Filler metal*	*C*	*Mn*	*Si*	*Cr*	*Ni*	*Mo*	*Mb*	*Al*
1	A-508	0.162	1.35	0.296	0.196	0.7	0.504	0.006	0.047
2	Alloy I	0.147	0.72	0.178	0.198	0.37	0.17	0.002	0.016
3	Alloy II	0.073	1.52	0.43	11.4	8.23	1.83	0.002	–
4	Alloy III	0.073	0.52	0.19	20.06	40.23	0.75	0.015	0.016

Note. Alloy I – 0.133 % Cu; alloy II – 0.22 % Ti.

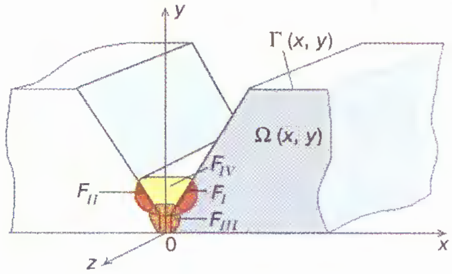

Рис. 1. Схема сечения сварного шва стыкового соединения — область $\Omega(x, y)$, ограниченная поверхностью $\Gamma(x, y)$, площадь F_q (где $q=I–IV$ — различные участки зоны проплавления второго прохода)

Fig. 1. Diagram of a weld cross-section in a butt joint: section $\Omega(x, y)$, limited by surface $\Gamma(x, y)$, area F_q (where $q=I–IV$ — are different sections of the penetration zone in the second pass)

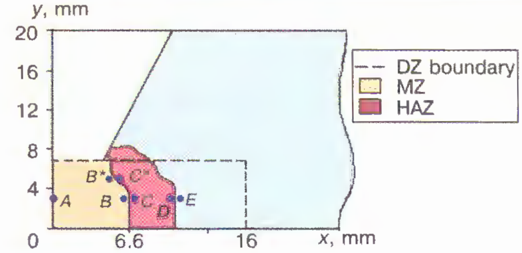

Рис. 3. Схема диффузионной зоны (ДЗ) в сочетании с зоной проплавления (ЗП) и ЗТВ; A, B, C, D, B*, C*, E — характерные точки указанных зон

Fig. 3. Diagram of diffusion zone (DZ) together with penetration zone (PZ) and HAZ; A, C, D, B*, C*, E are characteristic points of the above zones

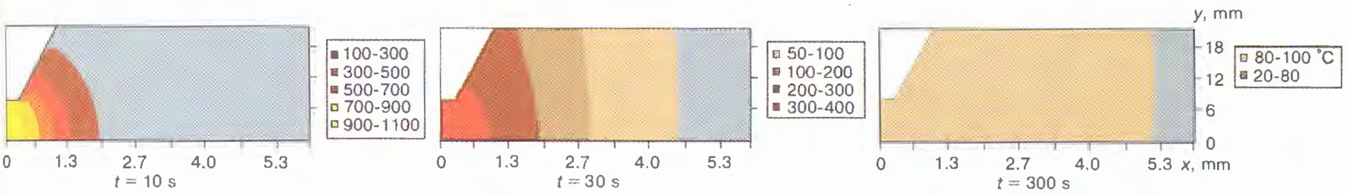

Рис. 2. Температурные зоны при сварке в зависимости от времени t в варианте № 1

Fig. 2. Temperature zones in welding, depending on time t in variant №1

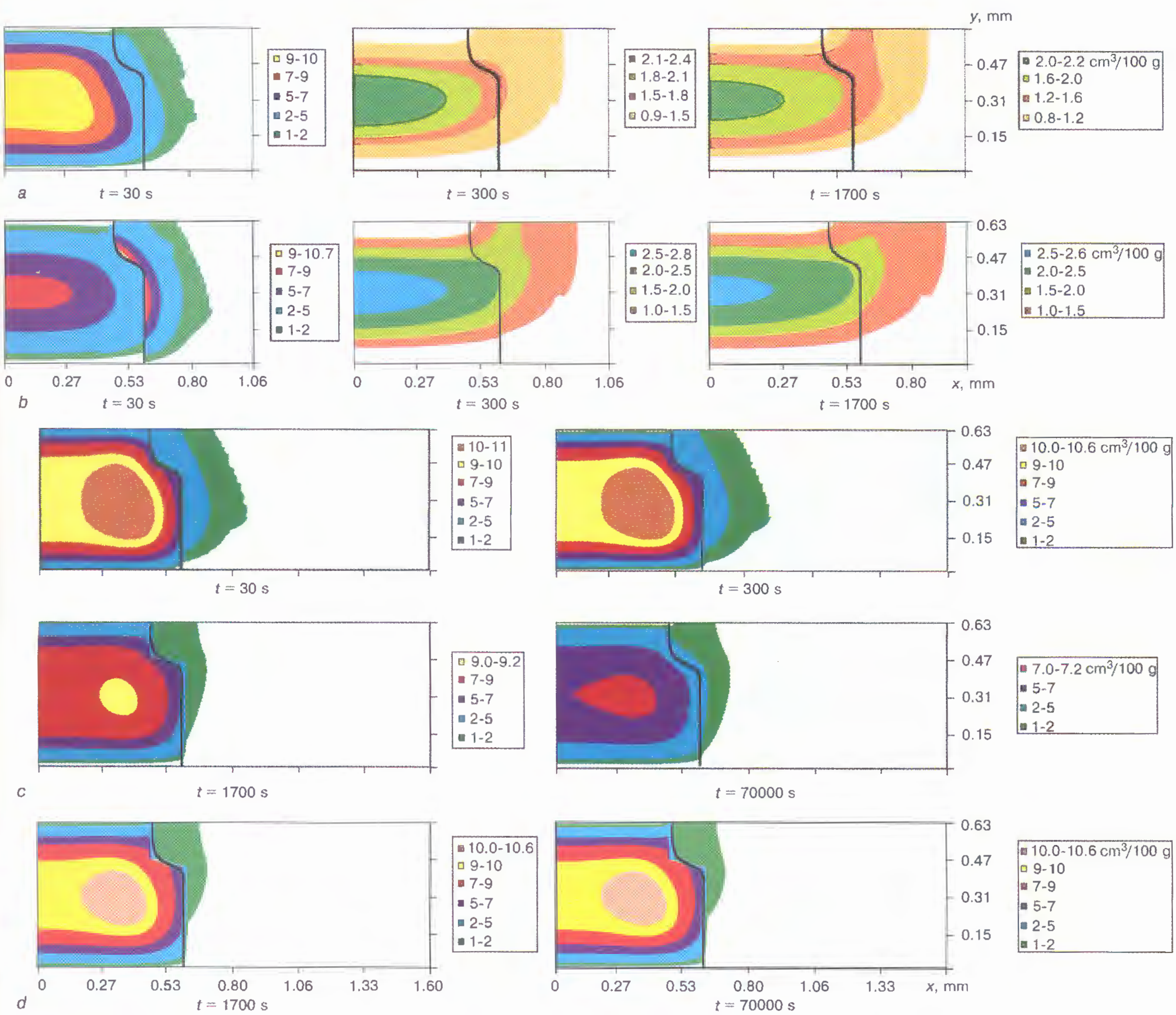

Рис. 4. Распределение диффузионного водорода H в поперечном сечении сварного соединения в различные моменты времени t для вариантов № 1 (*a*), 2 (*b*), 3 (*c*), 4 (*d*)

Fig. 4. Distribution of diffusive hydrogen H in the welded joint cross-section at different moments of time t for variants № 1 (*a*), 2(*b*), 3 (*c*), 4 (*d*)

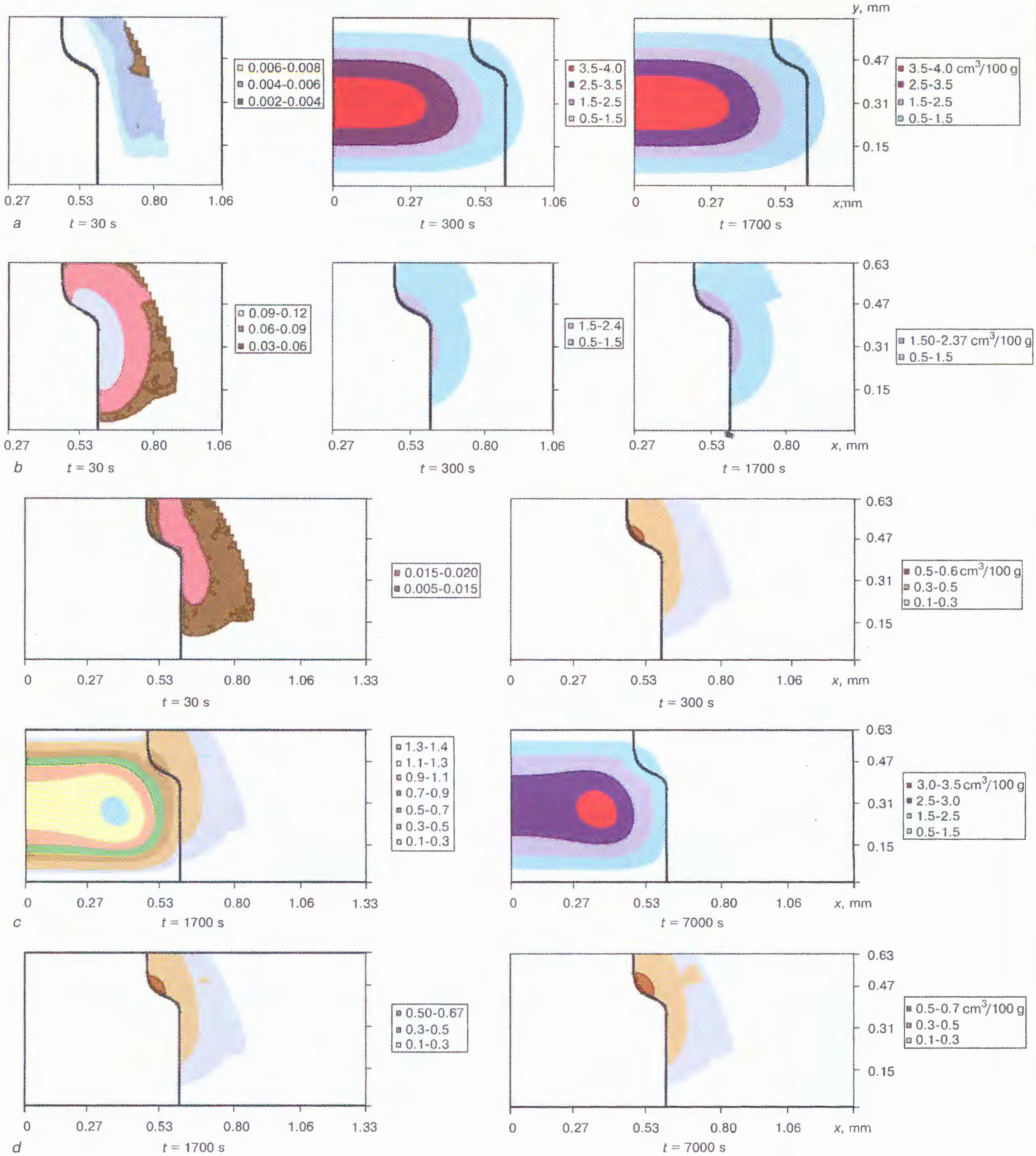

Рис. 5. Распределение водорода в ловушках (H_2) в поперечном сечении сварного соединения в различные моменты времени *t* для различных вариантов (*a*–*d* — см. рис. 4)

Fig. 5. Hydrogen distribution in traps (H_2) in the welded joint cross-section at different moments of time *t* for different variants (for *a*–*d* see Fig. 4)

being 4.5 kg/h. Such similar conditions were used for convenience of comparison, as for all the variants the sizes of MZ and HAZ, determined by properties of the base metal, were approximately the same. Figure 2 (see colour insert) shows temperature zones and sizes of MZ and HAZ in welding using wire with a composition close to that of steel of the A-508 type (variant No.1). Similar data were obtained also for the rest of the variants (No.2–4). They differ but very slightly, although it is possible to distinguish in them a mean chemical composition of MZ (Table 2). Based on the data on a chemical composition and kinetics of variations in temperature for MZ and HAZ, microstructural transformations in these zone can be calculated using the following dependencies:

$$\begin{gathered} \text{at } T > A_3 \; \nu_a = 1 - \nu_\delta,\; \nu_j = 0,\; j \neq a,\, \delta; \\ \text{at } T < A_3 \; d\nu_j = 0, \text{ if } \frac{\partial T}{\partial t} > 0, \\ \nu_j(x, y, t) = \nu_j^{\max}(x, y) f(T), \text{ if } \frac{\partial T}{\partial t} < 0, \end{gathered} \tag{16}$$

where $\nu_j^{\max}$ is the final microstructure of MZ or HAZ; $f(T)$ is the function of a current temperature $T(x, y, t)$ at a point with coordinates (x, y) and temperatures of the beginning, T_j^{st}, and end, T_j^{end}, of transformation of austenite into the j-microstructure for alloy of a given chemical composition [10]; and ν_δ is the amount of δ-ferrite from the Schaeffler diagram.

For the HAZ metal of all the variants and MZ metal of variant No.1 (see Table 2) the values of $\nu_j^{\max}$ were determined depending upon the chemical composition and cooling time $t_{8/5}$ (850–500 °C) from [8, 10].

For the MZ metal of variant No.2 ν_j was also determined depending upon the chemical composition and time $t_{8/5}$, but using description from [9]. For the melting zone of variants No.3 and 4 the use was made of the Schaeffler diagram. In the case of variants No.3 and 4, T_j^{st} for $j = \delta$ and $j = a$ was assumed to be equal to a solidus temperature of the alloy, i.e. 1350 °C. For variant No.3 T_m^{st} was calculated depending upon the composition from [12], i.e. at 0.03 < C < 0.35:

$$\begin{gathered} T_m^{st} = 454 - 210\mathrm{C} + 4.2/\mathrm{C} - \bar{A}\cdot\mathrm{Ni} - 16.8\mathrm{Cr} - 10.5\mathrm{Mn}, \\ \bar{A} = 21 \text{ at Ni} > 5.0\ \%, \\ \bar{A} = 1.6\mathrm{Ni} + 65/\mathrm{Ni} \text{ at } 1.4 < \mathrm{Ni} < 5.0, \\ T_m^{end} \approx T_m^{st} - 126\ ^\circ\mathrm{C}. \end{gathered} \tag{17}$$

For MZ of variants No.1 and 2 the values of temperatures T_j^{st} and T_j^{end} were taken from the corresponding TTT diagrams [13] (Table 3). This Table also gives maximum values of $\nu_j^{\max}$.

For HAZ, $\nu_m^{\max} = 0.65$–0.49, $\nu_b^{\max} = 0.35$–0.51, and T_j^{st} and T_j^{end} are similar to those for MZ (variant No.1). It follows from the data given that one may expect formation of martensitic-bainitic microstructure in MZ for this variant, bainitic-ferritic microstructure for variant No.2, martensitic microstructure for variant No.3 and austenitic one for variant No.4. A characteristic feature is that in variant No.3 transformation of austenite into martensite begins at +84 °C and ends at −46 °C, i.e. the microstructure will be austenitic-martensitic at a room temperature. As far as HAZ is concerned, it is expected that it will have a martensitic-bainitic microstructure, although in the initial state the material had a bainitic-ferritic microstructure, i.e. $\nu_b = 0.4$ and $\nu_f = 0.6$.

Naturally, at different stages of cooling of MZ the microstructural state may differ to a substantial degree from the final one (Table 3). It can be seen that variant No.2 is characterised by the fastest austentite transformation in MZ, variant No.3 — by the slowest austentite transformation, and variant No.4 — by the absence of such a transformation. It is of interest to estimate how this difference in microstructural transformations in MZ would affect distribution of hydrogen in the weld and HAZ metal. For this purpose the above problem (1) to (9) was numerically solved on an assumption of the following input conditions: in MZ the diffusible hydrogen concentration is $C = 10\ \mathrm{cm}^3/100$ g at a temperature of 1500 °C, and in the rest of the welded joint $C = 0.5\ \mathrm{cm}^3/100$ g. The diffusion and solubility coefficients are described by expressions (10). Allowing for a limited spatial effect of the diffusion process during a time of levelling of temperatures across the weld and the necessity of using finite elements with small linear sizes (10 times as small as those for the temperature problem), the spatial domain of the diffusion problem for the root weld is represented by part of a cross section (Figure 3, see colour insert), i.e. this domain includes MZ, HAZ and part of the cross section of the weld outside these zones. Condition (3) at $p_H = 0$ was assumed for the ends of this domain, coinciding with free surfaces (lower part of the plate and surface of the root weld). For the rest of the boundaries of this

Table 3. Characteristics of microstructure of the melting zone

Variant No.	$\nu_j^{\max}$				T_j^{st}, °C			T_j^{end}, °C		
	a	*f*	*b*	*m*	*f*	*b*	*m*	*f*	*b*	*m*
1	0	0	0.128	0.72	800	600	380	600	380	250
2	0	0.22	0.77	0	780	620	420	620	420	270
3	0	0	0	1.0	1300	–	84	84	–	46
4	1.0	0	0	0	–	–	–	–	–	–

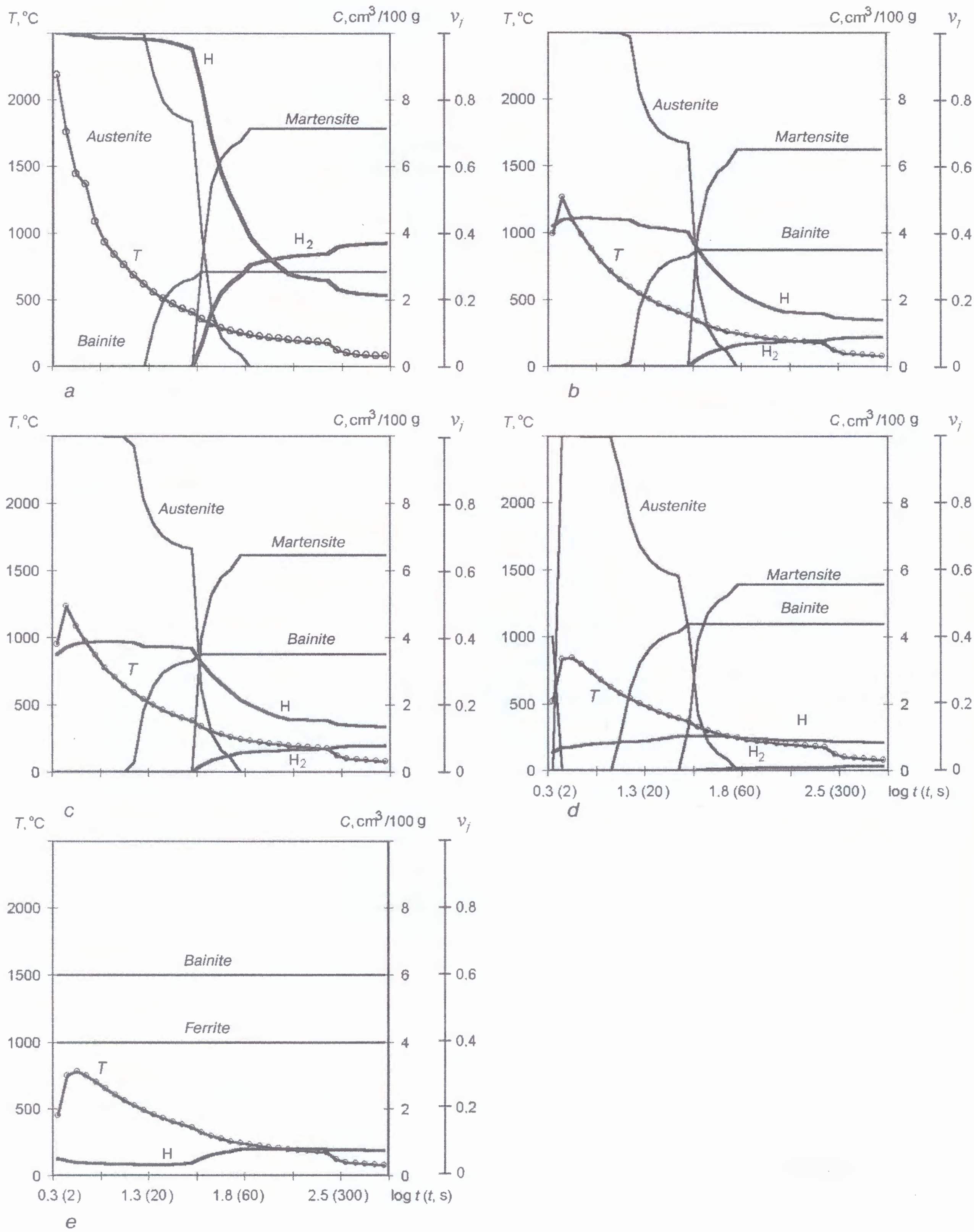

Figure 6. Kinetics of time variations of temperatures T, microstructural components v_j, concentration of diffusible hydrogen H and hydrogen in traps H_2 for variant No.1 at characteristic points A (a), B (b), C (c), D (d) and E (e) (see Figure 3)

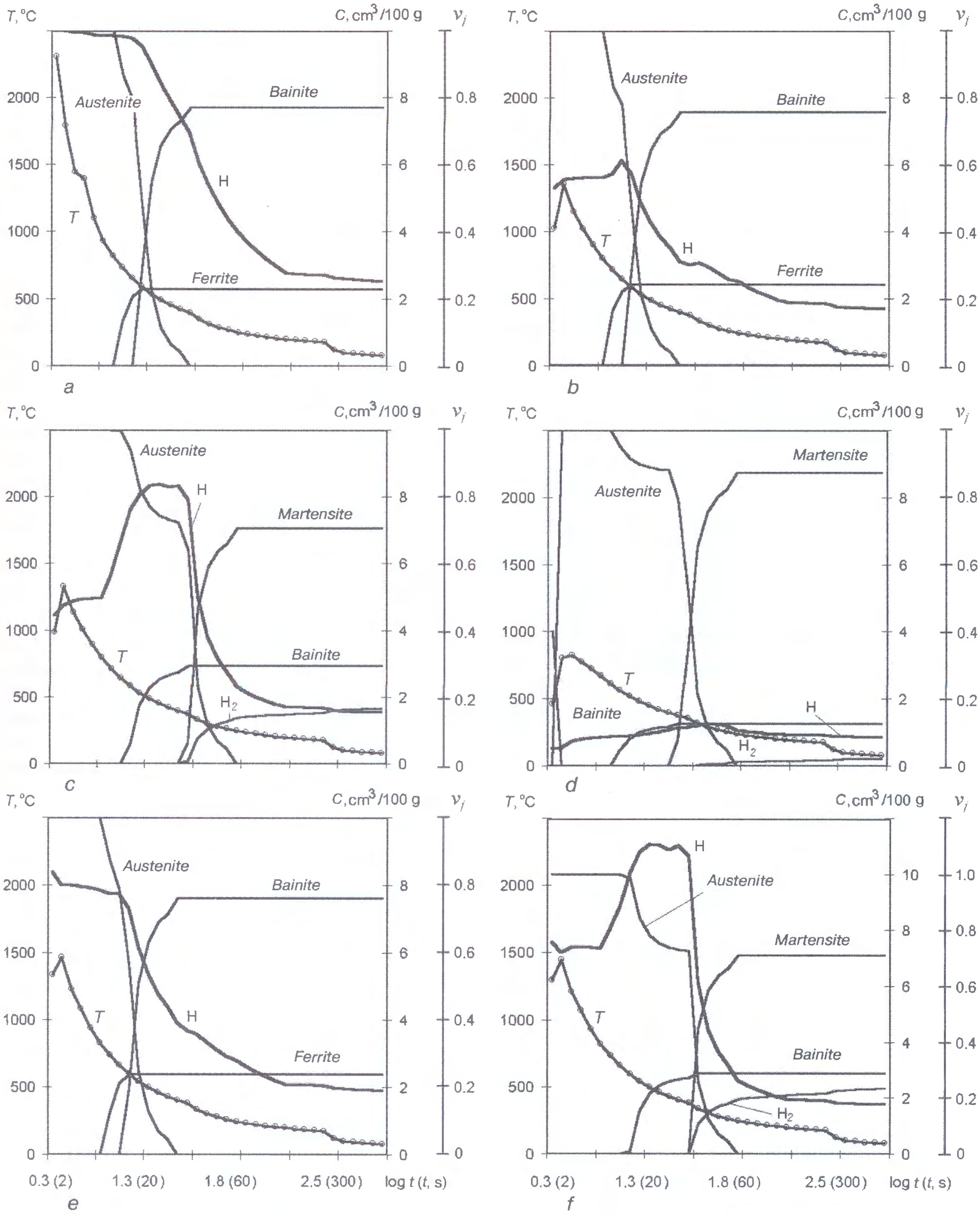

Figure 7. Kinetics of time variations of temperatures, microstructural components, concentrations of diffusible hydrogen and hydrogen in traps for variant No.2 at characteristic points *A* (*a*), *B* (*b*), *C* (*c*), *D* (*d*), *B*$^{\bullet}$ (*e*) and *C*$^{\bullet}$ (*f*)

Table 4. Concentration of hydrogen ($cm^3/100$ g) in HAZ at 50–100 °C

Variant No.	*H*	H_2	$H + H_2$	*H*	H_2	$H + H_2$
	at $T_C \approx 100$ *°C and* $t \approx 300$ *s*			*at* $T_C \approx 60$ *°C and* $t \approx 1700$ *s*		
1	1.4	0.76	2.16	1.3	0.79	2.09
2	1.58	1.62	3.2	1.49	1.68	3.17
3	1.12	0.36	1.48	1.59	0.39	1.97
4	1.12	0.35	1.47	1.09	0.38	1.47

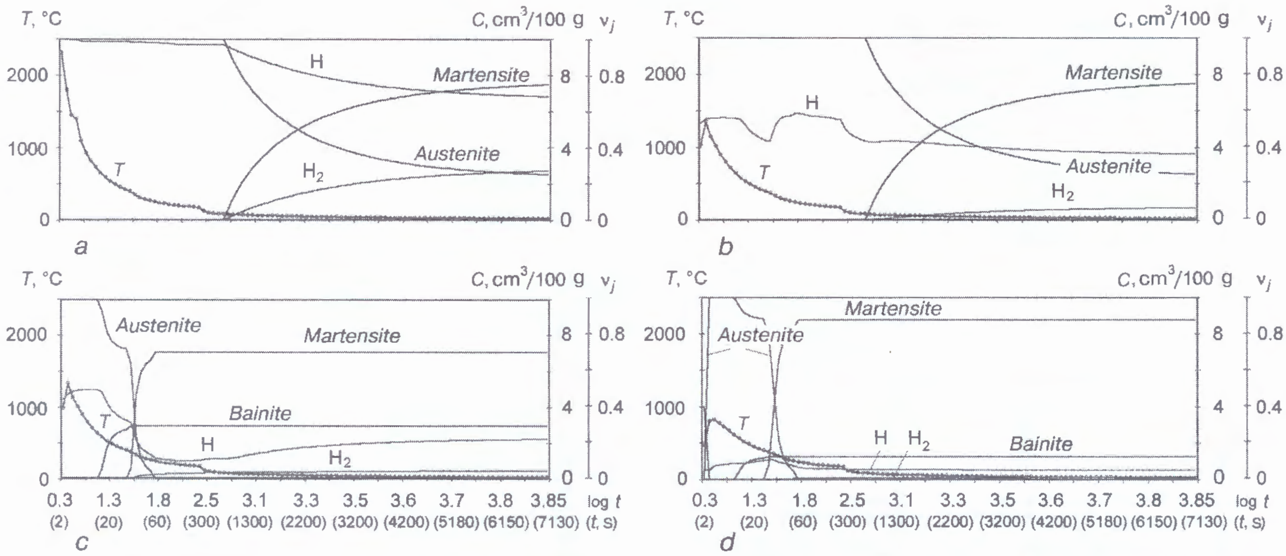

Figure 8. Kinetics of time variations of temperatures, microstructural components, concentration of diffusible hydrogen and hydrogen in traps for variant No.3 at points *A* (*a*), *B* (*b*), *C* (*c*) and *D* (*d*)

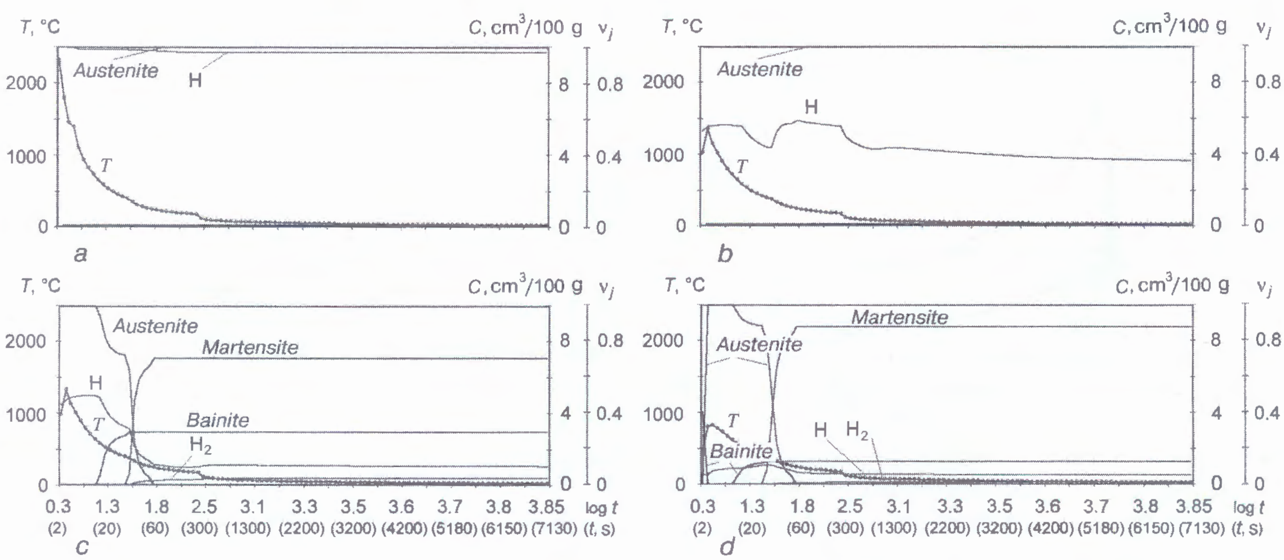

Figure 9. Kinetics of time variations of temperatures, microstructural components and concentrations of diffusible hydrogen and hydrogen in traps for variant No.4 (*a–d* — see Figure 8)

domain $\partial\Pi/\partial n = 0$, where n is the normal to the surface.

Considered also was the case of traps of the type of (5) and (6), but present in martensite at $T_{rev} = 300$ °C and $\beta_m = 0.05$. Results of calculations of distribution of diffusible hydrogen, H, and molecular hydrogen in traps, H_2, in a cross section of the weld at different time moments for the variants considered are shown in Figures 4 and 5 (see colour inserts). It can be seen from the data of Figures 4, *a* and 5, *a*, obtained for variant No.1 (base and weld metal — steel A-508), that distribution of H and H_2 is very non-uniform. The maximum concentration is observed far from the interface with the environment, where it is assumed that $p_H = 0$. At the boundaries of MZ and HAZ the concentration values gradually vary. Kinetics of variations of the H and H_2 concentrations with time at characteristic points of *A, B, C* and *D* (see Figure 3), shown in combination with temperature $T(t)$ and microstructures $v_j(t)$ for a given variant, yield curves shown in Figure 6. Here point *A* is located at the centre of MZ, *B* — at the boundary with HAZ, *C* — in HAZ at the boundary with MZ, *D* — in HAZ at the boundary with base metal and *E* — in base metal at the boundary with HAZ. Figures 4, *b*, 5, *b* and 7, *a–c*, show similar data for variant No.2, where the MZ metal (see Table 2) is low-carbon steel with minor additions of alloying elements and the microstructure contains no martensite. An earlier transformation in MZ, as compared with HAZ, which is characteristic of this variant, leads to a non-monotonous variation in the concentration of hydrogen in HAZ near the boundary with MZ, i.e. a burst of the concentration of hydrogen due to its displacement from MZ is seen not only in deep layers (Figure 7, *c*), but also near the surface (B^*, C^*, Figure 3), where a more rapid cooling makes this process rather pronounced (Figure 7, *e, f*).

The data of Figures 4, *c*, 5, *c*, and 8 correspond to variant No.3, where the metal microstructure is austenitic up to temperature $T_m^{st} = 84$ °C. In this case hydrogen is contained in the MZ metal, which has a corresponding effect on its concentration in HAZ. The latter is especially noticeable in variant No.4 (see Figures 4, *d*, 5, *d* and 9), in which MZ has a stable austenitic microstructure.

If the risk of formation of longitudinal cold (hydrogen) cracks in the root weld HAZ is related to the amount of hydrogen at characteristic points (C, C^*) at a temperature of 50–100 °C, the datas of Table 4 demonstrate this risk for all the variant under consideration.

It can be seen from Table 4 that variant No.2 has the highest risk of formation of cold cracks, then follow variants No.1 and 3, and variant No.4 is most favourable in this respect.

Therefore, the calculation results obtained in this study are in good agreement with the experiments described in [1, etc.]. This allows a suggestion of adequacy of the mathematical model described in this study, so that it can be applied to compare different variants of welding (different filler metal, parameters, preheating, etc.) by the kinetics of local concentrations of hydrogen in the cross section of a welded joint.

1. Hrivnyak, I. (1984) *Weldability of steels*. Moscow: Mashinostroyeniye.
2. Pokhodnya, I.K. (1998) Problems of welding of high-strength low-alloy steels. In: *Modern material science of XXI century*. Kyiv: Naukova Dumka,.
3. Oates, W.R., Saitta, A.M. (1998) *Welding handbook*. 8th ed., Vol. 4, Materials and applications, Part 2. Miami: AWS.
4. Michailov, V.G., Thomas, K., Wohlfahrt, H. (1996) Numerische Simulation der Wasserstoffverteilung in mehrlagigen Schweißverbindungen. *Schweißen und Schneiden*, **48**, 47–50.
5. Yorioka, N., Oshita, S., Nakamura, H. et al. (1980) An analysis of effects of microstructure, strain and stress on the hydrogen accumulation in the weld heat affected zone. *IIW Doc. IX-1161-80*.
6. Velkov, K., Palazov, A. (1983) On modeling of hydrogen distribution in connection with the formation of cold cracks in welding. In: *Proc. of II Symp. of CMEA on Application of Mathematical Methods to Study the Weldability*. Sofia.
7. Makhnenko, V.I., Demchenko, V.F., Ryabchuk, T.G. (1983) Calculation of diffusion of gases, produced pressures and stresses near micropores in weld metal and heat affected zone. *Ibid*.
8. Seyffarth, P., Kasatkin, O. (1982) Calculation of structural transformation in the welding process. *IIW Doc. IX-82*.
9. Jon, J.C., Saiminen, A.S., Sun, Z. (1996) Process diagrams for laser beam welding of carbon manganese steels. *Welding J.*, July, 225–232.
10. Makhnenko, V.I., Velikoivanenko, E.A., Makhnenko, O.V. et al. (2000) Investigation of effect of phase transformation on residual stresses in circumferential welding of pipes. *The Paton Welding J.*, **5**, 2–7.
11. Taljat, B., Zacharia, T., Wang, X-L. et al. (1998) Numerical analysis of residual stress distribution in tubes with spiral weld cladding. *Welding J.*, August, 328–335.
12. Beres, L. (1998) Proposed to Shaeffler diagram for chrome equivalents and carbon for more accurate prediction of martensite content. *Ibid.*, July, 273–276.
13. Seyffarth, P., Meyer, B., Scharff, A. (1992) *Grosser Atlas Schweiß-ZTU-Schaubilder*. Düsseldorf: DVS-Verlag.

EFFECT OF WELDING SPEED ON WELDING CURRENT MAGNETIC FIELD

V.I. SHCHETININA, S.V. SHCHETININ, N.I. CHAPNI, A.V. SHCHERBINA, A.E. MELNIKOV and **S.P. GOLUBKOV**
Priazovsky State Technical University, Mariupol, Ukraine

The induction equation has been derived and the effect of welding speed on the welding current electromagnetic field has been established. The electromagnetic theory of formation of undercuts in welding at an increased speed has been developed and experimentally proved.

Key words: *arc welding, undercuts, welding speed, electromagnetic field, induction equation*

Welding at an increased speed is one of the methods for decreasing material and power consumption and increasing process productivity. However, an increase in the welding speed has some limitations, as this may cause undercuts resulting from violation of the weld formation.

Considerable contribution into investigation of the nature of formation of undercuts and development of welding processes at an increased speed was made by B.E. Paton and S.L. Mandelberg [1]. However, the nature of formation of undercuts has not yet been sufficiently studied. N.N. Rykalin [2] attributes this phenomenon to overheating of the molten metal pool. Authors of studies [3–5] relate formation of undercuts to increase in the rate of cooling of molten metal, caused by enhanced heat removal. K. Andoh [6] and K. Ishizaki [7] think that undercuts are formed as a result of an increase in surface tension at the moment of solidification of molten metal.

Formation of the welds is determined to a considerable degree by the magnetic-hydrodynamic phenomena and the welding arc. Therefore, it is likely that the effect of thermal processes on the weld formation should be regarded as a result of changes in a direction of lines of the current and the welding circuit electromagnetic field. S.V. Gulakov and B.I. Nosovsky [8] state that with an increase in the welding speed under the effect of the arc on a thin interlayer the metal displaces only to the tailing part of the weld pool. The absence of transverse convection leads to formation of undercuts. At the same time, the molten metal flows in the weld pool are determined by pressure of the welding arc and the welding current electromagnetic forces. B.E. Paton and S.L. Mandelberg [1] are of the opinion that formation of undercuts with an increase in the welding speed results from violation of dynamic equilibrium of molten metal in the weld pool. An increase in the welding speed is accompanied by an increase in welding arc pressure P_a, and decrease in molten metal pressure P_{pool}. At $P_a > P_{pool}$ the arc pressure in a crater is not counterbalanced by the molten metal pressure, which leads to «throwing off» of molten metal to the tailing part of the weld pool. In studies [9, 10] formation of undercuts is attributed to an increase in the arc pressure.

Based on the fact that the arc pressure is a result of the pinch effect and that position of the arc in space depends upon the electromagnetic field, formation of undercuts greatly depends upon the welding circuit electromagnetic field. It is generated by the arc current and current flowing though base metal. As directions of its force lines coincide, then, according to the superposition principle, induction of the welding circuit electromagnetic field is determined as follows:

$$B = B_a + B_m, \tag{1}$$

where B_a and B_m are inductions of the electromagnetic fields generated by the arc and current flowing through the metal, respectively.

According to Biot–Savart law, induction of the electromagnetic field of a current conductor is determined from the following formula:

$$B = \mu \frac{I}{2\pi r}, \tag{2}$$

where μ is the magnetic permeability of environment; I is the welding current; and r is the distance from the current conductor to a point under consideration.

Induction of the electromagnetic field generated by the arc current is determined from the following expression:

$$B_a = \mu \mu_0 \frac{I}{2\pi r_a}, \tag{3}$$

where μ_0 is the magnetic constant equal to $4\pi \cdot 10^{-7}$ H/m and r_a is the distance of the point considered from the arc.

Induction of the electromagnetic field generated by the arc current flowing through the metal at a distance from the metal surface is determined from the following formula:

$$B_m = \mu \mu_0 \frac{I}{2\pi r_m}, \tag{4}$$

where r_m is the distance of the point considered with respect to a component of the current flowing through the base metal.

Then induction of the welding circuit electromagnetic field at a distance from the metal surface is described by the following expression:

$$B_a = \mu\,\mu_0\,\frac{I}{2\pi r_a} + \mu\,\mu_0\,\frac{I}{2\pi r_m}. \quad (5)$$

In the fusion zone the distance from the arc axis is half the weld width:

$$r_a = b_w/2. \quad (6)$$

Distance of the arc with respect to a component of the current flowing through the metal, which is measured from the centre through thickness of the metal, is equal to

$$r_m = h^2/4r_{m_0}, \quad (7)$$

where h is the base metal thickness and r_{m_0} is the distance from the centre through thickness of the metal.

Then induction of the welding circuit electromagnetic field on the metal surface within the fusion zone is determined from the following formula:

$$B = \mu\,\mu_0\,\frac{I}{\pi b_w} + \mu\,\mu_0\,\frac{2Ir}{\pi h^2}. \quad (8)$$

According to the equation derived, induction of the welding circuit electromagnetic field increases with an increase in the current and distance to the metal surface, and decreases with an increase in the weld width. The equation allows determination of induction in the weld pool, and these data are in good agreement with the experimental ones obtained from simulation of the welding process: induction increases with distance to the metal surface and decreases with an increase in the welded joint gap. As induction of the field increases with a decrease in distance to the metal surface, it is our opinion that the welding current electromagnetic field affects the formation of undercuts. The role of the electric current electromagnetic field is as follows. The current in the weld pool flows from an active spot through the molten metal. In a region of side edges of the pool the welding current and molten metal are affected by the field of the current flowing through the arc. Under its effect the molten metal of the pool is influenced by the electromagnetic force directed downward (Figure 1).

Increase in the welding speed enhances cooling of the active spots, leads to a concentration and decrease of heat input into the side edges of the pool, the electrical resistance of which decreases in this case. This results in growth of the current flowing through the side edges of the pool, induction of the electromagnetic field and electromagnetic pressure. The latter causes the molten metal to flow down from the pool edges, which leads to the formation of undercuts.

To confirm the role of the welding current electromagnetic field in the formation of undercuts, investigations were conducted to study the effect of the welding speed on the field. Induction of the welding current electromagnetic field during welding was measured at points located at a distance of $16\cdot10^{-3}$ m from the base metal and electrode, ahead of and behind the arc and in the fusion zone (Figure 2). Besides, in measurement of the electromagnetic induction behind the arc in the welding direction the distance from the rear wall of a composite electrode to the point con-

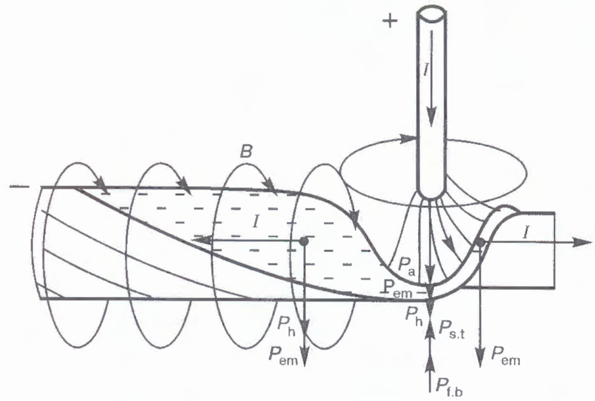

Figure 1. Schematic of forces acting on molten metal of the weld pool in one-sided welding on a flux backing: P_a — welding arc pressure; P_h — hydrodynamic pressure; P_{em} — electromagnetic pressure; $P_{s.t}$ — surface tension; $P_{f.b}$ — flux backing pressure

sidered was set at $16\cdot10^{-3}$ m and that ahead of the arc from the tip of a strip electrode was set at $8\cdot10^{-3}$ m. This provided an equal distance of the probe from the arc burning in the strip electrode zone, as the arc here melts out a straight-line region of the strip $(10-12)\cdot10^{-3}$ m long.

The data were obtained using the Sh1-7 electromagnetic induction meter based on the Hall effect. The probe for measuring the magnetic induction within a range of 0.01–0.16 T was placed in a quartz insulator rigidly fixed to the welding head, which provided a maximum possible approach of the Hall transducer to the arc and an insignificant heating of the probe during measurement (due to a low thermal conductivity of quartz). Relative magnetic permeability of molten metal was close to one and magnetic permeability of air. Therefore, the welding circuit electromagnetic field in the near-arc space can be determined from values of the magnetic induction at the measurement points.

As established as a result of the investigations conducted, increase in the welding speed is accompanied by an increase in induction of the electromagnetic field in the fusion zone (Figure 3). It is likely that this is a result of decrease in the amount of heat released in the side parts of the pool, decrease in the electrical resistance and increase in the current flow through the pool edges. Magnetic induction determines the electromagnetic force and electromagnetic pressure on molten metal of the pool in the fusion zone. Increase in the welding speed is accompanied

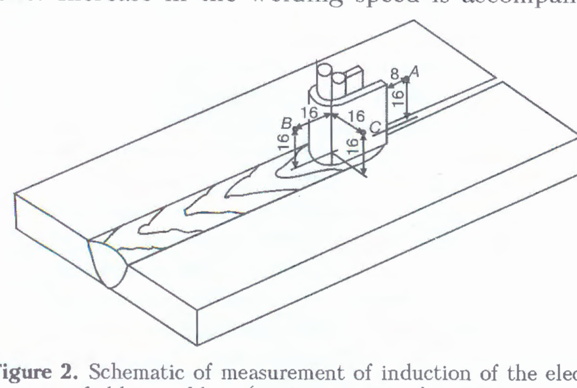

Figure 2. Schematic of measurement of induction of the electromagnetic field in welding (A–C — points of measurement of induction of the electromagnetic field ahead of and behind the arc and in the fusion zone, respectively)

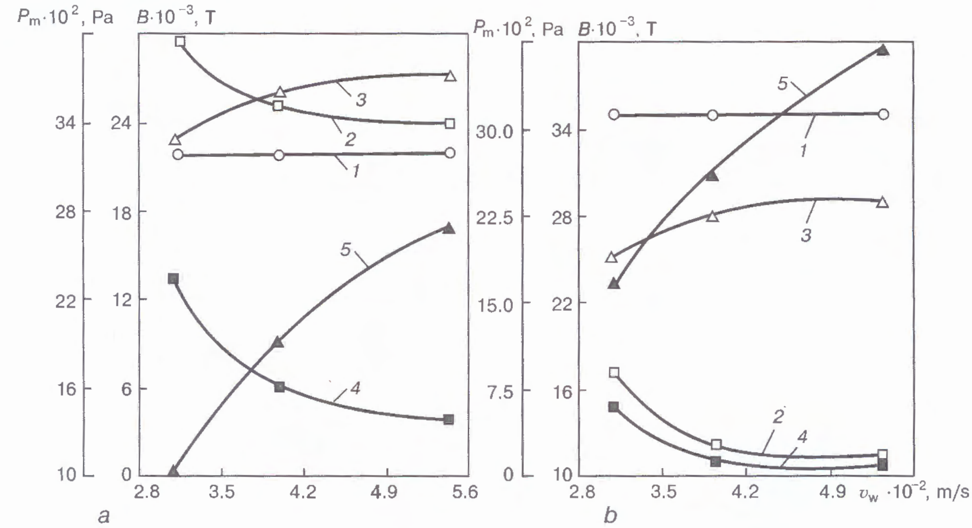

Figure 3. Dependence of electromagnetic induction (*1–3*) and electromagnetic pressure on molten metal (*4, 5*) upon welding speed v_w in a direction from the current conductor (*a*) and to the current conductor (*b*): *1* — ahead of the arc (point *A*); *2, 4* — behind the arc (point *B*); *3, 5* — in the fusion zone (point *C* in Figure 2)

by an increase in the downward electromagnetic field and magnetic pressure. Under the effect of the latter the molten metal flows down from the pool edges, which influences the formation of undercuts.

Induction of the electromagnetic field is particularly increased in the fusion zone during welding in a direction to the current conductor, which is a result of decrease in induction of the arc to 0.011 T. Undercuts resulting from an increase in induction in the fusion zone during welding in a direction from the current conductor cause violation of the weld formation.

During welding in a direction from the current conductor, under the effect of the electromagnetic field the arc deviates forward towards the lower field and heats edges of the pool. This causes increase in the electrical resistance and decrease in the current and the downward electromagnetic field in the fusion zone. As a result, the weld formation improves. The role of the welding current electromagnetic field in the formation of undercuts is proved by the effect of location of the current conductor point and direction of the current lines on the weld formation. Independently of the location of the current conductor point, as the welding speed increases, the magnetic induction ahead of the arc over the entire speed range remains constant. In this case the electromagnetic pressure on molten metal of the weld pool ahead of the arc does not change either.

Changes in directions of the current lines with an increase in the welding speed lead to a decrease in the current flow through the molten metal and induction of the welding circuit electromagnetic field behind the arc on the weld pool axis, which is caused by overheating of the molten metal. With an increase in the welding speed the downward electromagnetic pressure decreases in a squared dependence upon induction. This causes the molten metal to flow down from the weld pool. Decrease in the downward electromagnetic pressure leads to improvement in the back bead formation along the weld pool axis with an increase in the one-sided welding speed on a flux backing.

With an increase in the welding speed, due to a decrease in induction behind the arc the latter deviates backward towards a lower electromagnetic field, which leads to a decrease in the arc pressure. Here the speed of movement of molten metal into the tailing part of the pool grows, and the hydrodynamic pressure of molten metal decreases. Simultaneous decrease in the arc pressure, downward electromagnetic forces and hydrodynamic pressure of molten metal, increase in the rate of cooling and solidification and reduction of time during which the pool dwells in the liquid state lead to a substantial improvement in the back bead formation in one-sided welding on a flux backing. Increase in the welding speed due to an increase in the rate of cooling and solidification, refining of structure and decrease in size of the tempering zone also leads to an increase in impact toughness of welded joints.

To confirm the role of the welding current electromagnetic field in the formation of undercuts, investigations were conducted to study the effect of metal thickness on the welding circuit electromagnetic field. To study induction of the welding circuit electromagnetic field, according to the method developed, a direct current of 4800 A was passed through plates of different sizes. It was established that with a metal thickness increased from $4 \cdot 10^{-3}$ to $16 \cdot 10^{-3}$ m the electromagnetic field induction was maximum on the surface of the plates. It may grow from 0.035 to 0.150 T (Figure 4, *a*).

Increase in the electromagnetic field induction with growth of thickness is most probably a result of increase in the ferromagnetic mass, amount of magnetic moments and intensification of the field under the effect of a ferromagnetic.

Independently of the metal thickness, during the current flow the induction at the centre through thickness is equal to zero. It changes its direction to an opposite in transition from the upper to lower surface, according to a direction of the force lines of the field.

According to variations in induction with an increase in the metal thickness, the electromagnetic force grows from 50 to 216 N (Figure 4, *b*):

$$F_{em} = IBl, \tag{9}$$

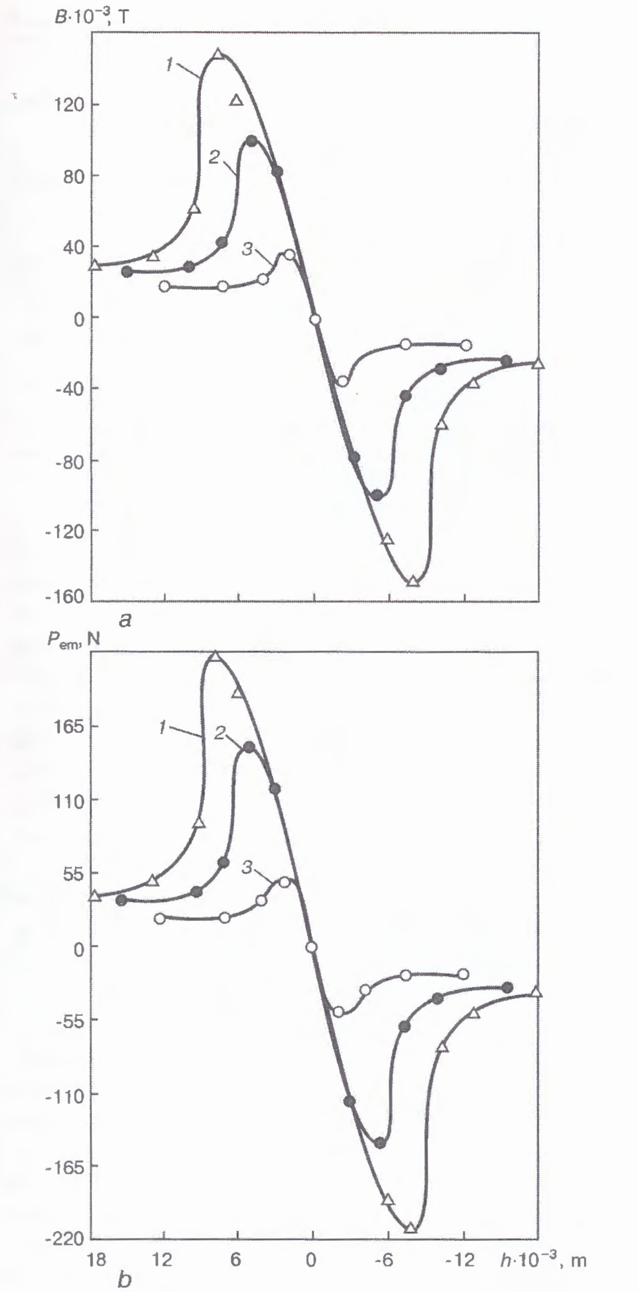

Figure 4. Dependence of induction B of the electromagnetic field (a) and electromagnetic force P_{em} (b) upon thickness h of the metal welded at I = 4800 A and welded joint gap of $2\cdot10^{-3}$ m: *1* — plate measuring $(16\times40\times300)\cdot10^{-3}$; *2* — $(10\times40\times300)\cdot10^{-3}$; *3* — $(4\times40\times300)\cdot10^{-3}$ m

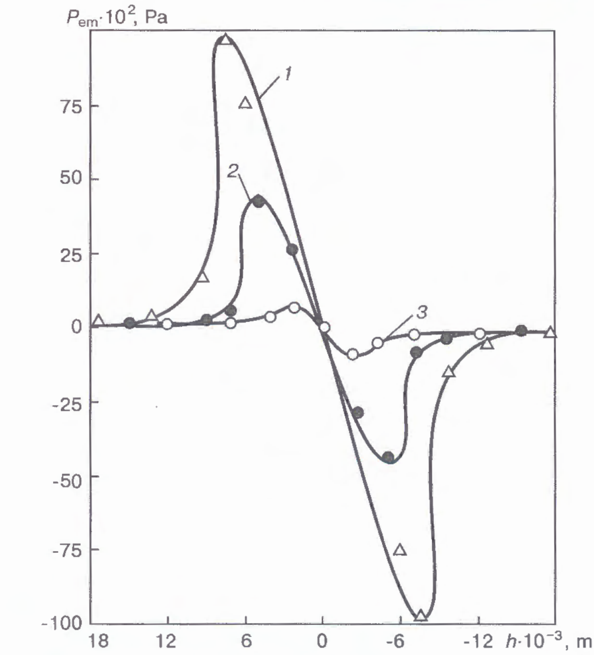

Figure 5. Dependence of electromagnetic pressure P_{em} upon thickness h of metal at I = 4800 A and width of the joint gap equal to $2\cdot10^{-3}$ m (*1–3* — see Figure 4)

where l is the length of the conductor with current I.

The downward electromagnetic field is maximum on the surface of the plates where undercuts are formed.

Induction is determined by the electromagnetic pressure acting on molten metal [11]:

$$P_{em} = \frac{B^2}{2\mu}. \quad (10)$$

With an increase in thickness of the metal welded, the electromagnetic pressure increases in a squared dependence upon the induction, i.e. from 0.49 to 9.00 kPa (Figure 5). Increase in the electromagnetic pressure on molten metal in a region of the pool side edges with an increase in the welding speed proved the effect of the electromagnetic field on the formation of undercuts.

Therefore, increase in the welding speed is accompanied by a decrease in heat input into the side edges of the pool, decrease in the electrical resistance in the fusion zone and increase in density of the current flowing through the pool edges, which causes a change in the welding current electromagnetic field.

This results in a decrease in induction of the welding current electromagnetic field behind the arc and increase in the electromagnetic induction in the fusion zone. The electromagnetic field and electromagnetic pressure on molten metal in the fusion zone increase. Under the effect of the electromagnetic pressure the molten metal flows down from the pool edges to form undercuts.

1. Paton, B.E., Mandelberg, S.L., Sidorenko, B.G. (1971) Some peculiarities of weld formation in welding at an increased speed. *Avtomatich. Svarka*, **8**, 1–6.
2. Rykalin, N.N. (1951) *Calculation of thermal processes in welding*. Moscow: Mashgiz.
3. Wealleans, J.W., Adams, P. (1969) Undercutting and weld bead turbulence in TIG-welding. *Welding & Metal Fabrication*, June, 225–257.
4. (1948) *Automatic sumberged-arc welding*. Ed. by E.O. Paton. Moscow-Kyiv: Mashgiz.
5. Savage, W.E., Lundin, C.D., Aronson, A.H. (1965) Weld metal solidification mechanics. *Welding J.*, **4**, 175–181.
6. Andoh, K., Nishikawa, J. (1968) Studies on and cathode energy of TIG arc. *IIW Doc. 212-158-67.*
7. Ishizaki, K., Karibe, Y. (1966) Theory of surface tension in arc welding. Penetrating power of the arc. *Yosetsu Gakkaishi*, **2**, 89–98.
8. Gulakov, S.V., Nosovsky, B.I. (1982) Influence of heat transfer by liquid metal flux on weld pool shape. *Svarochn. Proizvodstvo*, **10**, 2–3.
9. Erokhin, A.A., Bukarov, V.A., Ishchenko, Yu.S. (1972) Influence of tungsten electrode grinding angle on formation of undercuts and gas cavities during welding. *Ibid.*, **5**, 20–21.
10. Potekhin, V.P. (1986) Role of welding arc pressure in formation of undercuts. *Ibid.*, **6**, 12–13.
11. Abramovich, G.P. (1969) *Applied dynamics of gases*. Moscow: Nauka.

NON-CONSUMABLE ELECTRODE ARGON-ARC WELDING OF ALUMINIUM ALLOYS WITH ARC OSCILLATIONS

A.G. POKLYATSKY, A.Ya. ISHCHENKO, A.A. GRINUYK, A.A. CHAJKA and **V.E. FEDORCHUK**
The E.O. Paton Electric Welding Institute, NASU, Kyiv, Ukraine

The effect of arc oscillations occurring as a result of alternating current passing through the region of filler on the shape of penetration, hardness, structure and mechanical properties of welds in argon-arc non-consumable electrode welding aluminium alloys 1201, AMg6, 1420 and 1460 has been investigated. It is shown that the sizes of penetration of welds depend on values of current passing through the arc gap and the filler wire region, and the frequency of changing their polarities. It was established that at similar depth of penetration the width of welds and degree of weakening of welded joints produced by welding with arc oscillations are less than those in welding with a stationary arc. Intensive stirring of the molten metal and change in conditions of its solidification promote the formation of fine equiaxial dendrites, thus increasing the hardness of weld metal and its strength.

Key words: *argon-arc welding, non-consumable electrode, arc oscillation, aluminium alloys, mechanical properties, hardness, structure*

In welding advanced high-strength aluminium alloys with a non-consumable electrode the processes, causing intensive oscillations of the weld pool molten metal, find the more and more wide application. Here, the effective stirring of the parent metal with filler metal and refining of oxide inclusions in the pool bottom part are observed, the processes of gas evolution are activated and the conditions of metal solidification are changed leading to the formation of fine-crystalline structure of the weld metal. Oscillations of the molten metal in welding can occur owing to the intermittent feeding of the filler wire (filler), mechanical oscillations of the electrode, superposition of short-time pulses on the main welding current, application of a modulated current and action of auxiliary magnetic fields.

During mechanical oscillation of the non-consumable electrode the melt movement occurs as a result of changing a normal component of arc pressure, inversely proportional to the angle of the electrode deviation from vertical [1]. The intermittent feeding of filler wire leads to «shaking» of the weld pool by changing the volume of metal entered [2]. Using the superposition of short-time current pulses the oscillations in the molten metal occur due to an abrupt increase in arc pressure during the time of their passing [3], while in use of a modulated or asymmetric current they occur at the expense of difference of force action of arc on metal at the moments of pulse and pause or at straight and reverse polarity [4, 5]. The arc deviation from its vertical position, and, consequently, also oscillations of weld pool metal are created due to interaction of a volume electromagnetic force with an external magnetic field [6–8]. The variable magnetic field causes the periodic deviations of the arc column, whose amplitude and rate depend on the magnetic field intensity and frequency of changing its poles.

To realize the mechanical oscillations of the electrode and intermittent feeding of filler the use of the auxiliary equipment is required. The pulsed-arc welding is performed from special power sources allowing superposition of auxiliary pulses on the welding current or change in amplitude and duration of currents at straight and reverse polarity. Existing methods of electromagnetic action on arc include the use of solenoids on the torch, thus complicating its design and making the arc observation difficult.

The more simple method is the effect of electromagnetic field occurring as a result of passing alternating current through the filler wire region on the welding arc. The process of welding with a current passing through the filler was used by many researchers for the solution of different problems. In one cases it was used for improving efficiency of the process of welding or surfacing [9, 10], in another — for redistribution of temperature gradient in melt to change the structure of weld metal and to decrease its weakening [11, 12]. However, here the direct current was passed through the arc gap and filler wire, therefore, the changes of direction and values of induction of magnetic fields were not observed and arc deviations were not occurred. The use of alternating current led to arc deviation by changing magnetic field. This caused the dissipation of heat power and loss of arc penetrability and, as a consequence, the reduction in the process efficiency. In addition, to preheat the filler (especially from aluminium and its alloys) it is necessary to supply high current through it. As a result the arc is deviated at a considerable distance, filler wire is burnt before its contact with a workpiece and formation of arc discharge between them is occurred. As the welding of aluminium alloys with a non-consumable electrode is performed at alternating current, then even the direct current passing

Table 1. Conditions of welding butt joints

Alloy	Sheet thickness, mm	Filler grade	Welding current, A	Welding speed, m/h	Wire feed speed, m/h
AMg6 (Al–Mg–Mn)	4	Sv-AMg63 (Al–6.3Mg)	214	12	75
1420 (Al–Mg–Li)	4	Same	198	12	75
1460 (Al–Cu–Li)	3	Sv-1201 (Al–Cu)	200	14	82

Note. Diameter of filler was 1.6 mm; frequency of welding current – 250 Hz; I_f = 215 A.

through the filler region will lead to changing the magnetic induction causing the arc deviation from the vertical axis. Therefore, to stabilize the arc position, the currents passing through the arc gap and filler wire were synchronized [13].

The aim of investigations was to study the effect of arc oscillations, caused by passing the alternating current through the filler, on the parameters of penetration, structure, weakening and mechanical proper-

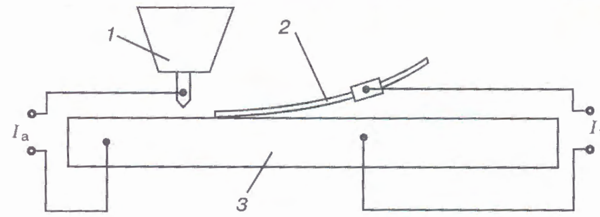

Figure 1. Scheme of non-consumable electrode argon-arc welding with a current passing through filler: *1* — welding torch; *2* — filler wire; *3* — workpiece; I_a, I_f — current passing through arc gap and filler, respectively

ties of high-strength aluminium alloy welded joints made in welding with a non-consumable electrode.

Procedure of investigations. Automatic surfacing of beads on δ = 6 mm thick sheets of alloy 1201 (Al–Cu) and single-pass welding of 4 mm thick sheets of alloys AMg6 and 1420 and also 3 mm thick sheets of alloy 1460 with a non-consumable electrode at alternating current in argon was made using welding head ASTV-2M. MW-450 (Fronius Company, Austria) was used as a welding arc power source, with the help of which the current frequency was changed within the ranges 50–250 Hz. To create the electromagnetic field around the filler wire, the alternating sinusoidal current of 50 Hz frequency was passed through its region using the transformer TDM-315

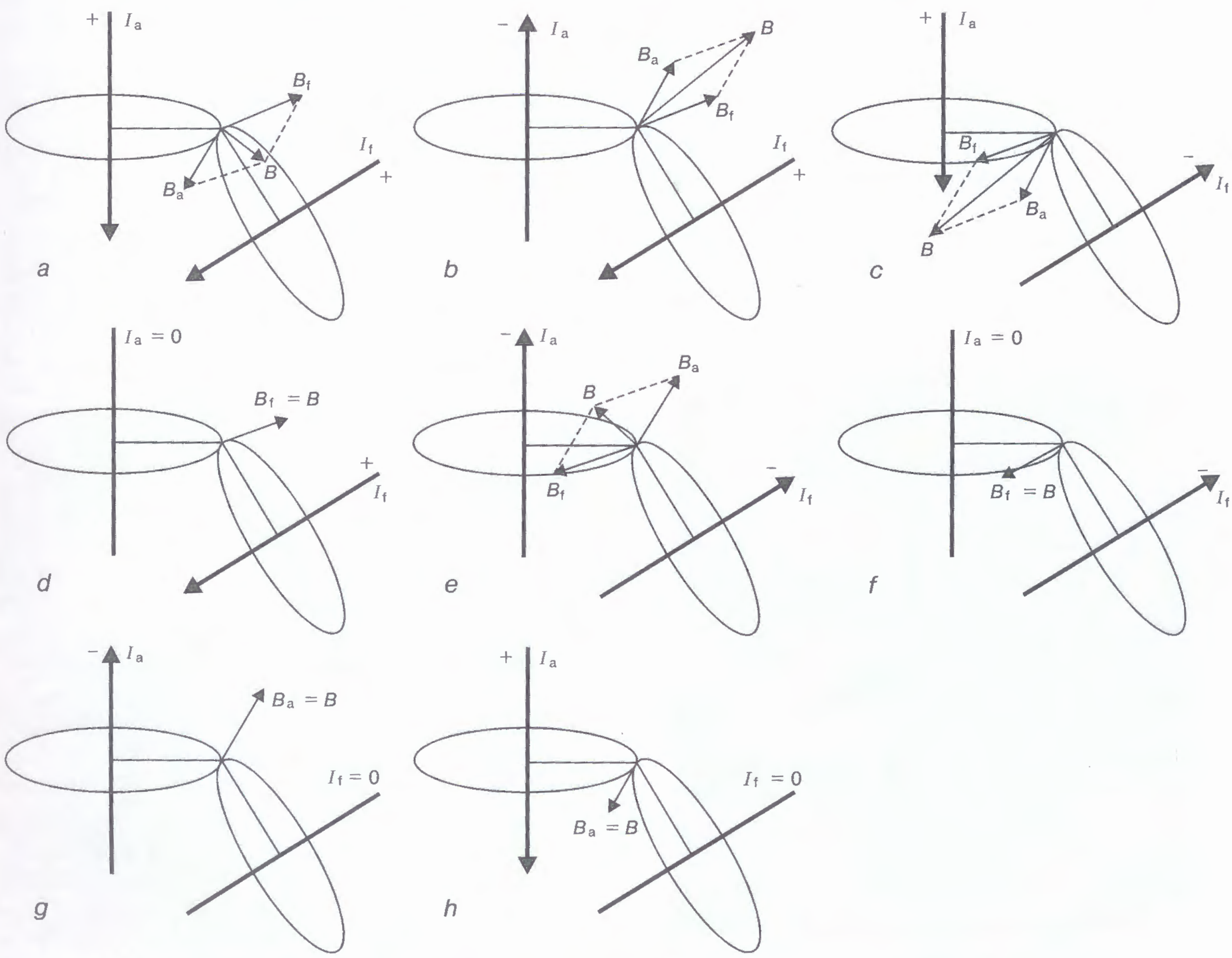

Figure 2. Scheme of changing direction of magnetic induction of resultant electromagnetic field occurring in passing currents through arc gap and filler: B_a and B_f — magnetic induction occurring as a result of I_a and I_f passing, respectively (*a*–*h* — see explanation in text)

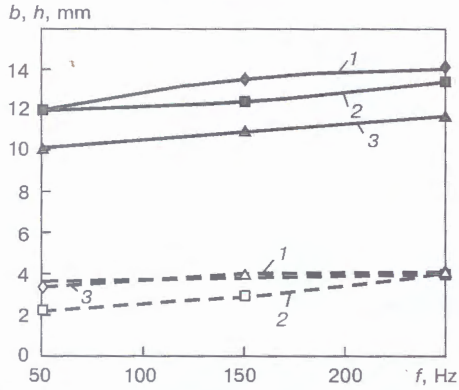

Figure 3. Dependence of width b (solid curves) and depth h (dash lines) of welds on frequency f of welding current at different values I_f: *1* — 0; *2* — 60; *3* — 210 A

and ballast rheostat RB-300 (Figure 1). This current was measured using transformer UTT-5.

Sheets, being welded and surfaced, and filler wires Sv-1201 and Sv-AMg63 of 1.6 mm diameter were etched using a standard technology, and their surfaces were cleaned mechanically for 0.1 mm depth. The welding conditions are given in Table 1.

Electromagnetic fields, occurring around the arc and filler wire, change the direction of lines of magnetic induction in accordance with a polarity of currents passing through them (Figure 2). As the currents into the arc gap and filler are supplied with a random shear of phases, then the resultant magnetic field changes constantly the direction and value of the magnetic induction B. The magnetic induction, passing through the conductors with current of similar (Figure 2, *a, e*) and variable (Figure 2, *b, c*) polarity, will be determined by the action of two fields, and in case of current absence in one of their conductors (in transition of current through zero) — by action of only one field (Figure 2, *d, f–h*). Depending on the polarity and amplitude of currents passing through

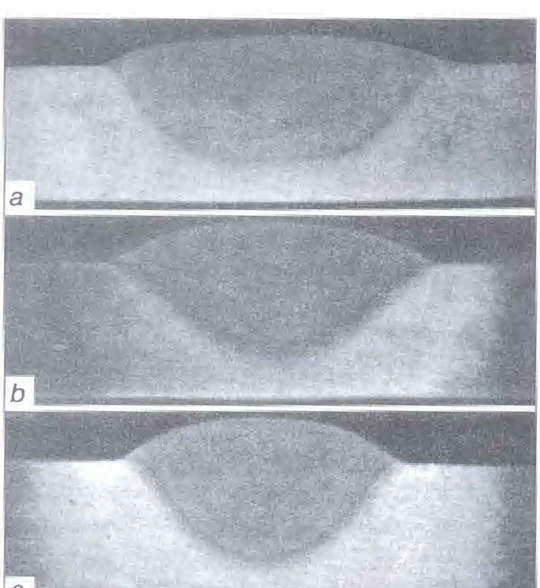

Figure 4. Macrosections of deposits on 6 mm thick plate of alloy 1201, made using non-consumable electrode with a filler wire Sv-1201 at 270 A current of 250 Hz frequency and variable value I_f (50 Hz frequency): *a* — 0; *b* — 60; *c* — 210 A

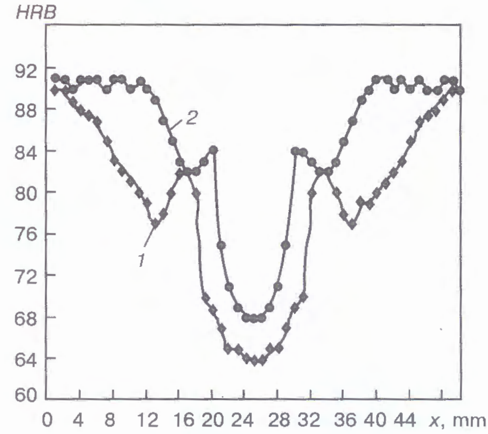

Figure 5. Change in hardness of alloy 1201 6 mm thick sheet welded joints produced using non-consumable electrode with filler wire Sv-1201 by conventional stationary arc and with oscillations caused by the passing alternating current through the filler: *1* — $I_f = 0$; *2* — $I_f = 210$ A

the arc gap and filler, the resultant magnetic induction B will change its value and direction causing the arc deviation relative to the vertical axis. Thus, the oscillations of the weld pool molten metal are occurred by changing the forced arc action due to constant changing of its position relative to the electrode that is stipulated by the action of variables of electromagnetic fields created by the welding arc and current-conducting filler region.

The beads on the sheets of alloy 1201 were deposited at 270 A current at 12 m/h rate of the torch displacement using filler wire Sv-1201. Its diameter was 1.6 mm, feed speed — 87 m/h. Alternating current of 50 Hz frequency was passed through the filler. Alternating current of 50, 150 and 250 Hz frequency was used for the welding arc supply. The amplitude of arc oscillations was changed depending on the value of current and frequency of changing the direction of magnetic induction. In case of 50 Hz frequency of welding current the stable formation of welds was provided if the value of current passing the filler was not more than 100 A. The increase in current increased the amplitude of arc deviations beyond the limits of point of filler wire contact the workpiece. Moreover, its fusion beyond the zone of shielding with an inert gas and formation of arc discharge between them were occurred. The use of welding current of 250 Hz frequency made it possible to increase the value of current passing through the filler to 300 A not disturbing the welding process stability. This is explained by the fact that at high frequency of changing the direction of the magnetic induction the arc has no time to reach its limiting deviations even at higher values of current passing through the filler.

Parameters of penetration of welds produced in surfacing with passing of alternating current through the filler were determined on transverse macrosections. Metal structure of the welded joints was examined on microsections. The mechanical tests were performed on standard flat samples. The effect of arc deviations under the action of electromagnetic field

Table 2. Mechanical properties of high-strength aluminium alloy welded joints produced in non-consumable electrode argon-arc welding

Alloy	*Filler grade*	*Conventional welding*				*Welding with weld pool oscillations*			
		σ_t^{w}, *MPa*	$\sigma_t^{w.m}$, *MPa*	$\alpha_n^{w.m}$, *J/cm*^{2}	α, *deg*	σ_t^{w}, *MPa*	$\sigma_t^{w.m}$, *MPa*	$\alpha_n^{w.m}$, *J/cm*^{2}	α, *deg*
AMg6	Sv-AMg63	$\frac{329.3–333.9}{331.2}$	$\frac{325.7–329.2}{326.9}$	$\frac{16.5–18.9}{17.6}$	$\frac{64–80}{78}$	$\frac{346.7–349.4}{348.3}$	$\frac{331.1–344.6}{334.8}$	$\frac{25.3–26.4}{26.0}$	$\frac{176–180}{177}$
1420	Same	$\frac{322.1–330.9}{326.5}$	$\frac{318.6–323.7}{321.5}$	$\frac{25.8–26.8}{26.2}$	$\frac{90–92}{91}$	$\frac{325.9–335.2}{330.5}$	$\frac{340.8–345.6}{342.8}$	$\frac{11.7–13.0}{12.5}$	$\frac{75–77}{76}$
1460	Sv-1201	$\frac{306.0–313.9}{309.8}$	$\frac{243.7–258.6}{251.2}$	$\frac{18.0–18.5}{18.3}$	$\frac{157–172}{161}$	$\frac{303.2–313.7}{308.9}$	$\frac{268.8–281.9}{274.6}$	$\frac{15.6–15.9}{15.8}$	$\frac{102–104}{103}$

Notes. 1. In numerator the minimum and maximum values of characteristics are given, while in denominator — their mean values obtained from results of testing 3–5 samples. 2. σ_t^{w}, $\sigma_t^{w.m}$ — ultimate strength of welded joint and weld metal, respectively.

on weakening of welded joints were examined on transverse sections using the standard procedure.

Results of investigations. The passing of alternating current through the filler in non-consumable electrode welding leads to a continuous change of arc position and oscillations of the weld pool molten metal. Parameters of penetration of welds in this case depend on the amplitude and frequency of arc displacements which are defined by the current passing through the arc gap and filler region, and on the frequency of changing its polarity. With increase in welding current frequency from 50 to 250 Hz the frequency of arc oscillations are also increased and their amplitude is decreased as the arc changes the direction of deviation, not reaching the extreme position. As a result, with a rise in welding current frequency the depth of penetration is increased (Figure 3). It should be noted that at small values of current passing through the filler, the depth is smaller than in welding with a stationary arc. With increase in I_f the loss in power caused by the arc deviations is compensated by preheating at the expense of I_f passing through it, thus leading to the increase in the weld penetration depth. In addition, the increase in the temperature of filler entered the weld pool leads to a significant decrease in weld width (Figure 4). Therefore, at a similar depth of penetration the degree of weld metal weakening in the HAZ is lower than in case of welding with arc oscillations caused by current passing through the filler (Figure 5).

The application of the non-consumable electrode argon-arc welding with weld pool oscillations, caused by the current passing through the filler, makes it possible to increase the mechanical properties of welded joints of alloy AMg6. The strength of weld metal produced using the filler wire Sv-AMg63 was increased by 2 %, and welded joints — by 5 %, impact strength of weld metal — by 47 %, and bending angle — by 127 % as compared with a conventional welding using a stationary arc (Table 2).

In welding with weld pool oscillations the strength of welded joints of alloy 1420 was not almost changed, and the weld metal strength increased by 6 % and reached the level which is provided after artificial

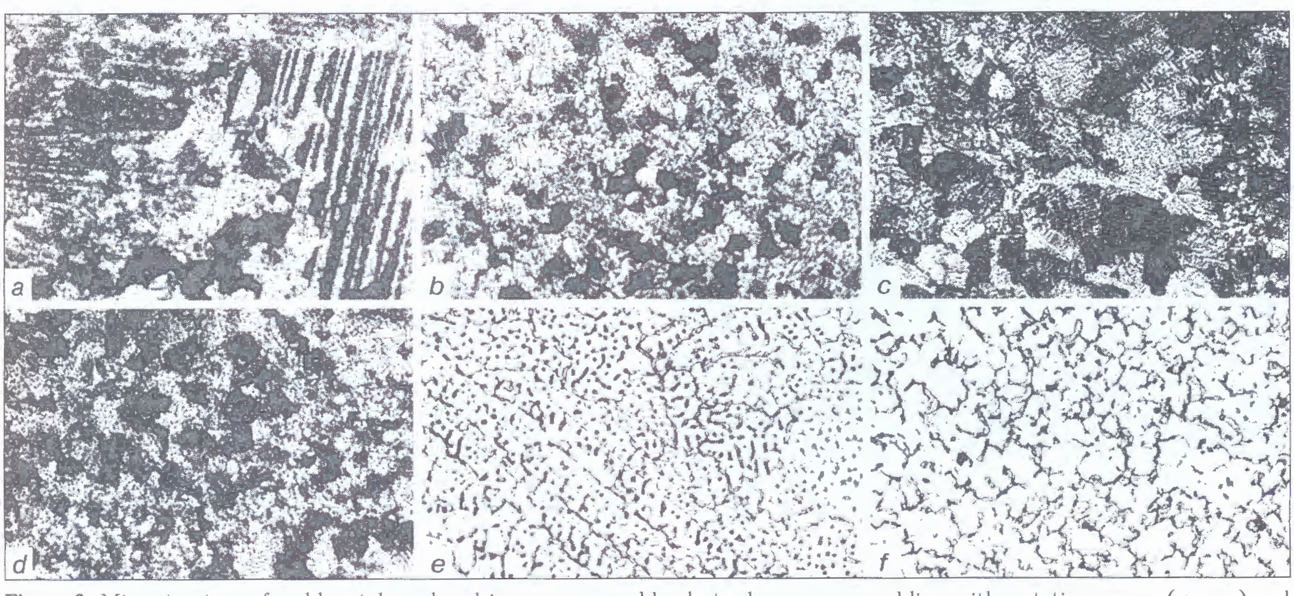

Figure 6. Microstructure of weld metal produced in non-consumable electrode argon-arc welding with a stationary arc (*a, c, e*) and with oscillations (*b, d, f*) caused by passing of alternating current I_f = 210 A 50 Hz frequency through the filler: *a, b* — alloy AMg6 + Sv-AMg63 (×100); *c, d* — alloy 1420 + Sv-AMg63 (×100); *e, f* — alloy 1460 + Sv-1201 (×1000)

ageing of welds. In this case the impact strength of weld metal decreased by 52 % , and bending angle — by 16 %.

The weld pool oscillations provide the increase in strength of weld metal of alloy 1460 by 9 % as compared with welding using a conventional stationary arc. Here, the tensile strength of welded joints is not changed and the impact strength of welds and bending angle are decreased by 14 and 36 %, respectively.

A dendritic structure with a central crystal is formed in structure of weld metal produced in non-consumable electrode stationary arc welding of alloys AMg6 and 1201 (Figure 6, *a*). In welding of sheets of Al–Li alloys 1420 and 1460 a finer dendritic structure with separate elements of the central crystallite, which manifest themselves in the formation of separate coarse crystals in weld midlle, is formed (Figure 6, *e*).

The arc oscillations in welding these alloys lead to the weld metal structure refining, disappearance of a central crystallite and formation of fine equiaxial dendrites across the entire section.

Figure 6, *b, d, f* presents a microstructure of welds produced in welding with arc oscillations. The fine equiaxial dendrites are formed instead of directed coarse dendrites in alloy AMg6, coarse equiaxial dendrites in alloy 1420 and mixed structure of equiaxial and directed dendrites in alloy 1460.

CONCLUSION

The passing of alternating current through the filler in non-consumable electrode argon-arc welding of aluminium alloys causes periodic deviations of arc from vertical axis that promotes oscillations of molten metal of weld pool. Amplitude values and frequency of arc oscillations depend on currents passing through the arc gap and filler wire region, and also on the frequency of changing their polarity.

Arc deviations cause the dissipation of heat power and loss in penetrability of the arc, but at the conditions, providing the similar depth of penetration, the width of welds is by 30 % smaller than that in case of welding using a conventional stationary arc.

The oscillations of the molten metal of weld pool lead to changing in conditions of its solidification and promote the formation of fine equiaxial dendrites. Moreover, the hardness of weld metal and its strength characteristics are increased.

1. Slavin, G.A. (1980) Formation of desoriented structure of weld metal in superposition of low-frequency perturbations on welding pool. *Svarochn. Proizvodstvo*, **6**, 3–5.
2. Zubrienko, G.L., Galkin, N.P., Gaponov, D.A. et al. (1972) Argon-arc welding of aluminium alloys with intermittent feed of filler wire. *Ibid.*, **4**, 46–47.
3. Slavin, G.A., Trokhinskaya, N.M., Ryazantsev, V.I. et al. (1986) Optimization of welding conditions of manual and automatic welding of thin sheet aluminium alloys in superposition of short period current pulses on arc. *Ibid.*, **1**, 14–15.
4. Ishchenko, A.Ya., Poklyatsky, A.G., Lozovskaya, A.V., et al. (1990) Influence of low-frequency modulation parameters of variable polarity current of rectangular shape on weld structure in welding of aluminium alloys. *Avtomatich. Svarka*, **9**, 23–27.
5. Maruo, H., Hirata, Y., Makino, H. (1989) Rectangular wave AC TIG arc welding of aluminium alloy. *Quart. J. of JWS*, **1**, 63–69.
6. Chernysh, V.P. (1964) Use of magnetic fields in arc welding. In: *Problems of mechanics and mechanical engineering*. Kyiv: KGU.
7. Bachelis, I.A. (1965) Magnetic control of welding arc. *Svarochn. Proizvodstvo*, **1**, 17–19.
8. Brodyagina, I.V. (1998) Arc welding of aluminium alloys with application of magnetic fields. *Ibid.*, **9**, 48–51.
9. (1973) WIG + Heiβdraht = MIG-Geschwindigkeit. *Betriebs Manag. Service*, **11**, 36.
10. Stol, I. (1989) Development of an advanced gas metal arc welding process. *Welding J.*, **8**, 313–326.
11. (1972) Le fil chaud donne une nouvelle dimension au soudage a l'arc. *Souder*, **104**, 7, 9–15, 57–59.
12. Lorenz, C., Nentwing, A.W.E. (2000) WIG-Heiβdrahtschweiβen von Aluminiumwerkstoffen. *Schweiβen und Schneiden*, **4**, 244–246.
13. Katsuyoshi, H., Yasuhio, B., Toshiaki, T. et al. *AC TIG welding apparatus using hot wire*. Pat. 4904843 USA, Int. Cl. B 23 K 9/10. Publ. 27.02.90.

RESULTS OF EXPERIMENTS ON MANUAL EBW IN A MANNED SPACE SIMULATION TEST CHAMBER

E.S. MIKHAJLOVSKAYA, V.F. SHULYM and A.A. ZAGREBELNY
The E.O. Paton Electric Welding Institute, NASU, Kyiv, Ukraine

The paper presents the results of investigation of samples of aluminium alloy welded joints, made during operator training in the manned spase simulation test chamber using «Universal» hardware for manual electron beam welding.

Key words: *manual electron beam welding, manned spase simulation test chamber, «Universal» hardware, aluminium alloys, mechanical testing, macrostructure, porosity, strength properties*

Experience of operation of long-term space vehicles, for instance, «Mir» orbital complex (OC), revealed the possibility of various often unexpected situations arising, that require the use of specific technological processes, which include welding and allied technologies (cutting, brazing, etc.).

After conducting the first in the world experiment on welding in space, the efforts of the researchers of the E.O. Paton Electric Welding Institute were focused on development of electron beam welding (EBW) as the most promising process for use under the conditions of space and, in particular, development of the hardware and technology for manual EBW. The first manual electron beam gun was developed and tested in 1974 [1], followed by development of a versatile hand tool (VHT) for manual EBW, cutting, brazing and coating deposition, tested in open space in 1984 and 1986 [2]. Analysis of the obtained samples of the joints and coatings is given in [3–5]. Experimental results demonstrated the possibility of the cosmonauts performing welding operations in open space, but insufficient output power (up to 350 W) and accelerating voltage (5 kW) of VHT did not allow welding aluminium alloys, used in space vehicle structures. In the next modification of the hardware for manual EBW – the «Universal» – the above parameters were raised as much as possible: up to 750 W and 10 kV, respectively, by agreement with the customer.

In 1989–1990, in addition to thermal and dynamic testing of «Universal» hardware, also testing in the manned space simulation test chamber was performed to check the correctness of the used design solutions, providing the ability to perform the main manual welding operations. In this case attention was focused on evaluation of the techniques of handling the electron beam hand tools, organization of the workplace of an operator, wearing a spacesuit, as well as spacesuit protection. As regards technological issues, just the fundamental possibility of welding aluminium alloys and conducting manual EBW with filler wire feed was evaluated, whereas all the technological retrofitting was intended to be further on combined with welder-operator training sessions. The range of materials to be used during the flight experiment was to be determined more precisely. Therefore, samples welded during testing, were not comprehensively studied, just their visual examination was performed.

During preparation for the International Space Welding Experiment (ISWE), an attempt was made to use flexible sleeves with gloves and a fragment of the pressure helmet, specially developed by ILC Dover, Inc., for preliminary retrofitting of manual welding operations, performed with «Universal» electron beam tools. They are shown in Figure 1. Testing demonstrated that a significant pressure gradient ($6.67 \cdot 10^{-3}$ Pa in the vacuum chamber) often resulted in a violation of the glove integrity. Moreover, their use could not allow a comprehensive assessment of the actions of an operator, wearing a spacesuit. Therefore, testing had to be restricted to performance by several operators (both Ukrainian and US) of welding of individual sections of a cell* of aluminum alloy 2219. The operators, not having sufficient skills of

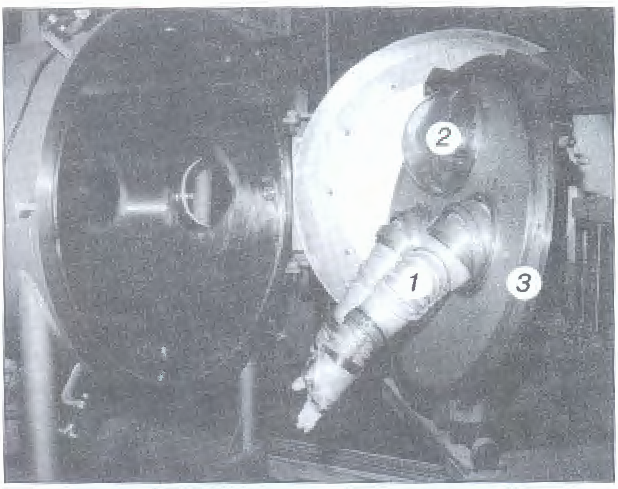

Figure 1. Flexible sleeves with gloves (*1*) and fragment of a pressure helmet (*2*), mounted on the vacuum chamber flange (*3*)

* Bodies of the modules of the ISS are honeycomb structures of alloy 2219 with cell sizes of 375×375×20 mm in the US modules and of alloys AMg6 (150×150×10 mm) in the Russian modules

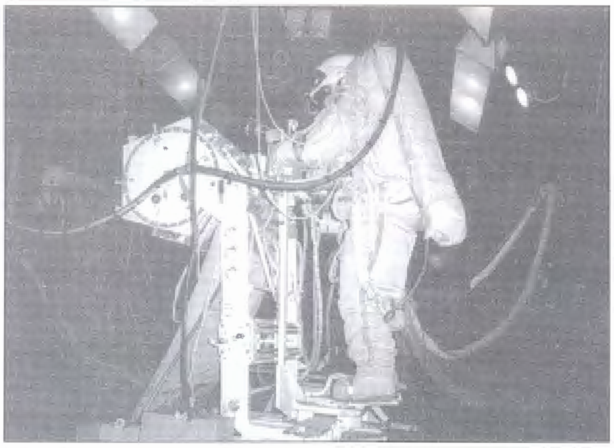

Figure 2. Work place of welder-operator in the space simulation test chamber

manual welding operation performance, noted the simplicity of the process and possibility of acquiring such skills.

Training sessions. Training of the primary and backup Russian crews to perform welding operations, using «Universal» system of electron beam hand tools, was carried out for preparation for the integrated «Flagman» experiment on board «Mir» OC. Training was conducted* in a vacuum chamber of 50 m^3 of TBK-50 facility in Joint Stock Company «Zvezda» (city of Tomilino, Moscow district, Russia), designed for retrofitting various cosmonaut extra-vehicular activity operations and fitted with «Orlan» spacesuit with a system for life support and body parameter monitoring during testing. The chamber is a horizontally located cylinder of 3.5 m diameter and ≈ 5.0 m length. Pumping system, using liquid-nitrogen filled freezing-out screen, maintained a pressure of $1.07\cdot10^{-1}$ Pa in the space simulation test chamber. Pressure was not measured directly in the zone, where welding operations were performed, but it was assumed to be somewhat higher there, because of gas evolution and in-leakage from the spacesuit.

An all-purpose multifunctional platform «Flagman», mounted in the flight experiment configuration, was used to provide the «support» conditions and relative comfort during the operator's activity. It allows the operator to move on a mobile platform along the base guide rail (and the drum with samples, accordingly) for up to 2 m distance (Figure 2). Results of the first altitude simulation were used for retrofitting the tool weight-neutralising system (its mounting on an independent carriage), and an additional lamp was installed. This greatly facilitated the operator's task during subsequent training sessions, although imperfection of weight-neutralising devices and poor lighting could not be eliminated completely, this, naturally, affecting the welded joints quality.

During training samples of the same US materials were used, that were intended to be processed in the flight experiment and had already been delivered to

Table 1. List of US materials, used during performance of processing experiments

Material	*Grade*	*Local analog*	*Sample thickness, mm*
Stainless steel	304SS	12Kh18N9T	1.6; 1.0
(C — 0.12; Cr — 17.0–19.0; Ni — 8.0–10.0 wt.%)			
Titanium alloy	Ti–6Al–4V	VT6	1.6; 1.0
Aluminium alloy	2219Al	1201	1.6; 1.0
(Cu — 5.8–6.8; Mn — 0.2–0.4; Fe — 0.3 wt.%)			
Aluminuim alloy *(Al–5Mg)*	5456Al	AMg5 type	1.6; 1.0
Filler wire *(Al–5Mg)*	5356Al	Same	1.0
Braze alloy *(Ag — 72.0; Cu — 28.0 wt.%)*	Lithobraze720	PSr-72	1.0

«Mir» OC. Their range is given in Table 1. Samples of the above materials were placed on replaceable cassettes, mounted on the faces of an all-purpose experimental drumlike sample holder of the work station, thus ensuring their convenient replacement, as well as welding operations performance.

In the course of training the operators made butt and overlap joints of all the materials, performed their cutting, as well as welding of covers to cells of bodies of the International Space Station (ISS) US and Russian modules (simulation of repair operations in the case of a hole made in the body). Samples of aluminium alloy 5456 were processed by a tool with filler wire feed. In addition holes in titanium tubes were welded up and stainless steel tubes were brazed. 98 samples of welded and brazed joints were made, of which 21 samples were made available to the US party for studying, and 27 samples were selected for conducting research at the PWI by a program, co-ordinated by the Russian and US parties.

Investigation results. Visual inspection of the selected samples of welded and brazed joints was followed by X-ray inspection, the results of which were used to prepare samples of butt and overlap joints to conduct mechanical tests. In addition, fracture surface was studied and metallographic examination and local X-ray microprobe analysis were performed.

Results of X-ray flaw detection, conducted in RAP-150/300 X-ray unit, revealed that welded joints of aluminium alloys, unlike those of stainless steel and titanium, are characterised by the presence of a great number of inner defects in the form of individual pores and cavities, as well as their clusters. Maximal size of individual pores was up to 2 mm. This is attributable to insufficient preparation of aluminium alloy samples for welding, as organisation of operations in the space simulation test chamber did not

* Training of the Russian crews of «Mir» OC, including G. Padalko, S. Avdeev, S. Zaletin and A. Kaleri, was conducted in April–May, 1998.

Table 2. Results of mechanical testing of butt joint samples

Sample No.	*Material*	*Ultimate tensile strength, σ_t, MPa*
1	304SS	640.0
2	Ti–6Al–4V	1011.4
3	2219	267.5
4	2219	232.3
5	2219	294.0
6	2219	260.0
7	5456	247.0
8	5456	326.0

Note. Samples No.1 and 2 failed in the HAZ, the others — in the weld.

permit their mechanical cleaning (scraping) to be performed directly before welding, as well as a not quite favourable vacuum level in the zone of welding operations performance. In all probability, however, this was not the main cause, for, as follows from [6], higher porosity of weld metal was also observed in welding similar samples, using «Universal» hardware in the automatic mode, with their preliminary scraping and in the vacuum of $6.67 \cdot 10^{-3}$ Pa.

Based on flaw detection results it was possible to cut out just 8 samples of butt joints with minimal number of inner defects for conducting mechanical testing. Such a number of samples were insufficient for statistical evaluation, so we can only speak of the general level of mechanical properties of the produced joints. Results of tensile mechanical testing, conducted in R-50 tensile testing machine, are presented in Table 2.

Results of testing welded joints of stainless steel 304SS and titanium alloy Ti–6Al–4V confirmed the data, obtained earlier in welding local materials 12Kh18N9T and VT1, using VHT [3, 4]. A practically complete absence of inner defects and high strength of weld metal, close to that of the base metal for stainless steel, or even exceeding it for titanium alloy, are indicative of the applicability of the «Universal» electron beam hand tools for performance of the operations of repair welding of items from these materials up to 2 mm thick.

Unfortunately, investigation results do not permit stating the same with respect to aluminium alloys. Given below are some results of analysis of samples of welded joints on these materials, that to a certain extent confirm the above-said. As can be seen from Table 2, the level of strength properties of welded joints on both the aluminium alloys is low, strength lowering being less characteristic for samples of alloy 5456. Studying the fractography of sample fracture surface after performance of mechanical testing and simultaneous determination of the elemental composition were performed using scanning electron microscope JSM-840, JEOL, with an X-ray energy spectrum analyser. Microstructure of the fracture surface

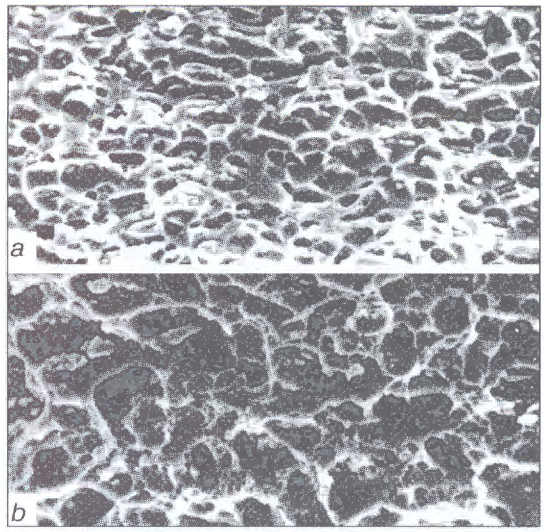

Figure 3. Microstructure of metal on the fracture surface of a welded butt joint on aluminium alloy 2219 (*a*) and base metal (*b*) after rupture testing (×800)

metal in welded joints of alloy 2219 is that of a non-uniform tough fracture with a great number of pores and other inclusions, enriched in copper. As is seen from Figure 3, *a*, microstructure of the metal of the surface of rupture, running through the weld of a butt joint (sample No.3) is more finely dispersed, than that of the base metal (Figure 3, *b*). Microstructure of the surface of rupture, running through the weld in joints of aluminium alloy 5456 is of a tough fracture type with a structure coarser, than that of the base metal. Coarse pores and numerous inclusions, enriched in iron, are found in the fracture zone.

A great number of pores and other inner defects in welded joints of aluminium alloys is largely accounted for by the results of their microstructural examinations in Neophot-2 optical microscope. Quantitative analysis of the secondary phases was performed using Omnimet image analyser, and the detectable phase composition and element distribution were determined in the scanning electron microscope JSM-840 in SEI mode, using a standard Link ZAF4/FLS program.

Microstructures of various zones of welded joints on aluminium alloy 2219 (Figures 4 and 5) demonstrate that the detected phases of the weld metal and HAZ have different dispersity. Considering the nature of distribution of copper, iron and manganese in the HAZ along the scanning line (Figure 5), it can be assumed that in addition to a homogeneous structure of Al-based α-solid solution also a number of chemical

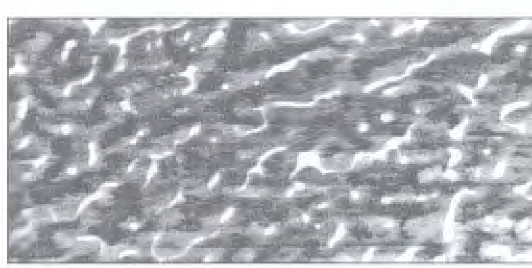

Figure 4. Microstructure of the metal of welded joint on aluminuim alloy 2219 of the large cell (SEI mode) (×900)

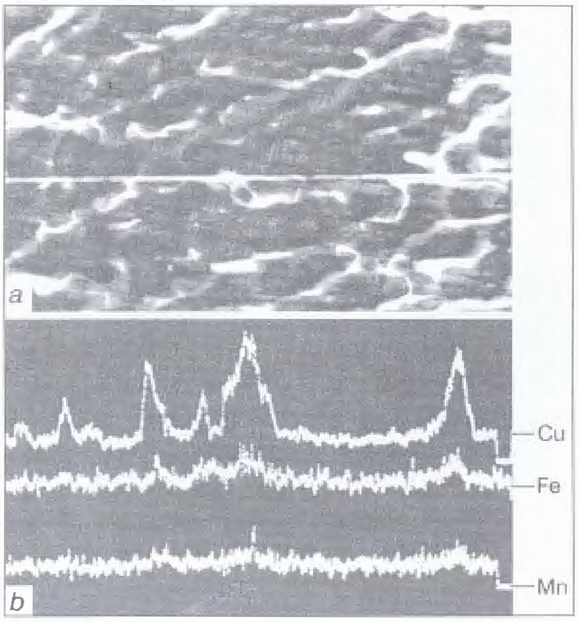

Figure 5. Microstructure of HAZ metal of welded joint on aluminium alloy 2219 of the large cell (SEI mode) (*a*) and copper, iron and manganese distribution along the scanning line (*b*) (×900)

compounds of $(FeMn)Al_6$ type form during welding. Examination of the microstructure of various zones of welded joints on aluminium alloy 5456 revealed a somewhat greater amount of inclusions in the HAZ, than in the weld metal. Proceeding from the nature of iron and manganese distribution in the HAS metal along the scanning line (Figure 6), it can be assumed, that complex compounds (for instance, AlFeSiMn), practically insoluble in aluminium, form during welding. They are the cause for considerable porosity along the fusion line.

Microstructural features of welded joints of aluminium alloys 2219 and 5456 indicate that weld metal develops a cellular-dendritic structure near the fusion line, and an equiaxed structure in its central part. The range of averaged values of welding speed was 10–19 m/h, when making butt joints, and 6–10 m/h in welding overlap joints and cells. However, even at such low welding speeds complete penetration was not achieved to produce sound joints. Individual sections of welded butt joints are an exception, as well as of welds in welding a cell of 5456 alloy at minimal welding speeds (10.3 and 6.3 m/h, respectively).

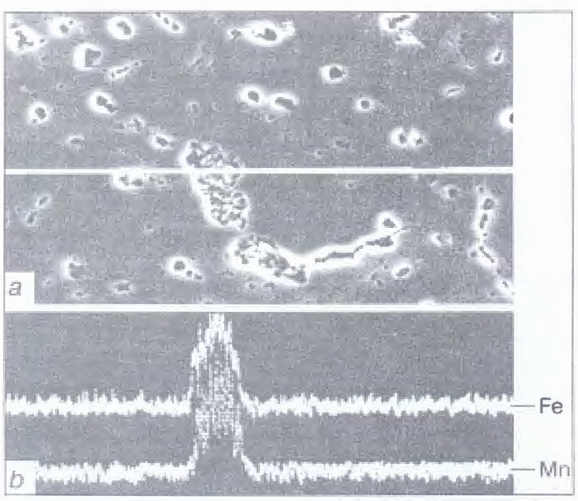

Figure 6. Microstructure of HAZ metal of welded joint on aluminium alloy 5456 of the small cell (SEI mode) (*a*) and iron and manganese distribution along the scanning line (*b*) (×850)

Capabilities of «Universal» hardware provided a certain (up to 20 %) increase of the electron beam power, but because of an insufficient number of training sessions (three altitude simulations for the principal crew member and two for the backup), the operators were not able to fully master control of the weld pool behaviour and the techniques of welding operations performance with the electron beam tools at maximal levels of their power. Considering the imperfection of weight-neutralizing devices, it is rather difficult for the welder-operator, wearing a spacesuit, to maintain a constant speed of the hand tool displacement that allows avoiding the welded material burn through. Therefore, the maximal level of electron beam power (750 W) was only used in the final altitude simulations, when welding the US module cell of 2219 alloy. Their scope should be significantly increased during similar training sessions in the future (not less than five altitude simulations for each operator).

It should be noted that the level of strength properties of welded joints of aluminium alloys, made with «Universal» hardware, is somewhat higher than the strength of welded joints of alloy 1201, welded during experiments on board the flying laboratory at short-term zero gravity (237–245 MPa) [7]. On the other hand, according to [8], EBW of aluminium alloys of 1201 type provides welded joint strength on the level of 320–330 MPa. The results of the performed experiments lead to the conclusion that a certain lowering of strength of aluminium alloy welded joints made at zero gravity, must be related to a significant increase of their porosity [9, 10]. Therefore, when welding these alloys in space, a whole range of problems will have to be solved, concerning hardware support and technology of welding aluminium alloys that minimises pore formation in welded joints.

This, primarily, is surface preparation of the items to be welded that should be carried out immediately before welding. Magneto-abrasive cleaning, proposed in [11], can be used as one of the possible variants. The electron beam gun should provide the appropriate parameters of the welding process, considering that use of sharper-focused beams and increase of their specific power and welding speed may lead to lower porosity. Electron beam oscillation by a certain preset law, increasing the intensity of stirring of the weld pool molten metal, as well as application of vibration technologies, can have a positive effect.

Thus, the results of the conducted training, using «Universal» hardware, and subsequent studies of the produced samples, pointed to the need to improve the strength properties of aluminium alloy welded joints. To a certain extent, this is achievable, using «Universal» hardware at maximal power levels and appropriate welding speeds, which requires additional trials in the space simulation test chamber. A significant improvement of the above characteristics will, probably, make it necessary to change the electron beam gun parameters and welding modes, in particular, increase the electron beam specific power, thus providing greater penetration depth and higher welding speed.

To enable performance of installation and repair work in ISS being under construction now, where the wall thickness is up to 3.2 mm, the electron beam power should be increased up to 1.5 to 2.0 kW. Performance of manual welding operations by a welder-operator, wearing a spacesuit, at electron beam power above 1.0 kW and high welding speeds seems problematic. Therefore, when developing the next generations of EBW hardware for space applications, it is expedient to envisage the possibility of its use both for manual and mechanised or automatic welding. Its parameters should be re-adjustable, respectively (as for instance is described in [12]). The above hardware can be used in the manual mode for performance of auxiliary repair or installation operations, and in the automatic mode in welding critical welds, when certain requirements are made of dynamic loads, vacuum-tightness, etc.

CONCLUSIONS

1. Welder-operator training, carried out in the manned space simulation test chamber, confirmed the principal possibility of conducting the process of manual EBW in space, as well as the possibility of quickly acquiring the necessary skills, compared to other welding processes. To provide the required level of operator training, the training sessions should include not less than five altitude simulations.

2. Results of investigation of samples of welded joints on stainless steel 304SS and titanium alloy Ti–6Al–4V, made during the training sessions, confirmed the possibility of producing welded joints with rather high properties, using «Universal» electron beam hand tools.

3. The results of the conducted training and investigations are indicative of the possibility of producing full penetration butt joints on aluminium alloys. Evaluation of the possibility of welding overlap joints and cells of the same materials, requires further trials, using «Universal» hardware at maximal power levels. The produced joints of aluminium alloys 2219 and 5456 are characterised by large amounts of inner defects and low strength properties.

4. To improve the quality of aluminium alloy welded joints it is necessary to provide a higher specific power of the electron beam in the next modifications of the hardware, this allowing increase of the penetration depth and welding speed.

5. In welding aluminium alloys in space a range of problems will have to be solved, related to preparation of the part surface immediately before the welding operations, minimising porosity, as well as welded joint quality control.

1. Paton, B.E., Gavrish, S.S., Shulym, V.F. et al. (1999) Manual electron beam processing operations in space. *Avtomatich. Svarka*, **10**, 7–22.
2. Nikitsky, V.P., Lapchinsky, V.F., Zagrebelny, A.A. et al. (1985) Testing electron beam hand tool in open space. In: *Problems of space technology of metals*. Kyiv: Naukova Dumka.
3. Paton, B.E., Lapchinsky, V.F., Mikhajlovskaya, E.S. et al. (1985) Analysis of the results of experiments, conducted using the versatile hand tool in space. *Ibid*.
4. Paton, B.E., Lapchinsky, V.F., Mikhajlovskaya, E.S. et al. (1998) Manual electron beam welding of sheet metal in open space. *Avtomatich. Svarka*, **10**, 3–8.
5. Paton, B.E., Lapchinsky, V.F., Mikhajlovskaya, E.S. et al. (1997) Some features of formation of silver coatings at different gravity levels. *Kosmichna Nauka i Tekhnol.*, **3/4**, 71–75.
6. Russel, C.C., Anderson, R.G. (1999) Technological testing of tools for materials processing in space. *Avtomatich. Svarka*, **10**, 23–30.
7. Rabkin, D.M., Lapchinsky, V.F., Ternovoj, E.G. et al. (1985) Investigation of the properties and structure of welded joints of alloy 1201, made by the electron beam at different gravity levels and low temperatures. In: *Problems of space technology of metals*. Kyiv: Naukova Dumka.
8. (1998) *Welding in aircraft construction*. Ed. by B.E. Paton. Kyiv: MIIVTs.
9. Ternovoj, E.G., Bondarev, A.A., Lapchinsky, V.F. et al. (1976) Studying some issues of weldability of aluminium alloys in electron beam welding at zero gravity. In: *Space research in Ukraine*, Issue 9.
10. Ternovoj, E.G., Lapchinsky, V.F., Bondarev, A.A. et al. (1977) Investigation of the influence of zero gravity on weldability and quality of aluminium alloy joints, welded by the electron beam. In: *Space materials science and technology*. Moscow: Nauka.
11. Khomich, N.S., Neznamova L.O. (1999) Magneto-abrasive cleaning of the surface. *Avtomatich. Svarka*, **10**, 120–121.
12. Lapchinskij, V.F., Rieek, U., Sobisch, Y. et al. (1993) Grundlagen orbitaler Fügetechnologien. Anforderungen an die Fügetechnik im Weltraum. In: *Vorträge der 3. Int. Tagung «Schweißtechik im Luft- und Raumfahrtzeugbau»*, Essen, Germany, Sept. 21–22. Düsseldorf: DVS.

SPECIAL CONDITIONS FOR FORMATION OF JOINTS IN SHOCK WAVE WELDING OF METALS

L.D. DOBRUSHIN, Yu.I. FADEENKO and **V.G. PETUSHKOV**
The E.O. Paton Electric Welding Institute, NASU, Kyiv, Ukraine

In explosion welding of pure aluminium, the initial region of a joint can be formed under special conditions, corresponding to a high-velocity movement of a contact point. This region of the joint is characterised by high porosity and low strength, and only special measures allow shortening its length or eliminating it completely. An interpretation of the mechanism of formation of cumulative jets is given, attributing it to the instability of flow of the surface metal layer, which is slowed down upon approaching the contact zone of plates. It is suggested that the same mechanism is responsible for the formation of «humps» under conditions of explosion welding involving wave generation.

Key words: *explosion welding, shock wave welding, contact point velocity, cumulative jet, centrifugal forces, wave generation mechanism*

Basic technological conditions of explosion welding, widely applied in practice, are those which involve generation of waves at the interface between metals joined. The range of existence of the wave mode in the coordinate plane «collision angle γ–contact point velocity v_c» on the side of «the right boundary of the weldability window» (at relatively high γ and/or v_c) is little investigated and rarely occurs in practice. This range, in particular, is characterised by the probability of realisation in it of special conditions, under which the peculiar «truss structures» are present at the interface of a joint, instead of waves. This profile of the interface of a joint was first mentioned in [1] in connection with discussion of the mechanism of spread of the deformation humps formed in explosion welding involving wave generation. This article discusses results of investigations into the special conditions of formation of a welded joint, in particular, in commercial purity aluminium, using the shock wave welding method developed by the E.O. Paton Electric Welding Institute [2]. Similar results were obtained with this method used to join copper and other ductile metals and alloys.

Flow diagram of the shock wave welding process, macrosection and microstructure of the resulting welded joint are shown in Figure 1. The main point of the process is that a through hole is preliminarily made in plates *1* to be welded, axis of the hole being normal to the mating surfaces. The plates are located with a required welding gap between them, and an elongated cylindrical explosive charge *2* is placed into a channel formed by the hole. The charge is initiated at point *3* at one of its ends, so that detonation wave D propagates along the channel axis. As a result of explosion, a high-power compressive wave with a very sharp front *4* in the form of a truncated cone, adjoining the detonation wave front *5*, is excited in metal (often such waves are called shock waves, which is not quite correct). Behind front *4* the cylindrical channel is subjected to an intensive expansion *6*, and the free (mating) surfaces of both plates in the gap approach each other and collide at a high velocity, which in a certain region near the channel is sufficient for a welded joint to be formed around the channel.

Under specific conditions the hole diameter increases almost 3 times after explosion, and a strong joint is formed in the ring with a width twice as large as the initial diameter of the channel (Figure 1, *b*). In this case only 0.3 g of an explosive is consumed per square centimetre of the area of the joint. It is important that velocity v_c is first high and then gradually decreases. In fact, formation of a welded joint begins from the surface of the channel and proceeds in a special high-velocity mode until v_c decreases to a value which is sufficient for changing into the mode of conventional wave generation. The remaining (main) portion of the joint is formed under conventional conditions with a gradually decreasing amplitude of the waves (Figure 1, *b*).

As the initial region of the joint formed under special conditions (first 15–20 % of the area of the joint) is characterised by the presence of coarse pores, which make up a substantial part of the total area of the joint within the above region, its strength is low, which results in a considerable deterioration of the quality of a weldment as a whole. Until recently these conditions have been little studied, despite the fact that conventional welding conditions involving wave generation, which accompany the above ones, have been described in detail in basic studies [1, 3] and in subsequent publications on explosion welding of metals.

This study suggests an explanation to the mechanism of formation of a welded joint with an abnormal structure of the near-weld zone (Figure 1, *c*). It is based on the concepts of formation of a rotary component of the strain field in the subsurface layers of metal in a region close to the contact line, and violation of stability of a metal flow in this region.

Complexity of physical mechanisms of the explosion welding process and lack of data on behaviour of metals under pressures of up to hundreds of thousands of atmospheres and deformation rates of more than 10^6 s^{-1} do not allow development of the comprehensive general theory of the process. In particular, although the main peculiarity of the process conditions, i.e. the presence of waves on the surface of the joint, can be modelled in numerical experiments, this involves a difference of several times between the calculated parameters and actual values [4]. Therefore, an extensive use until now has been made of a simplified model of the process, which considers an oblique collision of two jets of a fluid, instead of collision of elasto-plastic plates. This hydrodynamic flow would be stationary in the absence of instabilities and waves. The Bernoulli equation is met along the line of the current in a stationary fluid flow

$$\left(\frac{\rho v^2}{2}\right) + P = \left(\frac{\rho v_c^2}{2}\right) = \text{const}, \qquad (1)$$

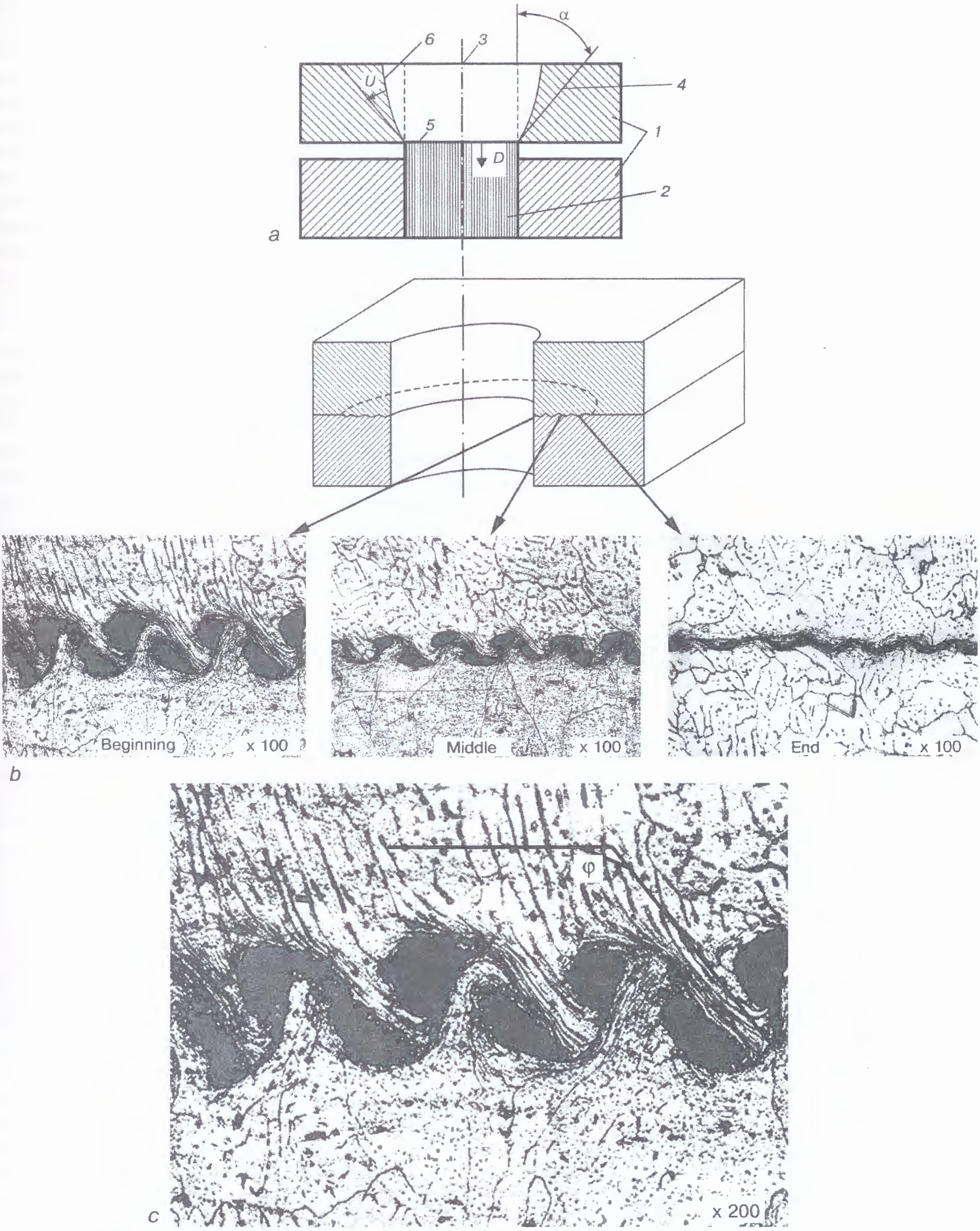

Figure 1. Schematic diagram of shock wave welding (*a*) and microstructures (*b, c*) of the resulting welded joint Al + Al

where v is the velocity of the fluid flow and ρ is the fluid density. It is assumed that at an infinite distance $v = v_c$ and pressure $P = 0$.

It is known from the theory of oblique collisions [1, 3] that high pressures developing in collision are concentrated in a small zone near the contact line between the mating surfaces. While flowing though this zone, components of a fluid decrease their velocity, according to expression (1). In this case the degree of the velocity decrease depends upon how deep a component of the fluid penetrates into the zone of high pressures, i.e. approaches the contact line. It is apparent that difference in the velocities along the different current lines results in rotation of components of the environment, moving between these current lines. Therefore, even in a simplified hydrodynamic statement the theory predicts inevitability of formation of a rotary component of the strain field near the contact point, which, because of the instability of the flow, takes the shape of vortices, looking like a vortex trail formed in a wake of a moving ship [1, 3].

In a more realistic statement, allowing for resistance of metal to deformation, an additional condition should be met for a loss in stability to take place, which in a general case can be written in the form of the following inequality:

$$\frac{\rho v^2}{\sigma} \geq B^*, \qquad (2)$$

where ρ is the density of the environment; v is the characteristic velocity; σ is the parameter characterising resistance of metal to deformation; and B^* is the critical value of a dimensionless ratio of inertia forces to deformation resistance forces, at which the flow of metal loses stability, similarly to the flow of fluid. For clearness, consider a quantitative picture of the mechanism of a loss of stability.

If an oblique collision of the jets is accompanied by formation of a cumulative jet, such a flow will contain a deceleration point at which the flow velocity is equal to zero in the moving coordinate system. In this case the maximum difference in velocities between the outside surface of a plate (where $P = 0$ and, according to (1), the velocity remains unchanged) and the deceleration point is a value equal to v_c. For the flow of an elasto-plastic environment expression (1) becomes more complicated, but the qualitative picture persists. In explosion welding the difference in velocities is much smaller, which is caused by the effect of strength of the plates, but it still remains approximately equal to v_c.

Therefore, in the case of explosion welding, the rotary movements at circumferential velocities compable with $v_c/2$ take place in the zone close to the contact line. An idea of sizes of this zone can be obtained from experimental data [3] on distribution of the end angles of turns of splashes through thickness of the near-contact metal layers. In a mode of stationary cumulation, components of the environment, which are parts of the cumulative jet, turn to angles close to 180°. Under the explosion welding conditions, the turning angles are much smaller. They gradually increase in value with distance to the contact surface, and at a level of the welding wave crests and valleys they usually amount to a few tens of degrees (turns amounting to 90° may take place at much smaller distances from the contact surface [5, 6]).

These facts are commonly known, but here there are two circumstances which usually miss attention of investigators and play a decisive role in formation of a welded joint:

- as explosion welding is performed at subsonic velocities ($v_c < C$, where C is the velocity of sound in metals welded), the field of pressures covers part of the region ahead of the contact point, and rotation of components of the inside (contact) surfaces of the plates joined begins as early as in the incoming flow. This circumstance is likely to be of a versatile importance for formation of the so-called «deformation humps» [1, 3] under all conditions of explosion welding, involving wave generation, at the interface of a welded joint;
- centrifugal forces are so high that even in the incoming flow (before reaching the contact point) they may cause formation and rapid growth of instabilities, which dramatically change the character of the flow near the contact point.

Consider some estimates. It is known from the elasticity theory [7] that the stressed state which precedes the onset of the plastic flow of rotating axisymmetric bodies of the type of disks and shafts is determined by the following relationship:

$$\sigma^* = A(\nu)\, \rho\, (v^*)^2, \qquad (3)$$

where $A(\nu)$ is the numerical coefficient, the value of which (of an order of 0.1–1.0) depends upon the geometrical shape of a body and the Poisson number ν; ρ is the density; σ^* is the fracture stress; v^* is the limiting value of the circumferential velocity v. For example, for a solid disk a radial tensile stress is maximum at the centre of the disk, where it is $\sigma = (3 + \nu/8)\rho v^2$. When v reaches a value at which the stress is comparable with a yield strength, a plastic zone is formed at the centre of the disk, whereas with further increase in the velocity the latter loses its stability and fractures. It follows from (3) that for a input geometry of the rotating body the limiting rotation velocity v^* is a material characteristic. For the majority of metals welded, it is equal to ≈ 100, and for steel disks it is equal to ≈ 300–600 m/s. On this basis, it can be assumed that in explosion welding, in a small region near the contact line, the metal components rotate so quickly that the circumferential velocities may exceed their limiting values. Therefore, the plastic flow and loss in stability begin even ahead of the contact line between the surfaces welded, thus leading to formation of the «deformation humps» and «lengths of jets» (formula (3) coincides in structure with condition (2)).

Suppose that a high-velocity «striking jet» hits against the inside surface of a disk rotating at a speed close to the limiting one. As a result of the impact the disk material locally loses stability, and part of it will be thrown out by the centrifugal forces. If mass of a material thrown out is sufficiently large, it may in turn play the role of such a striker for another similar disk. Drawing an analogy, it can be assumed that under the conditions considered a material in the incoming flow near the inside (contact) surfaces of the plates is in a state close to the limiting one. Therefore, in the absence of strong disturbances collision of the plates could have occurred either without formation of a welded joint or with welding under one of the conventional modes. However, the sufficiently strong local disturbance («seed striker») is capable of violating stability of the process and initiating formation of the special welding conditions.

Consider peculiarities of formation of structure of a joint shown in Figure 1, *c*. Examination of a microstructure of the zone of the joint gives an impression of a high degree of concentration of energy in this zone. Metal jets ejected alternately from the mating surfaces are similar in appearance to the head parts of the originating cumulative jets hitting against the opposite surface and spreading to form a characteristic «cap» («whiskers», according to the terminology of [1]). With respect to a material of the opposite surface, they play the role of spreading cutters that take off the chips which, upon turning, are transformed into a cutter for the opposite surface.

Another argument in favour of a high-velocity character of the jets is that the turning angles of the jets are about 120° (angle φ in Figure 1, *c*). This should have corresponded to an intermediate mode between the cumulative jet formation and welding conditions considered in [5, 6]. In fact, the observed values of the angles correspond not to the moment of formation of splashes, but to the state of drawing together of the plates and crushing of the «truss structure» of splashes, as a result of which the turning angles could increase from about 90 to 120°. But even if the true turning angles are only 90°, the «head» of the jet splash in a mobile coordinate system should have the following velocity components: longitudinal — zero, and close to v_c in a direction to the opposite surface. In this case collision of the «head» of the splash with the opposite surface, which slips by the splash at a velocity of v_c, should be of a character of impact with an angle of about 45° and velocity of about $v_c\sqrt{2}$.

The abovesaid is in good agreement with the observed qualitative picture of the phenomenon. However, there are no direct data of values of the velocities, and no appropriate measurement methods are available. Therefore, the problem of values of the velocities of the jets is open so far.

Consider evolution of γ and v_c during the shock wave welding process. Designate the velocity of detonation of an explosive as D, the compressive wave front velocity as U, the velocity of movement of the point at which this front escapes to the gap surface as W and the velocity at which surfaces of the closing gap approach each other as w. Absolute values of vectors **D**, **U** and **W** are related by the following geometrical relationship:

$$\left(\frac{U^2}{W^2}\right) = 1 - \left(\frac{U^2}{D^2}\right). \qquad (4)$$

The w/W ratio is determined by the collision angle $\mathrm{tg}2\gamma = w/W$. As distance r from the charge axis to the gap section considered increases, the W value decreases very slowly, whereas the w value does very quickly. The law of its variation is set with a satisfactory accuracy by relationship $w = w_0 \exp(-r/h)$, where h is the length dimension parameter, the value of which is of the same order of magnitude as the charge radius. The γ angle will also decrease following the same law. To estimate v_c, assume that the total time of closing the gap in a section with radius r is

$$t = (r/W) + (b/hw),$$

where r/W is the time of delay of arrival of the compressive wave front; b is the size of the gap; and b/w is the time of approach of the surfaces. Differentiating this relationship with respect to r, and allowing for the fact that $v_c = (dt/dr)^{-1}$ yield that $v_c = = [(1/W) + (b/hw)]^{-1}$. It follows therefrom that v_c also monotonously decreases with growth of r. Therefore, the range of special conditions, as it has been stated above, adjoins the range of conventional wave conditions on the side of the upper boundary.

The fact that special conditions occur in a range of relatively high values of the contact point velocity v_c, close to that of sound, allows the following interpretation of the mechanism of the process.

At the near-sonic velocities of the contact point the intensity of transfer of energy by the compressive waves into the incoming flow ahead of the contact point decreases, whereas the time available for the instabilities to develop decreases. Therefore, the conventional mechanism of growth of the instabilities and formation of waves becomes insufficiently effective. Dissipation of energy required for formation of a joint may occur only if the mechanism with splashes of the «striking jets», characterised by an extremely short time of growth of the instabilities, works. The process is realised if the dimensionless value $\rho v_2/\sigma$, characterising the ratio of inertia forces («hydrodynamic head») to forces of resistance of metal to deformation, is not high enough for the stable cumulative jet to form, but is already close to this threshold.

We think that the main point of this process is as follows. In a region ahead of the contact point between the plates to be joined the flow loses stability, so that short lengths («splashes») of the initiating cumulative jets are formed instead of the «deformation humps», traditional for explosion welding. The effect of strength of metal results in that the turning angle of these jets is less than that required for a stable cumulation. Therefore, they are ejected in a periodic mode, alternately hitting against the opposite surfaces, each impact by a previous length of the jet initiating ejection of the next one.

For this mechanism to take place, it is necessary to have a sufficiently strong initial push (the process has a high threshold of rigid excitation). The role of such an «initiating push» can be played by the first moment of closing the gap, when the mating surfaces collide at a velocity of about 1 km/s, radius of the hole in the upper plate at this moment being already larger than that of the lower hole by a value close to the gap size, and impact against the lower plate being made by a rectangular edge of the upper plate (see Figure 1, *a*). Further on the process of formation of a joint in shock wave welding occurs by the above mechanism up to the moment when the $\rho v_2/\sigma$ ratio decreases to the values corresponding to conventional wave generation conditions.

Therefore, in shock wave welding by the above method the process of formation of a welded joint occurs in two stages. The first 15–20 % of the area of the joint are formed under the special welding conditions, described in this study, and characterised by a decreased strength. The main part of the area of the joint is formed under conventional welding conditions, involving wave generation, and has strength not lower than that of the base metal. The presence of a region with a decreased strength is attributable to a high velocity of the contact point in the initial phase of the process. To reduce percentage of the total area of the joint occupied by this region, it is necessary to minimise the length of the region in which the contact point velocity is close to the sonic one. The authors have technological approaches which allow this condition to be met.

Within the framework of the concepts given in this study, it can be concluded that under all explosion welding conditions the wave generation process is realised due to formation of rapid rotating movements in the subsurface layers of metal near the contact line, violation of stability of the flow in this region and its deceleration. This interpretation allows the mechanism considered to be classified as a transition from conventional explosion welding conditions, involving wave generation, to an unstable cumulation, and vice versa. It is the opinion of the authors that this interpretation is a new approach to description of the mechanism of the explosion welding process and is worthy of further investigations.

1. Kudinov, V.M., Koroteev, A.Ya. (1978) *Explosion welding in metallurgy*. Moscow: Metallurgia.
2. Bushtedt, Yu.P., Volgin, L.A., Dobrushin, L.D. et al. *Explosion welding process*. USSR author's certificate 566433, Int. Cl. B 23 K. Publ. 15.06.86.
3. Deribas, A.A. (1972) *Physics of strengthening and explosion welding*. Novosibirsk: Nauka.
4. Surov, V.S. (1988) Oblique collision of metal plates. *Fizika Goreniya Vzryvom*, **6**, 115–120.
5. Bondar, M.P., Ogolikhin, V.M. (1988) Plastic strain and formation of the bond during explosion welding of copper plates. *Ibid.*, **1**, 122–127.
6. Bondar, M.P. (1995) Type of localisation of plastic strain in contacts, determining formation of a strong bond. *Ibid.*, **5**, 122–128.
7. Timoshenko, S.P., Gudier, J. (1979) *Theory of elasticity*. Moscow: Nauka.

WORKS OF THE E.O. PATON ELECTRIC WELDING INSTITUTE OF THE NAS OF UKRAINE IN THE FIELD OF MILITARY TANK CONSTRUCTION

B.E. PATON and V.G. GORDONNY
The E.O. Paton Electric Welding Institute, NASU, Kyiv, Ukraine

History of participation of the E.O. Paton Electric Welding Institute scientists in major works in the field of military tank construction is outlined. The role of the Institute in the development of the technology for automatic submerged-arc welding of armoured hulls and turrets of the legendary tank T-34 during the Great Patriotic Was is described. Stages of progress of work done in the field of arc and electron beam welding as well as special metallurgy for production of armoured hulls of medium and light tanks of different modifications in the post-war period are given.

Key words: *tank construction, armoured steels, armoured hull manufacturing, military tanks, automatic welding, gas electric welding, fused and agglomerated (ceramic) fluxes, flux-cored wire, electron beam welding, electroslag remelting, reinforced steel.*

The E.O. Paton Electric Welding Institute of NAS of Ukraine has started investigations on welding armoured steels as far back as pre-war years. At the beginning of the Great Patriotic War the number of these works was increased significantly. As is known, the Institute staff, by the initiative of E.O. Paton, was evacuated in autumn 1941 to Ural Railway Car Works «Uralvagonzavod» (UVZ) in Nizhnij Tagil. Komintern-named Kharkov Works, at which the first models of medium tank T-34 were manufactured in the pre-war period, was also moved there.

After arrival in Nizhnij Tagil the scientists of the PWI in collaboration with the workers of these plants started at once the development of technology and equipment for the automatic SAW of armoured structures of the tank T-34, manufactured from Si–Mn armour of 8S grade of thickness up to 45 mm.

In very limited periods the technology of high-speed automatic SAW of tank armour was developed, providing the use of alternating current, Si–Mn (Sv-18GS) and low-carbon electrode wires with embedding similar filler wires into a groove [1]. Two variants of flux were developed for the high-speed welding: high-silicon fused flux AN-2 of a wet granulation and a slag flux ASh, based on use of slag, enriched with manganese, from wood-coal blast furnaces of Ashinsk metallurgical plant [1, 2]. Simultaneously with the development of technology of welding a series of welding machines was designed and manufactured [1]. These machines were equipped with new welding heads, designed on the principle of self-adjusting of electric arc at a constant electrode feed speed. This could simplify significantly the design of the automatic machines and increase their serviceability [3].

In total 15 machines for SAW of different sub-assemblies of the military machine T-34 were designed, manufactured and put into service at UVZ [4].

Welding heads for automatic welding manufactured in the Institute workshops were also implemented at other plants. Thus, in 1943 the PWI staff implemented about 50 machines for automatic welding at the plants of Ministry (ex-Narkomat) of tank construction [5].

The implemented technology of the high-speed SAW of main joints of hulls and turrets of tank T-34, created in the severe conditions of war period, made it possible to increase the efficiency of welding by more than 5 times, to improve significantly the quality of welds and became basic for the organizing line manufacturing of the tank T-34. Until the middle of the 1950s it remained the main medium tank in the military equipment of the Soviet Army. More than 30 000 famous «thirty-fours» left the shops of UVZ during the war years [6].

In the post-war period, when the more powerful means of attack appeared, the tank protection caused the creation and use of new Cr–Ni–Mo armoured steels of large thickness (up to 100 mm). Possessing high armour-resistance, these steels, due to high content of carbon and presence of chromium, nickel and molybdenum, were characterized by a deteriorated weldability that was manifested, first of all, in the formation of cold near-weld cracks. By this reason, and also due to insufficient life of the welded joints at a shell attack the technology of the SAW, used successfully in mass manufacturing of tank T-34, became not suitable for the new modifications of the medium tank. The next its type, tank T-54, was manufactured exclusively by using manual welding with electrodes having a core of expensive high-alloyed austenitic wire Sv-06Kh21N10G6 (chemical composition of the wires used is given in Table 1). The weld metal of such composition was used by Germany in manufacture of tanks during the period of the World War II.

High ductility and toughness of austenitic welds, and also the favourable stressed state of welded joints provided the conditions for a significant improvement

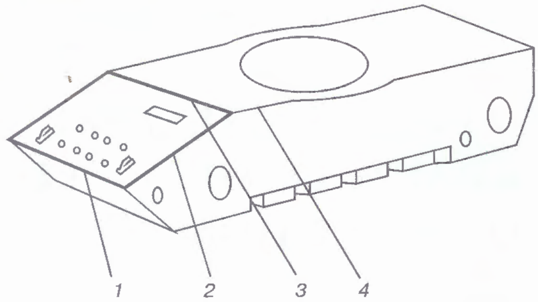

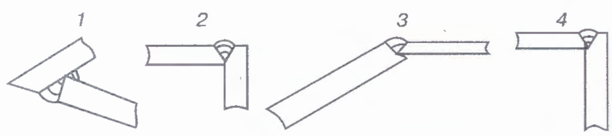

Figure 1. Scheme of welded joints of armoured hull of tank T-54: *1* — upper and lower sheet of sub-assembly «nose»; *2* — upper sheet of sub-assembly «nose» with a sheet «board»; *3* — upper sheet «nose» with sheet «roof»; *4* — front sheet «roof» with sheet «board»

of their resistance against the cold crack formation and brittle fractures at a shell attack. However, the efficiency of welding was reduced here to the level of the pre-war time that was a great obstacle for increasing the volume of production of the new tanks.

Below, we shall describe briefly the participation of the PWI in the major works on tank construction during the post-war period.

Armoured structures of medium tanks. In 1951 a special Statement of the USSR Government put forward the problem of automatic welding of armoured hull of medium tank T-54 before the PWI and V.A. Malyshev Works in Kharkov. As compared with the hull of tank T-34 the hull of tank of this model was characterized by the weld of larger sections, that increased the volume of the deposited metal. The scheme of main welded joints of armoured hull of tank T-54 is given in Figure 1. In the development of the technology of the SAW the austenitic wire Sv-08Kh21N10G6 was taken. Here, the welds, made by this wire, were characterized by a lower resistance to hot (crystalline) crack formation in weld metal that caused the necessity to limit the share of the parent metal in the weld formation. This is associated with certain difficulties for the high-efficient conditions of automatic welding of alloyed steels.

This problem was solved by the use of automatic welding at DCSP. In this method of welding the share of the parent metal in weld is significantly decreased [7]. To produce the quality welds the new austenitic wire EI-613 and fused low-silicon flux of a dry granulation of AN-14 grade were developed. As compared with wire Sv-08Kh21N10G6 the wire EI-613 was differed by some reduction in content of nickel and chromium, increased manganese and also by the presence of titanium. Modifying action of the latter made it possible to refine significantly the columnar structure of metal of austenitic welds, thus providing the increased their resistance to hot crack formation.

The use of direct current and flux of dry granulation promoted also the decrease in hydrogen content in the deposited metal that influenced favourably the resistance of metal of near-weld zone to the cold crack formation. At high quality of welded joints of armoured structures the efficiency of single-arc automatic welding, as compared with manual welding, increased by 4–5 times and was about 20 kg of deposited metal per hour.

In 1956 the technology of automatic welding with wire EI-613 under flux AN-14 at DCSP was implemented at V.A. Malyshev Works in Kharkov in manufacture of armoured hull of tank T-54 and cast-welded turret of the same tank at the Illjich Works in Mariupol. Later on the wire EI-613 was included under the grade Sv-08Kh20N9G7T into the State standard of the USSR for welding wires, and the flux AN-14, under the grade AN-22, found a wide spreading for welding structural steels [9].

At the beginning of the 1960s the technology of automatic welding with wire Sv-08Kh20N9G7T under flux AN-22 was widely used in manufacture of armoured hulls and turrets of tank T-55 at the machine-building plant in Omsk city. Somewhat later the more efficient technology of twin-arc automatic SAW using the same welding consumable that in single-arc welding was first used in this branch at the same plant. In this case, the efficiency of the process increased to 30–35 kg of the deposited metal per hour. As the results of investigations, carried out at the PWI and V.A. Malyshev Works, showed, the mentioned level of the efficiency of twin-arc automatic welding can be reached also in a single-arc automatic welding, preserving the required quality of the welded joints, at the expense of the extended stickout of the electrode. When the welding current is passed through the extended stickout of the electrode the Joule heat (effect I^2RT) is generated, the stickout is heated and the electrode melting rate is increased. Special nozzles were developed for the serial automatic machines for a practical realizing of this method to increase the welding efficiency [10].

In the middle of the 1960s the technology of the SAW with wire Sv-08Kh20N9G7T was approved at the above-mentioned plants for manufacture of armoured structures of medium tanks T-55 and T-64.

A part of internal welds of armoured hulls of these tanks was performed by the mechanized SAW. This increased the total level of the automatic and mechanized welding up to 60 % (in mass of deposited metal) and made it possible to realize the conveyor production of the armoured hulls. Welding of separate subassemblies and armoured hull during assembly in conveyor was performed by the machines of design of the PWI and serially-produced by industry.

In parallel with the above-mentioned technology, the technology developed in the middle of the 1950–1960s by the central armour laboratory (later VNII-stal) was used successfully in manufacture of similar armoured structures of medium tank and also heavy

Table 1. Chemical composition of the wires used, wt.%

Wire grades	*C*	*Cr*	*Ni*	*Mn*	*Si*	*Mo*	*Ti*
Sv-18GS	0.18			0.8	0.4		
Sv-06Kh21N10G6	0.06	21.0	10.0	6.0			
Sv-08Kh21N10G6	0.08	20.4	9.8	5.4	0.28	0.22	0.03
Sv-08Kh20N9G7T (EI-613)	0.08	19.8	9.2	7.1	0.44	0.06	0.76
Sv-08GSMT (EI-581)	0.08	up to 0.3	up to 0.3	1.1	0.6	0.2–0.4	0.05–0.12
Sv-10KhGSN2MT	0.1	1.0	2.0	1.0	1.0	0.8	0.3
Sv-08Kh10G32	0.08	10.0		32.0			
Sv-05Kh21N10G2T (PP-ANV8)	0.05	21.0	10.0	2.0			0.3
Sv-05Kh20N10M2T (EK-67) (PP-ANV9)	0.05	20.0	10.0	0.8		2.0	0.5

tank T-10M at the Ural plants of Chelyabinsk and Nizhnij Tagil. This is, respectively, the single-arc automatic welding with austenitic wire Sv-08Kh21N10G6 at alternating current under the ceramic dust-like flux of 11/5 grade and automatic three-phase arc welding with the same arc under the fused flux AN-20, which was developed at the PWI [8]. By the request of the workers of Chelyabinsk machine-building plant the PWI staff developed the new granulated ceramic flux of KGF-78 grade with improved sanitary-hygienic characteristics and increased resistance of weld metal to formation of pores and hot cracks, which was widely used in single-arc welding of armoured hulls and turrets of tanks T-10M and T-62, and implemented at the this plant and also at UVZ.

Technology of the automatic welding by three-phase arc, implemented at UVZ, in performance of main welds of armoured tanks T-62 and T-72, was characterized by the increased efficiency (comparable with twin-arc automatic welding), and also provided the high quality of welded joints of armoured structures. The results of investigations made in UVZ and the PWI for assessment of quality of the fusion zone of these joints, confirmed this [11].

Taking into account that both variants of the technology of automatic SAW envisaged the use of expensive austenitic wires containing up to 10 % of deficit nickel, the investigations were carried out at the PWI on the development of more cost-saving technology of the SAW of the tank armour.

Firstly, in the 1950s the technology of the automatic welding under the fused flux using the low-alloyed wire Sv-08GSMT was developed [12]. However, it was not managed to implement this technology of welding in manufacture of armoured hulls of tank T-64 due to necessity of preliminary heating to prevent the formation of cold cracks in the welded joints. Much more later and only in manufacture of turret of tank T-55 the automatic SAW with low-alloyed wire Sv-10KhGSN2MT [13] was used without preheating in manufacture of armoured hulls at Omsk machine-building plant.

Another cost-saving technology of welding the tank armour envisaged the use of high-alloyed, but Ni-free wire Sv-08Kh10G32 [14]. The technology of automatic welding using this wire under the ceramic low-oxidizing flux KM-78A proved the required quality of welded joints at 2-times reduction of cost of welding jobs. At the beginning of the 1960s it was used for manufacture of turrets of armoured hull of tank T-62 at Chelyabinsk machine-building plant.

The radically new approach to the solution of the problem of effective protection of molten metal in welding from atmospheric air is the method of gas electric welding in CO_2, developed by the PWI staff in collaboration with a number of organizations at the end of the 1950s and beginning of the 1960s, found its application also in armoured hull manufacture. The technology of mechanized welding in CO_2 with austenitic wire Sv-08Kh20N9G7T, developed at VNITI, forced out practically the mechanized SAW. The CO_2 welding was performed everywhere at DCRP and, as to the productivity, it was inferior to the earlier used mechanized SAW. The associates of the PWI and V.A. Malyshev Works showed a feasibility of realizing gas electric welding of armour using austenitic wire Sv-08Kh20N9G7T in CO_2 at DCSP. The efficiency of the mechanized welding was increased here by 1.5 times without deterioration of quality of welded joints of the armoured structures. Some increase in electrode metal spattering in this method of welding could be decreased significantly by an additional modifying wire Sv-08Kh20N9G7T with zirconium.

The further improvement of mechanized welding of armour in CO_2 was directed to the development of new austenitic flux-cored wires, stabilized by properties, which will provide the reduction in electrode metal spattering and increase in weld metal resistance against hot crack formation at increase in the welding efficiency. The new flux-cored wire of PP-ANV8 grade

Table 2. Mechanical properties of weld metal at different combinations of welding consumables

Combination of welding consumables	$\sigma_{0.2}$, *MPa*	σ_t, *MPa*	δ_5, *%*	ψ, *%*	a_n, *J/cm²*		v_{cr}, *mm/min*
					20 °C	*−40 °C*	
EK-67, AN-22	375	680	52	55	170	136	6.5
PP-ANV9, CO_2	445	678	36	54	150	110	8.0
EI-613, AN-22	350	610	33	46	140	118	3.0

Notes. 1. v_{cr} — resistance to hot crack formation in weld metal. 2. Mean values of 3–5 tests are given.

(Sv-05Kh21N10G2T) [15], satisfying all specified conditions and providing required quality of welded joints was developed at the PWI and used first in industry in CO_2 mechanized welding of hull of tank T-72 at UVZ.

All these years the main attention of the Institute staff was directed to the welding of hulls of armoured vehicles. But, as it sometimes happens, these were the welders who understood the need in improvement of materials used for manufacture armoured hulls. The understanding of the fact that the tank is the welded structure which after the artillery attack should preserve integrity of not only the welded material but also welded joints, led to the beginning of the first works at the PWI on the improvement of thick-sheet armour for the tank construction. It was established at the first stage of these investigations that new high-strength Cr–Ni–Mo armoured steels at satisfactory resistance to the shell attack do not possess sufficient toughness and, as consequence, do not satisfy the requirements of tank constructors and army to «life», i.e. absence of spallings at the internal side of the armoured hull at the shell attack. In definite situations, occurred at the end of the 1960s and beginning of the 1970s this meant that the new developed challenging machines would have a non-satisfactory level of armour protection. Only due to the efforts of scientists from the PWI in the carrying out comprehensive investigations of the electroslag remelting (ESR) of slag ingots of high-strength steels and all the metallurgical cycle of production of armoured steels (from melting to rolling and heat treatment) the reliable technology of production of tank armour was created. Moreover, the melting of such types of steels in oxygen converters with a subsequent ESR and, later on, their continuous casting, was first mastered.

At the end of the 1970s and beginning of the 1980s the new stronger armoured steels began to be produced using the ESR method suggested at the PWI [16]. Information about the effect of refining remelting of alloyed steels on their weldability were limited [17] and, sometimes, also contradictory [18]. Therefore, the associates of the PWI and VNIIstal carried out investigations and came to the conclusion that in welding new armoured ESR steels using austenitic materials, accepted in welding, the deterioration in quality of welded joints was not observed. The results of these investigations served the basis of the fact that technological processes of welding under flux AN-22 and in CO_2 using austenitic wire Sv-08Kh20N9G7T with a correction of conditions of welding root welds of steel became leading processes of welding also in manufacture of armoured hulls of medium tanks of next modifications T-80 and T-84 made from armoured steels of the new generation of 69Sh, 24Sh, 22Sh type. However, when wire Sv-08Kh20N9G7T was used, providing the strength of the weld metal at the level 600 MPa, the non-conformity of strength characteristics of weld metal and parent metal was expressed very clearly. In addition, the use of moderate conditions for improving technological strength of welds led to the noticeable decrease in the welding process efficiency.

As a result of investigations carried out at the PWI in the middle of the 1980s the new welding consumables were developed: austenitic wire EK-67 (Sv-05Kh20N10M2T) [20] for automatic welding under flux AN-22 and AN-22M [19] and austenitic flux-cored wire PP-ANV9 (Sv-05Kh20N10M2T) [15] for mechanized CO_2 welding. The new welding consumables provided higher, compared with a serial wire, mechanical properties and technological strength of weld metal (Table 2). As follows from the Table the strength of weld metal made by wires EK-67 and PP-ANV9 was increased by ≈ 10 % that provided higher characteristics of service properties of welded joints at some its increase in ductility and toughness.

After the comprehensive tests and experimental-industrial trials the technology of the automatic welding with wire Sv-05Kh20N10M2T under flux AN-22 (AN-22M) and technology of mechanized welding with wire PP-ANV9 in CO_2 were recommended to implementation in the manufacture of armoured hulls of tank T-80 from armoured ESR steels. The electroslag remelting found application in tank construction also for improving the quality of non-armoured steels used for manufacture of torsion bars of moving part of the hull and other parts of the tank.

The ESR variety, i. e. technology of electroslag hot topping of ingots [21] was used successfully in manufacture of cast turrets of tank T-62 and T-64, the their quality in this case was increased significantly. Moreover, the total consumptions of alloyed molten steel were reduced noticeably due to decrease in a crop part of the cast turrets.

The technology of electroslag casting, based also on the ESR, passed the industrial trial in manufacture of more quality armoured parts of armoured hull of tanks of the same modifications.

In the middle of the 1980s the scientists of the PWI developed the alternative variant of existing armoured steels, i.e. ESR, based on using method of producing radically new structural material, reinforced quasi-monolithic (RQM) steel [22]. This steel was not subjected to ESR and met all requirements specified to the tank armour.

The peculiar feature of this work was the innovatory proposal of associates of the PWI to decrease the carbon content in armoured steels by almost 2 times. This decision without essential change in alloying system led not only to the improvement of weldability, but also to the noticeable increase in toughness of thick-walled steel and its life as an armoured hull material.

The new armoured RQM steel and technology of its welding using above-mentioned serial welding consumables were used in manufacture of armoured hulls of tank T-80, and, owing to them and the new technology, the rolled-welded turrets of this tank were first manufactured. The improved weldability of armoured RQM steel provided the high-quality welded joints made using new technology of manufacture armoured hulls, namely the high-efficient electron beam welding (EBW). As compared with the arc multilayer welding of armour of up to 80 mm thickness the EBW is performed for one pass (Figure 2). High values of shell-resistance of joints made by EBW, close to the parent armoured metal, cannot be practically reached using the arc processes of welding.

Using the technology of EBW with a horizontal beam [23], a main front sub-assembly of armoured tank T-80 was welded successfully at the PWI. Macrosection of welded joint of this sub-assembly is given in Figure 3.

The 1980s are remarkable by investigations of the PWI on welding steel and aluminium armours to create the effective welded armoured structures from the dissimilar materials.

Technology has been developed, at which welding of armoured steel with aluminium armour of up to 100 mm thickness was realized using transition pieces of a special design. The latter were manufactured autonomously or with the help of hardfacing that made it possible to produce quality welded joints (butt, fillet, overlap). These welded joints withstood bullet or shell attacks and also mine explosion. Using the developed technology the armoured hulls of medium tanks with aluminium armour bottom were manufactured under the industrial conditions. At equal-mass variant the rigidity of this bottom was increased by several times.

Thus, the post-war period was remarkable by that the number of highly-efficient technological processes of welding and special electrometallurgy providing the necessary quality of parts and welded joints found application in armoured hull production in manufacture of medium tanks of different modifications.

At the end of the 1980s the level of mechanizing welding jobs was about 95 %. However, the share of

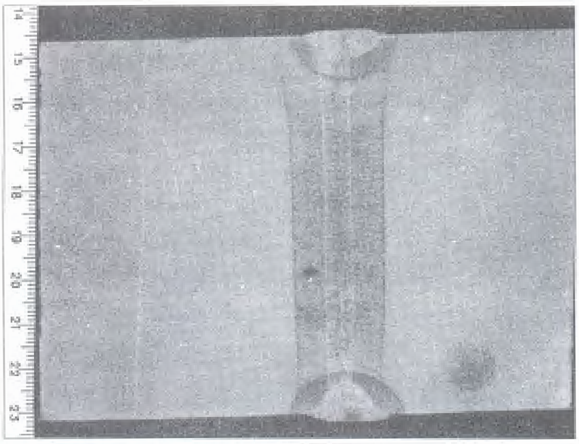

Figure 2. Macrosection of welded joint of armoured steel of 80 mm thickness, made by EBW

the automatic SAW was only 25 % (by volume of deposited metal) that was 2 times less than in manufacture of tank T-34. The main volume (≈ 70 %) in manufacture of armoured structures was mechanized CO_2 welding. Such wide use of the mechanized gas electric welding in armoured hull manufacture was stipulated by the versatility of the process which could realize welding of inner and hard-to-reach short and curvilinear welds, inconvenient for welding automation. However, the insufficient adaptability of welded joint design of armoured hulls limited the works for the further automation of welding. The attempts were made many times to use for these purposes the serially-produced welding automatic machines, but they were not efficient. In this connection the intensive investigations on the development of radically new specialized welding machines with automatic program control were started at the PWI during the 1980s.

These machines of a stationary type were based on the principle of a modular design. The new developments found concrete embodiment in the automatic machines of series AD-238 [24] (Figure 4). In 1986 two models of the new machines AD-241 from this series were first manufactured and mounted on the

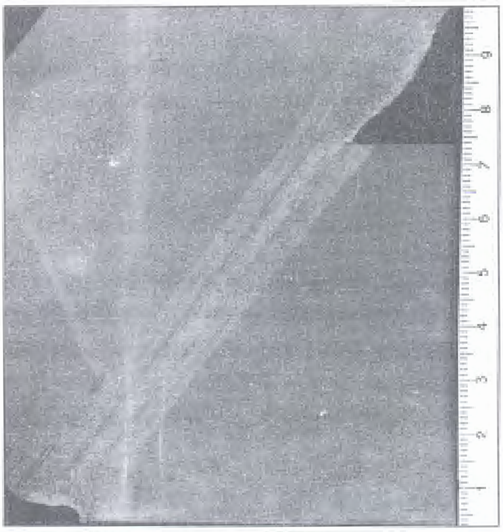

Figure 3. Macrosection of welded joint of mock-up of the front sub-assembly «nose» of armoured hull of medium tank, made by EBW

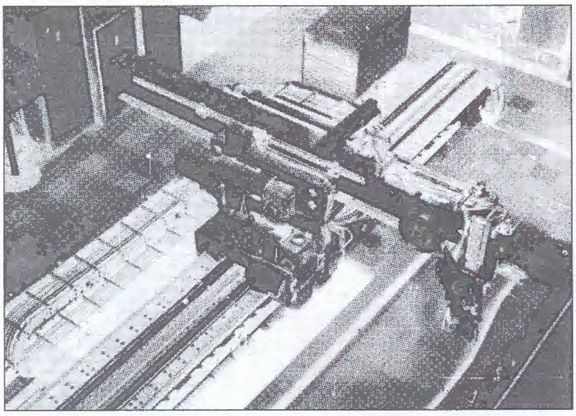

Figure 4. General view of welding automatic machine of series AD-238

new conveyor line of UVZ for gas electric welding of inner welds of armoured hull of tank T-72. They provided the automation of welding head feed to the site of welding, search for the weld beginning, tracking the weld during welding, layout of beads of multipass welds according to the program. Several automatic machines of series AD-238 were also designed for welding of external and internal welds of this armoured hull, including the automatic machine for welding up of bosses to the armoured sheets. It was supposed that with their implementation the volume of automation of welding jobs in manufacture of armoured hulls would increase at the UVZ up to 50 %. Simultaneously with works for UVZ the Institute carried out works on the designing, manufacture and implementation of new automatic machines for welding joints of armoured hull of tank T-80.

Armoured structures of light tanks. At about the same time with the works on automatic welding of armoured hull of medium tank T-54, the associates of the PWI started the investigations on the development of the technology of welding armoured structure of a light tank, manufactured from the Si–Mn–Mo steel of grade 2P of up to 20 mm thickness. The small thickness, and also low content of carbon and alloying elements in this steel could prevent the formation of cold cracks in welded joints in welding with a low-alloyed wire without using preheating. In comparatively short terms the technology of automatic welding under fused flux AN-42 using a low-alloyed wire Sv-08GSMT (EI-581) was developed. At the end of the 1950s this technology was implemented in welding of armoured hulls of light amphibian tank PT-76 at Volgograd plant.

After several years, the technology of mechanized welding in CO_2 using the same wire that in SAW was developed at the PWI and implemented in manufacture of armoured structures of tank of this type.

At the same time at the Volgograd plant the technology of automatic CO_2 welding up of bosses to the armoured sheets was first used by a portable machine A-1077 developed at the PWI.

The technology of gas electric welding with wire Sv-08GSMT found rapid and wide spreading in armoured hull manufacture and became the main process practically at all the plants for manufacture of light tanks and armoured troops carrier of different modifications such as PT-76, BMP-1, BMP-2, BTR-50, etc.

To increase the bullet-resistance of separate welded joints of armoured hulls the associates of the PWI have developed and implemented technology of gas electric finishing welding of welds using the new flux-cored wire PP-AN-180 at Kurgan machine-building plant.

In mass manufacture of thin-armoured vehicles, it seemed necessary to reduce the labour intensity for cleaning electrode metal spatters from armour and also to increase the efficiency of the gas electric welding whose volume by mass of the deposited metal exceeded 95 %. The gas electric welding with wire Sv-08GSMT in mixture of gases ($Ar + CO_2$) was developed and implemented in the production of the above-mentioned machines that could decrease significantly the electrode metal spattering and decrease, respectively, the expenses for the armour cleaning from the welded-on spatters. The use of the mechanized welding in shielding mixture of gases was very useful for the fulfilment of the automatic welding of armoured structures of infantry military machines BMP-1.

As regards to this machine and its modifications, manufactured at Kurgan machine-building plant, many works were carried out at the PWI on the creation and industrial implementation of specialized automatic machines for gas electric welding which showed a high efficiency in welding separate joints of armoured hull and turret of BMP-1.

With use of the new aluminium armour the demand was appeared for the development of more efficient technology of its welding.

In the middle of the 1980s the associates of the PWI developed the new technology of the highly-efficient automatic consumable electrode argon welding of armour on the base of aluminium and alloy AMg6. The technology envisaged the optimizing of conditions of welding different types of joints of metal thickness from 8 to 60 mm and was used in manufacture of hulls of light troops landing tanks and armoured machines of infantry at the Volgograd plant and Kurgan machine-building plant. The challenging process of welding at narrow gap was also suggested [25], which passed the successful test under the industrial conditions. At the beginning of the 1990s the scientists of the PWI developed the equipment UD-474 and new technology of welding structures of stamped-welded aluminium alloy AMg6 rollers for military machines of infantry for the Kharkov tractor plant. Its application made it possible to decrease significantly the number of defects in welds, to increase the efficiency of welding jobs and serviceability of military machinery.

Naturally, that the present article cannot cover all the trends of investigations which were carried out at the PWI in the field of the tank construction. The authors suppose that over the decades of active work the close cooperation of welders and metallurgists, from design bureaus of tank construction to metallurgical plants and further up to assembly of armoured hulls and test grounds was most important in this direction. It was the process of mutual exchange of ideas of scientists and production workers that has led to the development of the most technical solutions which were widely implemented in the field of the tank construction.

At present, when the production of domestic tanks is renewed in Ukraine [26], it seems reasonable to use the above-mentioned developments of the PWI.

1. (1943) *Guideline on automatic welding of armoured structures*. Ed. by E.O. Paton. Kyiv: AN USSR.
2. Korennoj, A.I. (1948) Experience of industrial application of automatic machines of E.O. Paton Electric Welding Institute of AS USSR. *Trudy po Avtomat. Svarke*, **9**, 57–65.
3. Dyatlov, V.I. (1943) New principle of design of automatic welding machines. *Vestnik Mashinostroyeniya*, **9/10**, 15–18.
4. Strunets, V.K. (1986) 50th anniversary of welding manufacturing at PO «Uralvagonzavod». *Avtomatich. Svarka*, **9**, 47–52.
5. Kornienko, A.N. (1997) Welding technique in years of the World War II. Part 1. Welding in manufacturing of armament in the USSR. *Ibid.*, **7**, 41–60.
6. (1986) 50th anniversary of F.E. Dzerzhinsky Ural Railway Car Works. *Ibid.*, **9**, 46.
7. Makara, A.M., Slutskaya, T.M. (1956) About resistance of near-weld zone of medium-alloying steels in welding at direct and alternative current. *Ibid.*, **6**, 31–37.
8. (1974) *Technology of electric fusion welding of metals and alloys*. Ed. by B.E. Paton. Moscow: Mashinostroyeniye.
9. Pokhodnya, I.K., Alter, V.F. Galinich, V.I. et al. (1981) Manufacturing of welding consumables. In: *Welding in the USSR*, Vol. 2. Moscow: Nauka.
10. Dibets, A.T., Gordonny, V.G., Vashchenko, N.M. (1976) Automatic submerged-arc welding with increased electrode stickout. *Avtomatich. Svarka*, **10**, 68–69.
11. Strunets, V.K., Nikopov, I.P., Gordonny, V.G. et al. (1980) Structure and properties of intermediate layer in fusion zone of medium-alloyed steel with austenitic weld. *Ibid.*, **11**, 24–27.
12. Makara, A.M., Novikov, I.V., Lutsuk, V.A. (1959) Development of technology of electroslag welding of AK medium-alloyed steel shells. *Ibid.*, **4**, 55–65.
13. Makara, A.M., Gordonny, V.G., Vasiliev, V.G. (1967) Alloying of welds from nonheat-treated high-strength steels of 30KhN2M type. *Ibid.*, **11**, 5–9.
14. Kabatsky, V.I., Kiriakov, V.M., Parfesso, G.I. et al. (1982) Structure and properties of fusion zone of welded joints of pearlitic class steels with austenitic welds. *Ibid.*, **8**, 13–15.
15. Kiriakov, V.M., Chertov, A.I. (1991) High-alloy flux-cored wires PP-ANV8 and PP-ANV9 for welding of hardening steels. In: *Proc. of Int. Seminar on Welding Consumables for Mechanized Arc Welding of Steels*, Nikopol, Oct. 1990. Kyiv: PWI.
16. Medovar, B.I., Latash, Yu.V., Maksimovich, B.I. et al. (1962) *Electroslag remelting*. Moscow: Metallurgizdat.
17. Makara, A.M., Gordonny, V.G., Dibets, A.T. et al. (1973) Remelting of high-strength steels as means of improvement of their cold crack resistance in welding. *Avtomatich. Svarka*, **8**, 1–5.
18. Smith, N., Bagnall, B. (1968) The influence of sulphur on heat-affected zone cracking of carbon-manganese steel welds. *British Welding J.*, **2**, 82–89.
19. Tokarev, V.S., Sarzhevsky, V.A., Avrakhova, L.I., et al. *Fused flux for mechanized welding*. USSR author's certificate 1756080, Int. Cl. B 23 K 36/362. Publ. 23.08.92.
20. (1994) *Consumables for welding of steels and cast iron*. Handbook. Kyiv.
21. Medovar, B.I. (1984) Electroslag technology today and tomorrow. In: *Welding and special electrometallurgy*. Kyiv: Naukova Dumka.
22. Saenko, V.Ya., Medovar, L.B., Us, V.I. (1984) *New structural material — RQM steel*. Kyiv: Znaniye.
23. Nazarenko, O.K. (1984) State-of-the-art of electron beam welding. In: *Welding and special electrometallurgy*. Kyiv: Naukova Dumka.
24. Paton, B.E., Moshkin, V.F., Pritula, S.I. et al. (1990) Prospects of development of electric arc welding equipment. In: *Problems of welding and special electrometallurgy*. Kyiv: Naukova Dumka.
25. Zaviryukha, V.I., Ryabets, Yu.A., Steblovsky, B.A. et al. (1981) Technological peculiarities of consumable electrode narrow gap welding of thick aluminium alloys. In: *Actual problems of non-ferrous metals*. Moscow.
26. Veretennikov, A.I., Rasskazov, I.I., Basok, S.N. et al. (1998) *A.A. Morosov design office on mechanical engineering*. Kharkov: Iris.

ERECTION ASSEMBLY-WELDING OF TUBULAR STRUCTURES OF NIOBIUM ALLOYS IN THE JIG

V.E. BLASHCHUK
The E.O. Paton Electric Welding Institute, NASU, Kyiv, Ukraine

Technology of erection assembly-welding of tubular structures of a niobium alloy in the jig and equipment for its performance have been developed. A heat-hydraulic model of a lithium-niobium loop has been welded of individual blocks in site. Control-technological and corrosion testing and testing in a space-vacuum chamber demonstrated the high quality of the field welded joints.

Key words: *niobium alloys, arc welding, erection assembly-welding in the jig, liquid lithium, corrosion resistance, control, lithium-niobium loop*

Presented below is part of the integrated research and developmental work, performed in 1980s at the E.O. Paton Electric Welding Institute of the NAS of Ukraine together with Research-Production Association «Energiya» on development of a nuclear electric jet propulsion system of refractory materials. It was not published earlier for obvious reasons. It should be noted that the results of the performed studies are still important even to-day, in connection with development of investigations related to construction of reactors with liquid-metal heat-transport fluid, as well as application of refractory metals in other branches of engineering.

Progress of modern engineering required application of advanced structural metallic materials, one of such materials being niobium alloys, having high corrosion resistance in the medium of liquid-metal heat-transport fluids [1–4]. Investigation of the behaviour of niobium contaminated with oxygen in lithium that is a liquid-metal heat-transport fluid, showed that even at small concentrations niobium releases the oxygen into lithium. The process of lithium interaction with oxygen, contained in niobium, leads to embrittlement and corrosion of the latter [1].

Therefore, higher requirements to the content of gaseous impurities (particularly oxygen content) are made of niobium as a structural material, exposed to liquid lithium at T ≥ 1200 K.

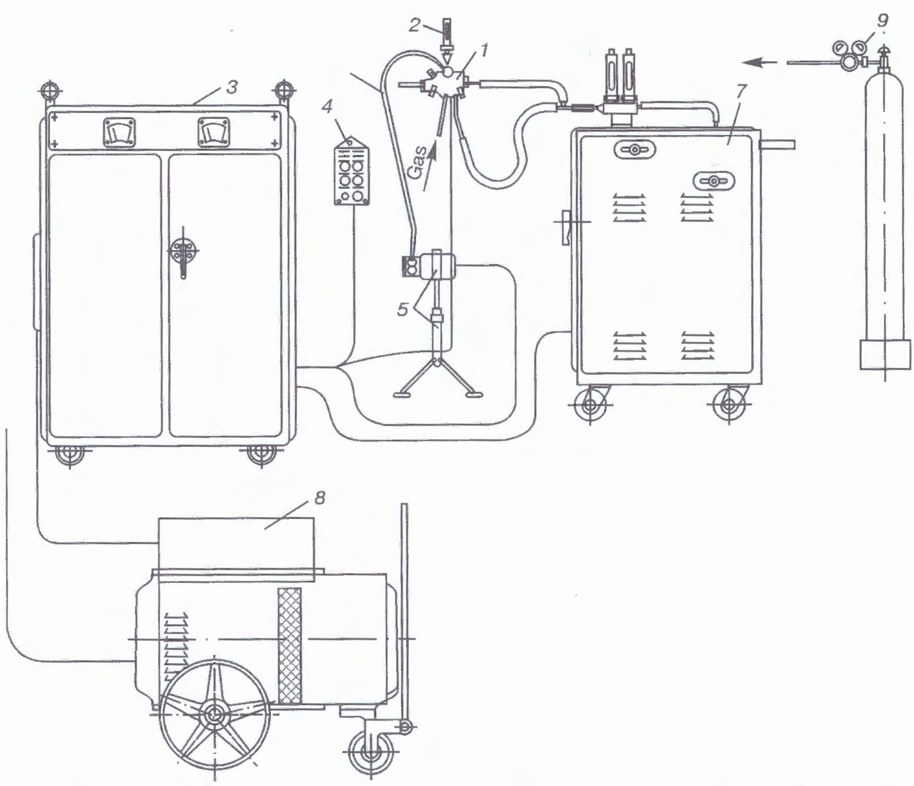

Figure 1. Schematic of A1129M unit: *1* — control cabinet; *2* — control panel; *3* — flexible shaft; *4* — spring suspension of chambers to the frame; *5* — welding chamber; *6* — vacuum station for checking and setting up the chambers; *7* — cylinder with super pure helium and pressure regulator; *8* — drive mechanism with a rack; *9* — power source

Nb-based alloys (with oxygen content of $5\cdot10^{-3}$–$2\cdot10^{-2}$ wt.%) have a high corrosion resistance in the liquid lithium medium [5] and are applied to manufacture a heat-hydraulic model of a Li–Nb loop of up to 300 kW heat power, where lithium is used as the working medium. Investigations demonstrated, that in welding it is necessary to provide the oxygen content in the metal of the weld and the HAZ on the level of $(1-2)\cdot10^{-4}$ vol.% and that of moisture – dew point not lower than –70 °C in the shielding gas atmosphere. In this case, the corrosion resistance of welded joints in liquid lithium will be on the level of the base metal [6–9].

The heat-hydraulic model of the Li–Nb loop is a large-sized tubular structure, consisting of individual blocks, welded by the electron beam process and in a chamber with a controlled atmosphere of super pure helium [6, 8, 10]. In non-consumable electrode welding of individual components of tubular structures, the required purity of the inert atmosphere can be achieved and high-quality joints can be produced, however, welding of field butt joints in the jigs runs into serious difficulties.

The aim of this study is to develop the technology and equipment for erection assembly-welding in the jig of a model of a Li–Nb loop, providing the high quality and reliability of welded joints and the entire item as a whole.

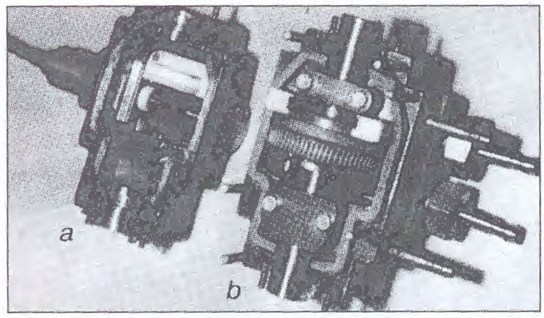

Figure 2. Chambers for welding niobium alloy tubing of Ø 12×1 (*a*) and Ø 28×1(*b*) mm size, shown with the removed covers

Large-sized manned welding chambers of «Atmosfera» type became used for assembly-welding of complex tubular structures of reactive materials (for instance, titanium) [6, 11]. They, however, turned out to be unsuitable to manufacture niobium components, because of the difficulty of producing the super pure atmosphere, controlling the content of impurities in a large gas volume, great losses of expensive inert gases, complexity of providing the working conditions for the welder in such a chamber, high equipment cost, etc.

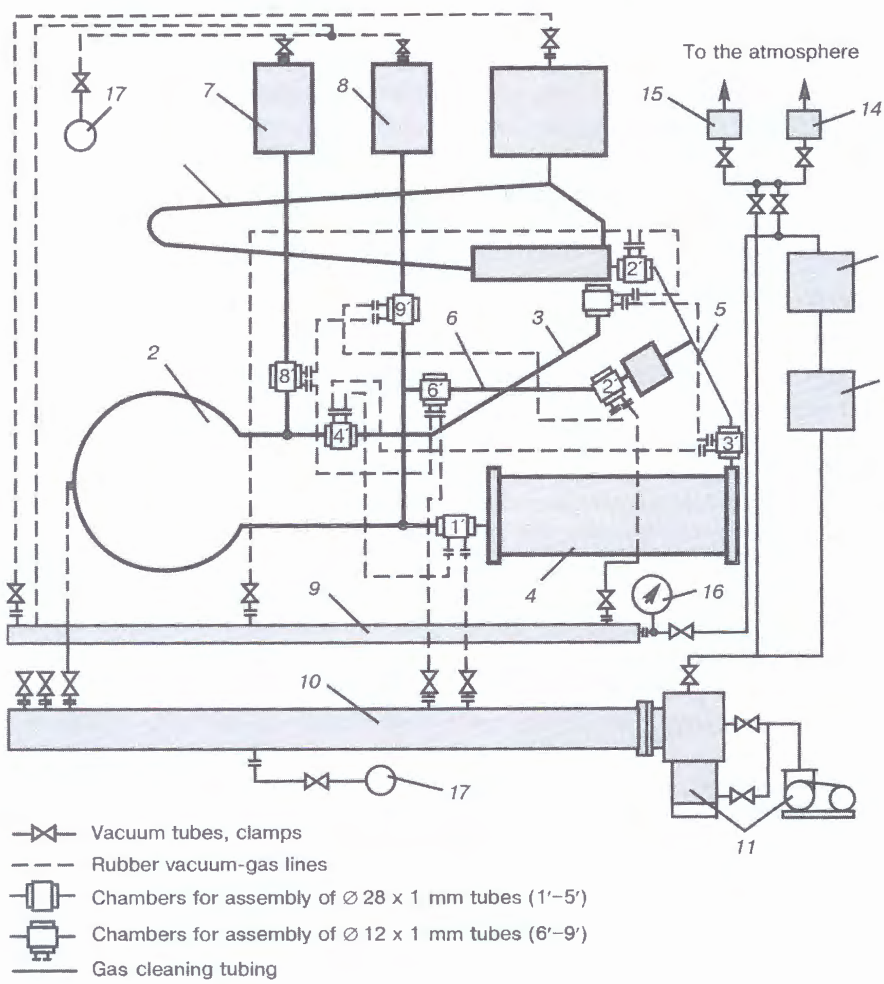

Figure 3. Schematic of connection of the item and welding chambers to the unit for gas cleaning and vacuum system in erection welding in the jig: *1–8* – blocks; *9, 10* – gas and vacuum collectors, respectively; *11* – vacuum unit; *12* – compressor; *13* – gas cleaning block; *14* – KhG chromatograph; *15* – hygrometer; *16* – compound pressure and vacuum gauge; *17* – manometric tube

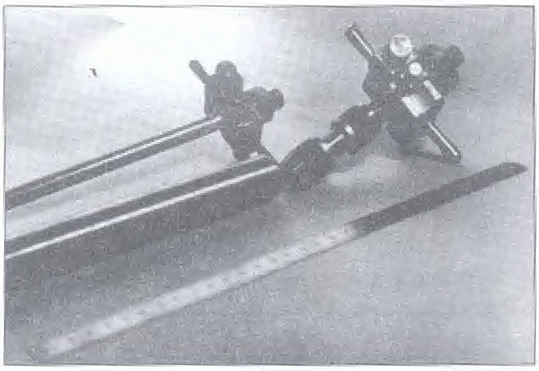

Figure 4. Manual edge trimmer

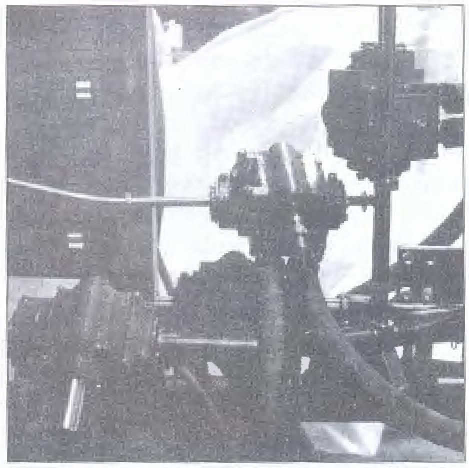

Figure 5. Part of niobium loop with the mounted captive chambers (chambers *1, 4, 8, 9*) (see Figure 3)

The fundamental feature of the developed technology is achieving a minimal sealed volume of the shielding atmosphere, limited by the dimensions of microchambers (mounted on field butts) and inner cavities of welding equipment. In view of the small dimensions of the chambers and the item being welded, it allows producing, maintaining and reliably controlling the composition of super pure atmosphere during welding.

Special equipment was developed to conduct the erection assembly-welding of the niobium loop in the jig:

- jig with vacuum and gas systems for 3-D arrangement of the blocks and microchamber fastening;
- A1129M welding unit for non-consumable tungsten electrode welding of position butts of tubes in the atmosphere of super pure helium in site. The unit consists of sealed small-sized captive chambers for assembly and welding of tubes of Ø 12×1 and 28×1 mm size, separate drive mechanism and control cabinet. Detachable welded microchambers are used for welding the butts and spatial orientation of the tubing to be welded [6, 12] (Figures 1 and 2).

Technological operations were optimized on a mock-up of high-alloyed Cr–Ni steel. Optimal modes of welding niobium tubes were established on samples that were later on used for corrosion testing.

Figure 3 gives the schematic of the item, places of mounting the microchambers, connections of the item and microchambers to the vacuum and gas cleaning systems. The tubes of the abutted blocks were cut to size and the butt locations were treated by a special manual trimmer to provide the normality of the end face to the tube axis (Figure 4). Item correspondence to the drawing was checked after its assembly in the jig with cramps. After removal of the cramps the butts to be welded were degreased, etched in the reactive of 30 % fluorspar acid (1.15 g/cm^3 density) + 30 % nitric acid (1.34 g/cm^3 density) + 40 % water, washed in cold water and dried. Captive chambers were mounted on the thus prepared butts (the gap in the butt and edges misalignment did not exceed 0.1 mm, which was checked with a thickness gauge), the chambers being suspended from the jig, using a spring balance to reduce the load on the tubes. The gap between the tungsten electrode and the tube was set to be about 0.9 mm, using a thickness gauge. The tube free ends were closed by special bypass plugs, that were later on used to conduct the control-technological operations. The chambers and plugs were connected to the vacuum and gas collectors by vacuum rubber hoses. The jig vacuum system was used to pump down the item, microchambers, vacuum and gas collectors. After a rarefaction of $5 \cdot 10^{-3}$ Torr has been achieved, the vacuum system was switched off, and the item with the microchambers was filled with helium from the gas cleaning system up to excess pressure of 0.3 atm. The vacuum and gas collectors were disconnected and circulation gas cleaning was switched on (see Figure 3). KhG type chromatograph was used to control the purity of helium at the system outlet. Welding of field butt joints was performed, when the specified purity of helium by the impurities was achieved. The selected modes (see the Table) provided reliable penetration over the entire tube perimeter, absence of pores or lacks-of-fusion, minimal narrowing of the tube section.

Erection welding was performed in two stages:

Welding stage	*Tube diameter, mm*	*Welding conditions*		*Welding mode*			
		Pressure in the system, atm	*Atmosphere composition at the system outlet*	$U_{o.-c}$, *V*	U_a, *V*	I_w, *A*	v_w, *m/h*
I	28×1	0.11–0.13	$8.5 \cdot 10^{-5}$ vol.% [O] $5.6 \cdot 10^{-4}$ vol.% [N] dew point −70 °C	80	16–17	95–100	40
II	12×1	0.10–0.13	$4.6 \cdot 10^{-5}$ vol.% [O] $1.6 \cdot 10^{-4}$ vol.% [N] dew point −72 °C	80	16–17	70–75	40

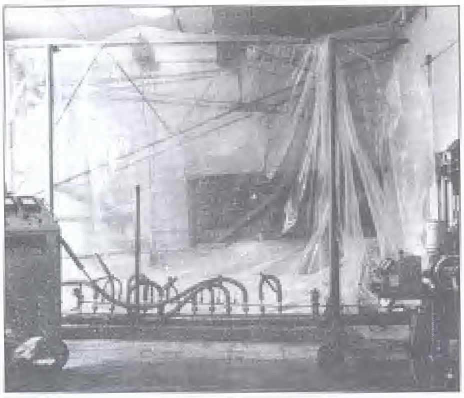

Figure 6. Use of a polyethylene chamber, filled with helium, for determination of the total lack of tightness of a heat-hydraulic model of a niobium alloy

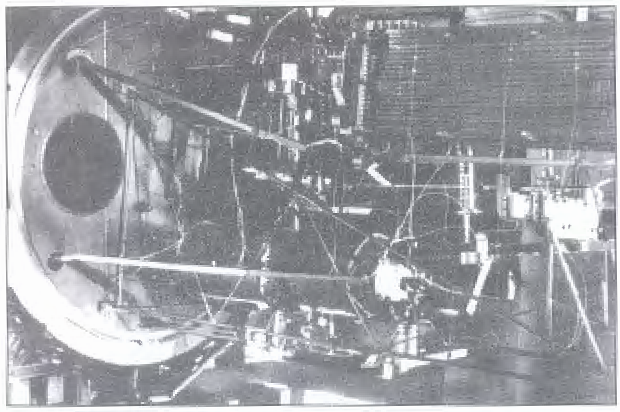

Figure 7. Mounting the lithium-niobium loop into the space-vacuum chamber

I stage — successive welding of butts *1′*, *4′*, *3′*, *5′* and *2′* on ∅ 28×1 mm tubes (see Figure 3);

II stage — successive welding of butts *7′*, *9′*, *8′* and *6′* on ∅ 12×1 mm tubes (see Figures 3 and 5).

After welding the captive microchambers were dismantled and the item in the jig was subjected to the following control-technological tests [13]:

- visual examination of welded joints that did not reveal any cracks or pores, coming to the surface or craters in the field welded joints;
- vacuum testing for local leaks. For this purpose a helium leak detector of PTI type was connected to the jig vacuum system;
- pneumatic testing at the pressure of 13.5 atm of pure helium for 10 min;
- repeated vacuum testing for local leaks, that demonstrated their absence;
- determination of the total lack of tightness by the mass-spectrometric method. The item was placed in a polyethylene shell, filled with helium (Figure 6), with the inserted calibrated leak. The total lack of tightness was 0.4 Pa, this being not more than the value, indicated by the item specification.

Corrosion testing of welded tubular samples in liquid lithium demonstrated that their corrosion resistance is close to that of monolithic tubular samples of the same niobium alloy. Control- technological testing and subsequent testing of the heat-hydraulic model of a niobium alloy, filled with lithium, in a space-vacuum chamber (Figure 7), demonstrated the high quality of welds, made in site [5].

CONCLUSIONS

1. Technology of erection assembly-welding of complex tubular structures in the jig has been developed.

2. Special equipment has been developed to conduct erection assembly-welding of ramified tubular structures of reactive metals in the jig.

3. A welded heat-hydraulic model of a niobium alloy with the heat power of 300 kW has been made. Corrosion studies of welded samples in liquid lithium and model testing under the conditions of subsequent service demonstrated the high quality of the welds, made in site.

1. Balandin, Yu.F., Markov, V.G. (1961) *Structural materials for units with liquid-metal heat-transfer liquids*. Leningrad: Sudpromgiz.
2. Distefano, I.R., Hoffman, E.E. (1964) *The science and technology of tungsten, tantalum, molybdenum, niobium and their alloys*. New York: Pergamon Press.
3. Nikitin, V.I. (1967) *Physico-chemical phenomena at the action of liquid metals on solid metals*. Moscow: Atomizdat.
4. Popovich, V.V., Voznyj, T.D. (1976) Short-time strength of 5VMTs alloy at elevated pressure of liquid-metal media. *Fiz.-Khim. Mekhanika Materialov*, **6**, 64–67.
5. (1996) *S.P. Korolyov Rocket Space Corporation «Energiya»*. Ed. by Yu.P. Semenov. Moscow: RKK «Energiya».
6. Gurevich, S.M., Nerodenko, M.M., Kharchenko, G.K. et al. (1982) *Metallurgy and technology of welding of refractory metals and alloys on their base*. Kyiv: Naukova Dumka.
7. (1991) *Welding and materials being welded*. Vol. 1. Weldability of materials. Ed. by E.L. Makarov. Moscow: Metallurgia.
8. Asnis, A.E., Goncharov, A.B., Nerodenko, M.M. et al. (1995) Welding of refractory metals. *Welding and Surfacing Rev.*, Vol. 5, Part 1. Harwood A.P.
9. (1998) *Welding Handbook*. 8th ed. Miami: AWS.
10. Nazarenko, O.K., Kajdalov, A.A., Kovbasenko, S.N. et al. (1987) *Electron beam welding*. Ed. by B.E. Paton. Kyiv: Naukova Dumka.
11. Gurevich, S.M., Zamkov, V.N., Blashchuk, V.E. et al. (1986) *Metallurgy and technology of welding of titanium and its alloys*. 2nd ed. Kyiv: Naukova Dumka.
12. Gurevich, S.M. (1990) *Handbook on welding of non-ferrous metals*. 2nd ed. Ed. by V.N. Zamkov. Kyiv: Naukova Dumka.
13. Troitsky, V.A. (1997) *Quick-reference guide on quality control of welded joints*. Kyiv: PWI.

DEPOSITION OF OXIDE COATINGS ON SURFACES OF PRODUCTS OF ALUMINIUM-BASED ALLOYS

Yu.N. TYURIN[1], **M.L. ZHADKEVICH**[1], **S.I. GOLOVENKO**[1] and **N.M. CHIGRINOVA**[2]
[1]The E.O. Paton Electric Welding Institute, NASU, Kyiv, Ukraine
[2]NIIPM with PP, Minsk, Belarus

The theory of conductivity of the electrolyte in a microdischarge process of oxidising of the working surfaces of products from the aluminium-based alloys is considered. Technology and technological fixture for the formation of a porous oxide coating on the surface of piston combustion chamber and a compact coating of up to 150 μm thickness and hardness up to 8 GPa on the inner surface of the cylinder are developed. The technology makes it possible to form the composite coatings with introducing dispersed ceramic particles. The offered technological fixture provides the coating formation on the working surfaces of the products manufactured from the metals used for valves.

Key words: *microarc oxidising, oxide coatings, aluminium-based alloys, technology, equipment*

Industry is widely using light-alloy products, where the working surfaces are inaccessible for thermal spraying of coatings (inner surfaces of cylinders, mounting surfaces of cases and structures, inner cavities of pistons, engine combustion chambers, etc.). As shown by service experience, it is rational to deposit a wear-resistant compact coating with a low surface roughness on the working surfaces of the cylinders. A porous coating should be formed on the walls of the combustion chamber. The latter is made so that the porosity on the surface were up to 50 %, and that at the base up to 10 %. In addition, it is alloyed with rare-earth metals, mineral fibres and dispersed materials. In any case it should have a minimal level of stresses and high degree of adhesion to the substrate.

Technologies of producing coatings, based on anode-spark processes in water-base electrolytes, are extensively used now [1, 2]. They feature low consumption of material and energy resources and simplicity of equipment. Application of these technologies is limited, however, by the absence of specific procedural decisions, concerning coating deposition in difficult-of-access places. The paper proposes solutions and principles of developing a technology for coating application on surfaces of various products.

An electrolytic cell with minimal electrode spacing and a schematic of feeding the electrolyte and dispersed mineral powders or salts have been developed that are universal for different technological solutions. Application of the developments allows simplification of the technology of producing various composite coatings on the surface of complex-shaped products.

Electrolytic-plasma cell. A feature of the anode-spark processes or, as they are also called microarc oxidising (MAO) is application of the electric discharge energy for processing of the product surface in the electrolyte. These processes are chiefly used in the technologies of coating deposition on products of metals, used to make valves, for instance, aluminium. Extensive research [1–10] revealed the features of oxide formation at the electric field intensity, causing the coating microbreakdowns. Investigation results allowed forecasting the thickness of oxide coatings, depending on the electric field intensity in the range of 3 to 1000 μm [4].

Oxidising was performed with microarc discharges that form on the surface in the case of application of process modes with a forced increase of the electric field voltage after formation of an oxide layer of a certain thickness. Discharge time is varied between $1\cdot10^{-1}$ and $1\cdot10^{-3}$ s. The start of the oxide layer breakdown is of a massive nature, being accompanied by an abrupt (up to 10 A/cm^2) rise of electric current. Discharges are gradually extinguished with time and with the increase of coating thickness and electric strength. Addition of rare-earth element salts to the electrolyte or dispersed mineral powders allows the coating to be alloyed. Anode-cathode mode or mode of alternation of the anode and the cathode components of current allow intensification of the technology and production of compact coatings [5].

The process of microplasma oxidising is accompanied by formation of complex oxides of aluminium and metals, included into the complex anion of the electrolyte [6]. For instance, addition of iron and copper anions to the electrolyte provides formation of composite oxide coatings with high service properties. In the steady-state mode of oxidising the current density is 0.1–0.5 A/cm^2.

Specialised power sources were developed for microarc oxidising that provide regulation of amplitude values of current (0–170 A) and voltage (0–1 kV), both in the anode and the cathode pulse modes and the ability of making the anode half-period longer than the cathode half-period [7].

The main parameters, allowing control of the process of microarc oxidising and coating properties, are electrolyte concentration, current voltage and density, temperature, duration of the process, alloy composition and modes of its heat treatment [8]. Corrosion resistance and wear resistance of samples change several dozen times, depending on these parameters.

Microarc oxidising technology mostly uses parts immersion into the electrolyte [9]. Depending on the electrolyte composition, coatings of a colour from milk-white to black and with a high resistance to atmospheric corrosion are produced on the surface of aluminium alloy products. Anhydride coatings are formed on titanium alloys, which allows the friction factors to be reduced by 2 to 3 times.

From publications on anode-spark and cathode processes of surface modifying [1–10] it follows, that technology developers do not use the possibility of technology optimisation by controlling the conductivity of the electrolyte inter-electrode layer. This paper proposes such a method of regulation of the electrolyte conductivity. A special electrolyte cell was developed with this purpose (Figure 1) that incorporates a casing of a dielectric material and a metal electrode (anode) of diameter D. Electrolyte is fed to the product surface through holes in the electrode. Geometrical relationships of the cell characteristic dimensions and values of electrolyte pressure influence the rate of its flowing in the inter-electrode gap.

Cross effects are known to take place between the electrodes in the electrolyte volume [11]. On the one hand, the electric field creates in the flowing medium bulk «ponderomotive» forces of a mechanical nature, that in the hydrodynamics equations are summed up with the forces of the inertia, gravity, baric and viscous nature. On the other hand, convective currents form in the hydrodynamic flows of electrolyte ions. Current density in the electrolyte is the sum of densities of three independent currents, namely conduction or «migration», diffusion and convective currents. The ions of conduction current are moving in the liquid under the impact of electrostatic forces, irrespective of their own concentration or motion of the entire liquid. In the case of diffusion current, ions of the same kind diffuse under the impact of osmotic pressure relative to the surrounding liquid, independent of the electric field intensity or liquid motion. At convective current the ions are moved by the flowing solution, as if they were «frozen» into the neutral fluid, independent of the field intensity or their concentration gradient.

A linear combination of currents of three densities in the approximation of complete dissociation is described for each kind of ions by Nerist–Planck relation [12]:

$$J_i = u_i p_i E - \varphi_0 u_i / z_i \operatorname{grad} p_i + v p_i, \qquad (1)$$

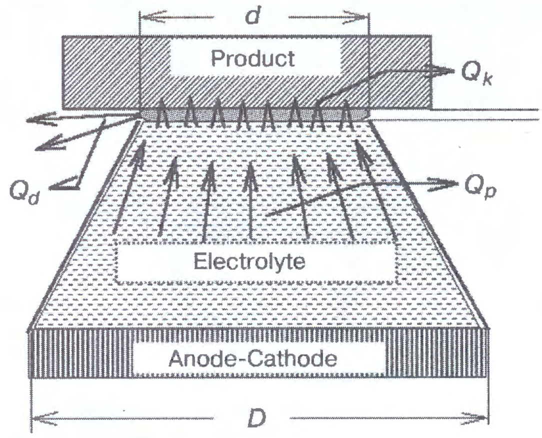

Figure 1. Schematic of a hydrodynamic electrolytic cell for microarc oxidising: d — diameter of outlet nozzle of the cell (cathode); D — diameter of metal electrode (anode)

where J_i is the current density, due to ions of kind i; u_i is the mobility of ions of kind $i = 1, 2, 3, ..., n$; $p_i = n_i z_i e$ is the local density of electric charge distribution (here n_i is the ion concentration; z_i is the valency of ions of kind $i = 1, 2, 3 ..., n$; e is the modulus of the electron charge); E is the electric field intensity; $\varphi_0 = kT/e$ is the specific osmotic potential, equal to 25.9 mV for water solutions at room temperature (k is the Boltzmann constant; T is the electrolyte temperature); v is the velocity of the electrolyte flow.

Simple and complex ions form in the water solution of salts. Anions release the excess electrons, when passing through the anode hole, cations are entrained by the hydrodynamic flow of electrolyte and recombine on the cathode — the solid surface of the product.

Ions interact in a quite complicated manner with each other, the electrodes and the insulating walls of the heater. At a large charge and high velocity of the electrolyte flowing, convection current is much higher, than the diffusion and migration currents, allowing them to be ignored in calculations. Experimental results demonstrated that the electrolyte conductivity can be increased 3 to 4 times and its heating losses can be significantly reduced just at the expense of the hydrodynamic component. Electric energy conversion proceeds in the main layer on the modified surface of the product. Energy distribution in the electrolyte cell can be represented in the following form (Figure 1):

$$Q_k = UJ - Q_p - Q_d, \qquad (2)$$

where Q_k is the energy, consumed in formation of electric discharges; U is the voltage between the anode and the cathode; I is the electric current, flowing through the electrolytic cell from the metal cathode to the product surface; Q_p is the energy consumed in heating and evaporation of electrolyte; Q_d is the radiation energy.

As the microarc power is not high, dissipation of the radiation energy can be neglected. Electrolyte heating results from the diffusion and migration currents. As

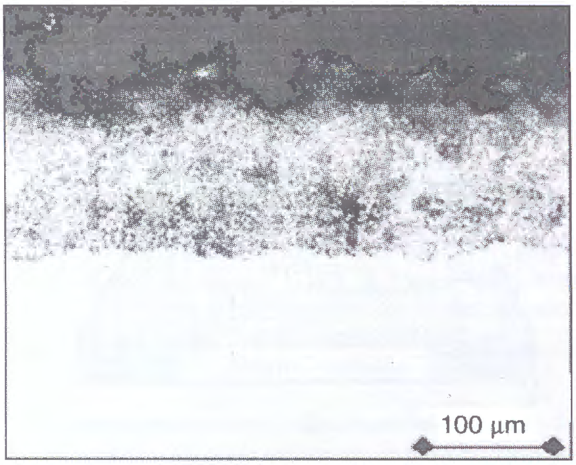

Figure 2. A layer of oxide coating on the surface of a piston combustion chamber

the diffusion mechanism of conductivity is mostly implemented in the cell, this accounts for the low power losses for the electrolyte heating. Experiments showed, that they amount up to 10 % of the entire consumed power. The main amount of energy is consumed for microarc formation and local heating of the surface layer of oxides before the start of melting.

Energy is transferred to the surface through the plasma layer in the form of non-equilibrium electric discharges of a specific shape [13]. By Yu.P. Raizer classification the discharges can be considered to be distributed (film) discharges with a low temperature of gas. The discharges have a diffusion fixation to the surface of electrolyte — «liquid electrode». Under the impact of varying pressure in the places of discharge fixation, the electrolyte surface is imparted oscillatory motion. As a result the gap between the surfaces of liquid electrolyte and the solid changes periodically. Electric field intensity is not high (up to 80 to 200 V/m) in the electrolyte proper, but in the layer, adjacent to the product surface (boundary), it has a variable magnitude ($1\cdot10^4$–$11\cdot10^6$ V/m). The intensity primarily depends on the voltage and distance between the boundaries of the media with different conductivity. Voltage drop in the electrolyte layer between the electrodes is not more than 25 V, and in the near-boundary layer it is 300 to 1000 V.

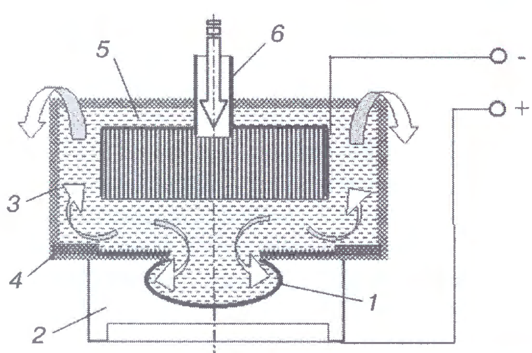

Figure 3. Schematic of a unit for coating application on the walls of the piston combustion chamber (*1*–*5* — see explanation in the text)

Characteristic modes of interaction of the surfaces of the liquid and solid electrode can be traced, depending on voltage and temperature of the electrolyte. At the initial moment, when the oxide layer has not formed, a local overheating and electrolysis of the electrolyte are observed. Voltage U = 120–200 V is sufficient for this process to proceed. Oscillation of the electrolyte surface provides a local increase of the electric field intensity in the gap. Microarc discharges run between the electrolyte and the conducting sections on the product surface. At the same time the surfaces are cooled by the electrolyte. Variation of the discharge luminosity on the anode layer and abrupt changes of the current magnitude, as well as electrolyte boiling and electrolysis are observed simultaneously.

Electrolysis results in evolution of oxygen on the anode that is activated by the electric discharges and oxidises the product metal. To maintain the electric mode of oxidation as the oxide layer becomes thicker, the electric field intensity should be increased until the microarc discharges become stabilised. The oxidising process is of a gradually extinguishing kind, its resumption requiring an increase of the electric field intensity up to a value, resulting in the oxide layer breakdown and discharge running.

Experience of technology application. The main purpose of electrolytic cells (see Figure 1) is to provide a high intensity of the electric field on the surface being oxidised, lower the power losses in the electrolyte and stabilise the temperature in the near-boundary layer. All this eventually improves the process efficiency and provides formation of compact coatings on the working surfaces of the products.

The proposed technology was used to apply a heat-protection layer on the walls of a piston combustion chamber. The piston was made of alloy Al + 6 % Si. Metallographic analysis showed that the produced layer of more than 120 μm thickness, is more dense near the substrate (Figure 2). On the surface it is loose and porous, the thickness of the porous layer is 30 to 50 μm. Microhardness of the oxidised layer depends on the substrate material and is equal to 4.5 to 7.0 GPa. Oxidising was performed in KOH alkali electrolyte at the maximal voltage of 340 V. In pure aluminium oxidising an oxide film 250 μm thick of 7.0 to 8.0 GPa microhardness formed on the product surface.

A special unit was developed for microarc oxidising of the bottom on the piston working surfaces (Figure 3). In this unit the electrolytic cell includes wall *1* and bottom *2* of the piston combustion chamber. Cell casing *4* is made of a non-electrically conducting material, that is fastened to the piston bottom by rubber collar *3*. The unit has the capability of a forced feed of electrolyte. Electrolyte is fed through piping *6* from the top of the cell via metal porous electrode

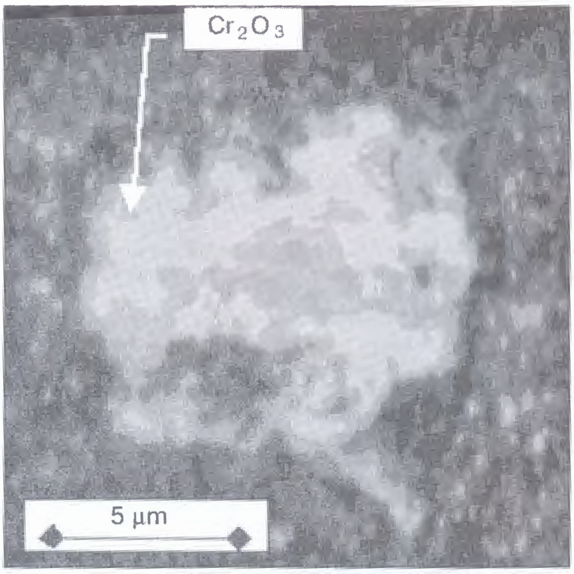

Figure 4. Appearance of a chromium oxide particle in the oxide coating layer

5. Electrode *5* has channels, where recombination of positive ions and formation of negative ions proceed. In implementation of the technology the electrolyte closes the electric circuit between the surfaces of the product and channels in the electrode. The number of negative ions that move from the cathode to the walls of the combustion chamber (anode) depends on the electric field intensity and on the velocity (volume) of the flowing electrolyte (see expression (1)). In Figure 3 arrows indicate the flow of electrolyte (together with the ions) from the cathode to the product surface.

The unit allows conducting oxidation at inter-electrode gaps of 20 to 30 mm, this lowering the power losses and provides formation of the oxide layer up to 150 μm thick. Voltage is ≈ 340 V. It is known that the optimal temperature of electrolyte for implementation of the technology is equal to 50–60 °C. Such a temperature is due to heat losses in the electrolytic cell.

Oxidising of the surface of aluminium alloy was conducted in a water solution of KOH salt + Cr_2O_3 powder. Addition of solid particles of 10 μm size to the electrolyte creates the necessary conditions for their displacement to the product surface and increase of the weight fraction of these particles near the surface being oxidised, thus enhancing the effectiveness of the technology of producing composite coatings. For instance, addition of chromium oxide particles of up to 10 μm size (their weight fraction in the electrolyte being 2–3 %) results in about 15 % weight fraction of particles at the product surface.

Product oxidising was conducted as follows. At the initial moment of time electric current at 110 V voltage was connected to the inter-electrode gap. As a result, an oxide film formed on the product surface in 60 s, lowering the current density by 50 times (to 10 mA/cm^2). Then voltage was increased up to

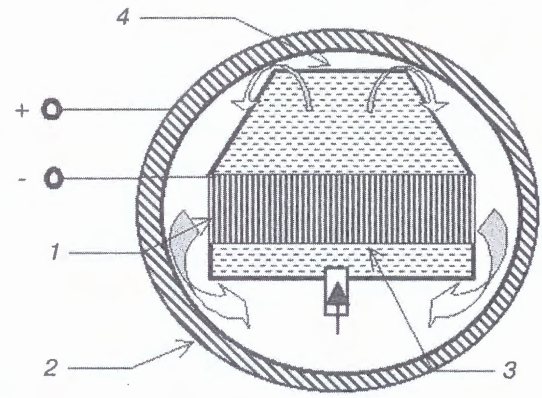

Figure 5. Schematic of a unit for oxidising the cylinder inner surface (*1–4* – see explanation in the text)

200 V, current density being 2 mA/cm^2. After soaking for 5 min, voltage was increased up to 270 V. Its further increase up to 340 V provided formation of a coating of 150 μm thickness, containing fused-in particles of chromium oxide. Figure 4 shows the appearance of a disperse particle in a layer of an oxide coating on aluminium, produced by microarc oxidising. X-ray phase analysis revealed that the coating base is a mixture of aluminium oxide γ-, δ- and α-Al_2O_3. The latter is mainly concentrated at the oxide–metal boundary.

The proposed technological sequence ensures addition of dispersed non-metallic particles to the electrolyte, their displacement and fixation on the product surface in the layer of aluminium oxide. Powders of diamond, metal oxides, carbides, nitrides, spinels, etc. can be used.

Electrolyte anions deposit mainly on the surface of dispersed particles, this giving them a negative charge and providing their displacement to the product surface under the impact of electrophoretic forces. When anion concentration is increased and the electrolyte temperature is decreased, the effect of adding dispersed particles to the coating together with the anions, is enhanced.

The above technology was used for processing a test batch of diesel engine pistons that passed bench thermal cycling tests. Testing results showed that the coating stood $1.5 \cdot 10^6$ cycles without fracture.

In order to form coatings of oxides on the inner surface of the cylinder we proposed a device (Fi-

Figure 6. A layer on the inner surface of the cylinder, produced by simultaneous oxidising and abrasive treatment

gure 5) to introduce electrolytic cell *3* inside cylinder *2*. It incorporates porous electrode *1*, through which electrolyte is passed. The latter closes the electric circuit between the electrode and cylinder surface in gap *4*, then flows over the cylinder surface and is removed from the product being strengthened. In the hydraulic system the electrolyte is cleaned, cooled, the quantity of dispersed particles is replenished and then the electrolyte is fed again into the electrolytic cell.

To produce a hard compact coating, performance of abrasive treatment of the cylinder surface simultaneously with oxidising is also envisaged. This destroys the upper, porous, loose layer of the coating and creates conditions for defect melting and improvement of the coating density.

Figure 6 gives a section of the coating, produced by microarc oxidising with simultaneous processing with abrasive sticks. A compact oxide coating of up to 150 μm thickness of a uniform density across the entire thickness was produced, its hardness reaching 10 GPa, adhesion of the coating layer to the base being 300 MPa, surface roughness after oxidation being 3 to 5 μm.

CONCLUSIONS

1. Analysis of electrolyte conductivity was the basis to develop the technology and fixture that provide a high-quality local oxide coating in difficult-of-access places of a product, made of Al-base alloys.

2. Developed principles of the technology are versatile and allow designing a device for application of high-quality oxide coatings on difficult-of-access surfaces of products, for instance, on inner surfaces of a cylinder or piston bottom.

1. Chernenko, V.I., Snezhko, L.A., Papanova, I.I. (1991) *Producing coatings by anode-spark electrolysis*. Leningrad: Khimiya.
2. Chernenko, V.I., Snezhko, L.A., Papanova, I.I. et al. (1995) *Theory and technology of anode processes at high stresses*. Kyiv: Naukova Dumka.
3. Gordienko, P.S. (1996) *Formation of coatings on anode-polarized electrodes in aqueous electrolytes at arcing and disruption potentials*. Vladivostok: Dalnauka.
4. Atroshchenko, E.S., Kazantsev, I.A., Rozen, A.E. (1996) Technology of producing coatings by microarc oxidising. *Nov. Promyshl. Tekhnologii*, **1**, 28–33.
5. Markov, G.A., Slonova, A.I., Terleeva, O.P. (1997) Chemical composition, structure and morphology of microplasma coatings. *Zashchita Metallov*, **3**, 289–294.
6. Timoshenko, A.V., Magurova, Yu.V., Artyomova, S.Yu. (1996) Influence of additives to electrolyte for oxidising of complex compounds on process of deposition of microplasma coatings and their properties. *Fizika i Khimiya Obrab. Materialov*, **2**, 57–64.
7. Gorchakov, A.I., Karpoukhov, A.N., Oshepkov, D.A. (1997) Development of power electric circuit for microarc oxidising unit. In: *Problems of modern materials and technologies*. Perm.
8. Atroshchenko, E.S., Kazantsev, I.A., Rozen, A.E. et al. (1996) Applications of coatings produced by microarc oxidising. *Fizika i Khimiya Obrab. Materialov*, **3**, 8–11.
9. Korkosh, S.V. (1998) Experience of microarc oxidising of products from titanium and aluminium alloys. *Voprosy Materialoved.*, **1**, 40–42.
10. Yerokhin, A.L., Nie, X., Leyland, A. et al. (1999) Plasma electrolysis for surface engineering. *Surface and Coating Technology*, **122**, 73–93.
11. Ostroumov, G.A. (1979) *Interaction between electric and hydrodynamic fields*. Moscow: Nauka.
12. Plank, M. (1980) Über die Erzeugung von Elektrzität und Wärme in Elektrolyten. *Ann. Phys. Chem.*, **39**, 161–186.
13. Raizer, Yu.P. (1987) *Physics of gas discharge*. Moscow: Nauka.

NEW MACHINE FOR ELECTROSLAG WELDING OF LARGE PARTS AT JSC «NKMBF»

V.A. NEVIDOMSKY[1], **S.G. KRASILNIKOV**[1], **A.D. PANIN**[1], **V.P. GULIDA**[1] and **I.I. LYCHKO**[2]
[1]JSC «NKMBF», Kramatorsk, Ukraine
[2]The E.O. Paton Electric Welding Institute, NASU, Kyiv, Ukraine

Versatile machine for electroslag welding of large-size plates for welded-forged die blocks of forge-and-press equipment is described. Parallel upgrading of the steel-making technology and starting up of a new machine made it possible to produce quality electroslag welded joints in plates for presses with a capacity of 750 MN.

Key words: electroslag welding, versatile machine, die blocks, large-size billets, metal quality

Joint-Stock Company «Novo-Kramatorsky Machine-Building Factory» (JSC «NKMBF») was the first to apply, in collaboration with the E.O. Paton Electric Welding Institute, the electroslag welding (ESW) technology for heavy engineering. Technologies for manufacture of large and heavy members with a weight of up to 300 t for the fabrication of unique forge-and-press, rolling, power generation and other facilities exported by the Factory to many countries all over the world were developed and mastered on the basis of a 50-year experience of the successful application of ESW [1–4].

Under conditions of economic difficulties of the last decade and a drastic decrease in demand for traditional heavy engineering products, the Factory succeeded in retaining its high-skilled staff and unique production base and raised the level and competitiveness of its equipment and technologies, including in the field of producing large billets using ESW.

Today, when major metallurgical enterprises of Western and CIS countries are going through a restructuring period and standing on the threshold of renovation and reconstruction, as their last projects were completed more than 20 years ago [5], JSC «NKMBF» is prepared to meet the customers' demands. This is evidenced by inquiries the Factory receives from Russia and European countries.

Within the frames of reconstruction of powerful hydraulic stamping presses with a capacity of 750 MN (earlier made by JSC «NKMBF»), Russian metallurgical enterprises, such as Open Joint-Stock Company «Association «Siberian Aluminium» (Samara) and JSC «VSMPO» (Verkhnyaya Salda), ordered to the Factory to manufacture die blocks consisting of large base plates.

For the manufacture of the above welded-forged plates, as well as expecting new orders, the Factory built and commissioned a new versatile machine of a gantry type (see cover page 1) for ESW of thick-walled large-size billets. It meets the highest requirements and is superior in its technical capabilities to machines of a similar type available in the CIS countries and abroad. The machine is capable of making joints in sections of up to 5000×6000 mm in size (thickness of parts welded by weld length). The ESW technology provides for automated computer monitoring of welding and thermal-deformation cycle parameters.

The machine is equipped with a welding hardware of the PWI, custom-made according to the work statement of the Factory. The hardware includes two automatic devices ASh-110, each fitted with three-electrode feed mechanisms for consumable-nozzle (12 pcs) ESW, power units, i.e. transformers A-481E (4 pcs), and panels with control cabinets. Reliability of the ESW process performed using this hardware is achieved owing to the system of automatic backing up of wires, allowing a continuous feed of electrode wires (72 pcs) to the welding zone. In the initial state, during the ESW process, while working wires are fed to the welding zone the backup ones are in a standby mode. In the case of interruption of the feed of the working wires, the control system automatically switches up the feed of the backup ones. Upon repair of a malfunction in the feed of the working wires, the system is brought up into the initial state.

Main units and mechanisms of the machine are intended for performing the following functions.

Gantry of the machine with a hoisting cross-arm, welding hardware and service devices for the ESW process moves on a track over the pit stand deck along its length (the deck is 6300×20000 mm in size).

Each of the two posts of the gantry has a platform with the A-535 automatic device and a service elevator. The A-535 platforms and elevators have drives for vertical and horizontal displacement. They serve for formation of the weld using a forming shoe and visual tracking of the consumable-nozzle ESW process using the ASh-110 automatic devices. In addition, the platforms with the A-535 automatic devices and elevators can be used to perform electrode-wire ESW of parts with thickness of up to 450 mm.

Panels with control cabinets for the ASh-110 automatic devices are located on the first floor of the two-floor cross-arm. Two self-propelled cars are located on the second floor, the ASh-110 automatic device, system of holders for 36 spools with welding

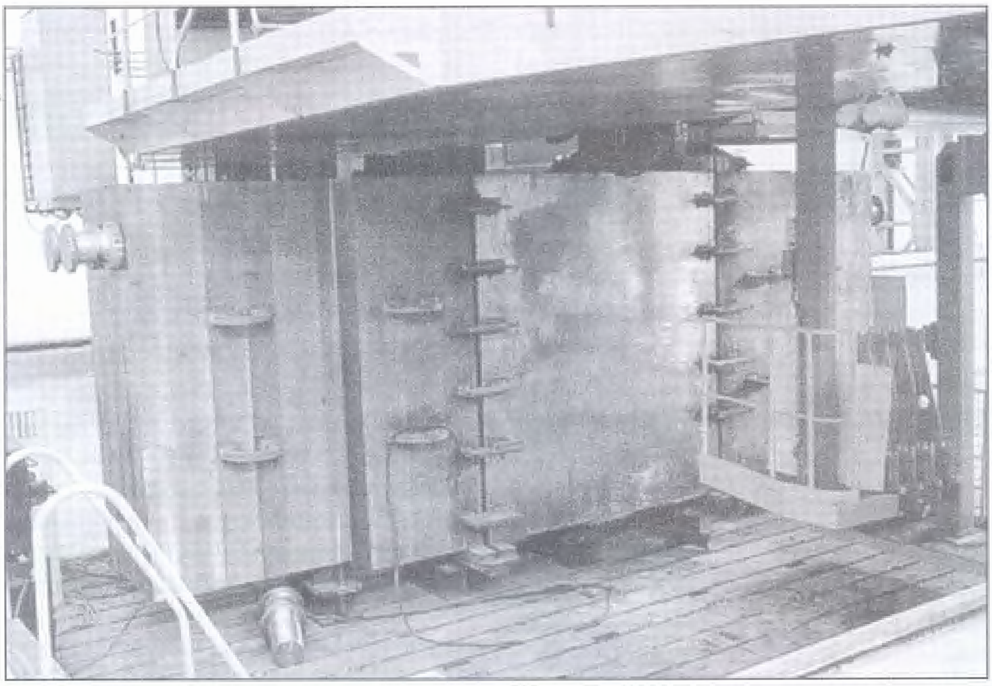

General view of the upper base plate 170 t in weight for the 750 MN stamping press, assembled for ESW

wire and two A-481E welding transformers being mounted on each of the cars. The automatic devices with nozzle holders are hung under the cars and located in the cross-arm space between the floors. The cross-arm provides positioning of the ASh-110 automatic devices at a required height from the stand deck, depending upon dimensions of a workpiece and length of the joints welded. The cars move along the cross-arm and fixed, depending upon location of the joints assembled for ESW. Consumable-nozzle welding using the ASh-110 automatic devices can be carried out into one weld pool for workpieces over 2500 mm thick, or into two weld pools used separately for simultaneous or successive welding of two joints each up to 2500 mm thick. The cross-arm drive has a gradually regulated vertical displacement speed, which makes it possible to perform ESW using plate electrodes or electroslag surfacing using consumable electrodes (surfacing of rolls with cast iron tubular electrode).

To ensure a liquid start in excitation of the electroslag process, the machine is equipped with two flux-melting devices.

The machine is completed with an independent pumping station for emergency water supply to water cool forming shoes and welding transformers.

To perform hoisting operations in preparation of workpieces for ESW, the gantry of the machine is equipped with a telpher and an overhead travelling crane with a capacity of 0.5 t.

The new equipment and technology were originally used for ESW of two plates, each welded from three forgings.

Manufacture of large billets of low-alloy Fe–Mn–Ni–Mo–V and Fe–Cr–Ni–Mo–V steels of medium and increased strength for critical heavy-loaded parts of different machines and facilities involves metallurgical problems associated with processes of forging, ESW and heat treatment, which are characterized by high-temperature cycling [6, 7].

Peculiarities of ESW of large-size billets include a considerable heat input, which leads to formation of marked strains and a high level of residual welding stresses. A coarse-grained structure due to overheating, which is characterized by low values of ductility and impact toughness, is formed in the weld and HAZ metal under the effect of a thermal cycle of ESW. The presence of the above main alloying elements may decrease resistance of the ES welded joints to hot cracking of the weld metal and tear-type cracking of the near-weld zone, aggravate consequences of overheating and increase susceptibility of welded joints to brittle fracture. An increase in strength and degree of alloying of steels welded is accompanied by deterioration in their technological properties and decrease in permissible sizes of defects under the brittle fracture conditions.

The risk of brittle fracture depends in many respects upon the quality of metal, its sulphur and phosphorus content, contamination with non-metallic inclusions and hydrogen content. Therefore, the paramount consideration should be given to improvement of the quality of metal and its mechanical properties.

In the last years the Factory has mastered a number of advanced processes on upgrading of the steel-making technology, which allowed a substantial improvement in the quality indicators of steel used for large forged and pressed ingots. Thus, processing of metal with the ladle-furnace unit provides a sulphur content of down to 0.005–0.01 % and phosphorus content of down to 0.008 %. Vacuum processing of metal using a steam-ejection pump (degassing in the jet and ladle and double degassing) provides the following content of gases: H_2 — 1.8–2.2 (2.0–2.5 $cm^3/100$ g), O_2 — 25.0–45.0 and N_2 — 35.0– 45.0 ppm.

Mastering of the new technologies for production of large billets to manufacture welded-forged parts provided prerequisites for making sound electroslag welded joints in the fabrication of plates for the 750 MN presses.

Forgings for electroslag welding were preliminarily heat treated by annealing. The ESW plates of steel 20KhN3MFA (C — 0.2; Cr — 1.0; Ni — 3.0; V — 0.3; Mo – 0.7 wt.%) were made in two stages: assembly and ESW of two parts of a plate with subsequent immediate loading into the furnace for heat treatment (normalizing + tempering), then abutting the third billet and ESW of the second weld followed by final heat treatment (double normalizing + tempering) to ensure the required level of mechanical properties of the product.

ESW of two joints in the second steel plate (see the Figure) was performed without intermediate heat treatment. Heat treatment (normalizing + tempering) was carried out after successive performance of ESW of all the joints of the plate.

Visual examination of the welds revealed no external defects. The 100 % ultrasonic inspection of the welded joints confirmed the high quality of the welds. In addition, the welds were subjected to metallography. No defects of the type of discontinuities, nonmetallic inclusions and tear-type cracks were detected on the Bauman imprints and in a transversely etched macrostructure of the external regions of the root and top sides of the welds and HAZ.

The machine put into operation and combined with the improved technology is reliable and convenient to control and maintain in terms of providing stability of a complicated electroslag process.

Therefore, commercial validation by JSC «NKMBF» of the new ESW machine in manufacture of plates for the 750 MN stamping presses, using a package of arrangements that improve quality of metal of billets, showed a new technological potential for making large high-quality weldments and opened up new prospects for widening services that could be rendered to companies and enterprises dealing with reconstruction and building of advanced unique machines and facilities.

1. Chernykh, V.V., Vinokurov, V.A., Eregin, A.P. et al. (1989) Solution of problems of supersized welded part manufacturing in heavy engineering. *Avtomatich. Svarka*, **7**, 53–55.
2. Gulida, V.P., Nevidomsky, V.A., Chernykh, V.V. (1999) Electroslag welding and prospectives of his development at the Novokramatorsky machine-building factory. *Ibid.*, **9**, 41–43, 60.
3. Eregin, A.P., Malaj, A.E. (1985) Electroslag welding of large-sized prefabrications for press-forged equipment. *Kuznechno-Shtamp. Proizvodstvo*, **11**, 19–20.
4. Adamenko, V.Ya., Eregin, A.P., Malaj, A.E. (1977) Technological features of welding of 65000 t forse press. *Svarochn. Proizvodstvo*, **11**, 15–17.
5. Werme, A., Eckelsbach, K., Kneppe, G. (1997) The new SSAB Oxelosung heavy plate mill. *Metallurgical Plant and Technology Int.*, **4**, 134–144.
6. Eregin, A.P., Malaj, A.E. (1978) Conditions of formation of near-weld cracks-tears in electroslag welding of Cr–Ni–Mo steels. *Svarochn. Proizvodstvo*, **10**, 26.
7. Modzhuk, M.D., Potapov, N.N. (1988) Metallurgical problems of electroslag welding of low-alloy steels at power engineering. In: *Technology, industrial engineering and management,* Issue 10. TsNIITEItyazhmash.

TECHNOLOGY OF RESTORATION OF GAS TURBINE BLADES

M.L. ZHADKEVICH[1], **A.A. BONDAREV**[1], **V.I. ZELENIN**[1], **V.M. TEPLYUK**[1], **S.I. SIDORENKO**[2], **V.A. MOKHORT**[2], **Yu.V. NESTERENKO**[2] and **O.V. ZELENIN**[2]
[1]The E.O. Paton Electric Welding Institute, NASU, Kyiv, Ukraine
[2]NTUU «KPI»

Technology envisages preliminary deposition by microplasma process of a protective coating on high-nickel alloy blade with its subsequent remelting by the electron beam. Programmed heat input provides partial melting of the matrix to not less than 30–50 μm depth.

Key words: *microplasma deposition of coatings, electron beam processing, gas turbine blades, high-temperature high-nickel alloys, defects*

In high-temperature operation the gas turbine blades are exposed to alternating loads, as well as corrosive and abrasive wear. High-temperature high-nickel alloys are used as blade material. The working surfaces of the parts develop microdefects in operation. Their elimination is related to prevention of the alloy cracking in the HAZ during application of the protective coating by surfacing or spraying or during its heat treatment [1, 2].

Structural state of the applied coatings (for instance, those based on Ni–Cr–W–Mo–Al (ChS-40) and Ni–Co–W–Mo–Al (ChS-70) alloys) is characterized by the presence of γ-solid solution of the alloying elements, γ′-phase (for instance, Ni_3Al), γ–γ′ eutectics. Carbides of different dispersity, more seldom carbonitrides and other compounds of the alloying and impurity elements of the alloy can be located in the solid solution along the grain boundaries. In surfacing by the arc or plasma process at significant thermal impact, the presence of dispersed phase precipitations leads to internal stress concentration in the deposited layer, preventing the occurrence of the diffusion processes, which is exactly what promotes cracking.

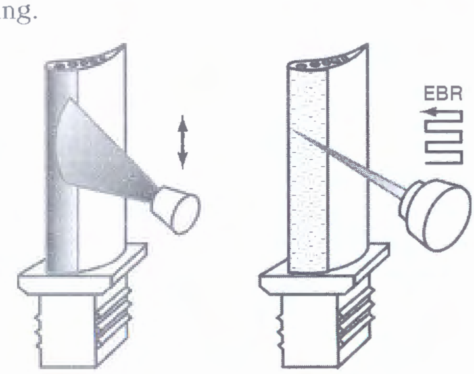

Figure 1. Flow chart of applying a powder-like filler in a section of blade restoration (*a*) and electron beam remelting of a blade in the restoration zone (*b*)

The E.O. Paton Electric Welding Institute developed a new technology of restoration of parts of high-temperature high-nickel alloys. Its fundamental difference from the traditional technologies consists in a separate application of a powder-like material of the appropriate composition on a prepared surface and subsequent surface melting of the produced layer by the electron beam (Figure 1).

The protective coating material is deposited by the microplasma process without formation of the liquid phase with controlling of the applied layer thickness (by using ingenious powder metering devices) and the base material temperature. Subsequent surface melting is performed by a highly concentrated electron beam with a programmable heat input, so as to provide partial melting of the base material to the depth of not more, than 30–50 μm. Investigations showed that separate performance of these operations leads to minimizing the thermal impact on the base material, limits the mixing of the matrix metal and the deposited layer, this resulting in formation of a deposited layer with the required surface properties. This allows restoring the gas turbine blades with the inner cooling channels with the wall thickness below 1 mm. Residual welding deformations of the parts are absent and cracks do not form. It is found that the coating layer thickness of 150–200 μm is optimal. In the case of a greater depth of the corrosive attack repetition of such processing operations is allowed without the risk of development of hot cracks or evident changes in the structure of various sections of the processed zone.

Microstructural investigations of the coatings performed by the method of scanning electron microscopy and X-ray microprobe analysis demonstrated the high homogeneity of the structure, absence of gas porosity and non-metallic inclusions.

Microstructure of the surface layer of the filler surface-melted by the electron beam in the defect zone on the blade of ChS-70 alloy is shown in Figure 2. No defects were found in the coating material or in

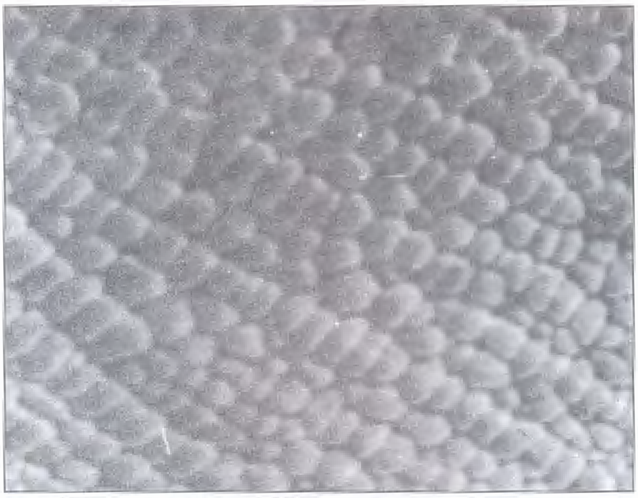

Figure 2. Microstructure of a section surface-melted by the electron beam in the zone of defect restoration (×1740)

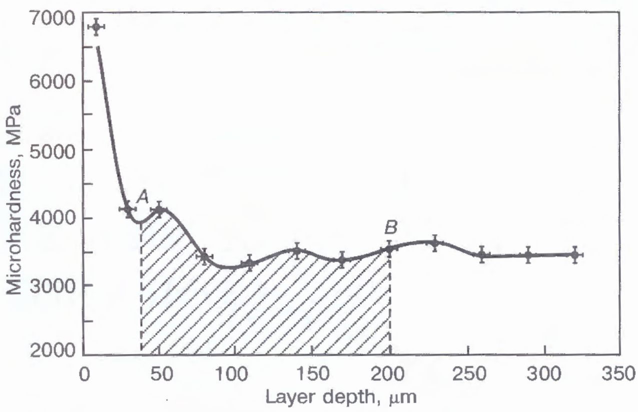

Figure 3. Dependence of microhardness on the depth of the deposited layer (A–B is the damping zone)

the zone of transition from the deposited layer to the base metal of the blade.

The results of X-ray diffraction and electron microscopy investigations demonstrate that the amount and morphology of the γ-phase are practically unchanged after the filler surface melting by the electron beam.

Figure 3 shows the graph of microhardness dependence on the depth of the surface-melted layer. Investigation results indicate that the deposited layer has good adhesion to the matrix material and high mechanical properties (microhardness is up to 7000 MPa at the surface). Another characteristic feature of such surfacing conditions is the presence of a damping zone (section A–B in Figure 3). Formation of such a zone is highly desirable, as it will damp and relieve the alternating stresses to a certain extent in operation.

The results of this work not only provide a deeper insight into the physical concepts of the fundamentals of protective-restoration coating formation on high-temperature nickel alloys, but also allow optimizing the technologies of producing the coatings, reduce the cost of the currently available technologies of defective parts restoration, as it becomes possible to avoid the stage of remelting and casting new parts of expensive high-nickel alloys (their manufacturing cost sometimes is up to several thousand US dollars).

1. Adam, P. (1981) Welding of high-strength alloys for gas turbines. In: *High-temperature alloys for gas turbines*. Ed. by M. Shanin. Moscow: Metallurgia.
2. Dudko, D.A., Bondarev, A.A., Zelenin, V.I. et al. (1998) New method of modifying the surface of parts, operating under extreme conditions. In: *Proc. of Int. Conf. on Welding and Allied Technologies in the XXI Century*. Kyev: PWI.

OPTIMIZATION OF CHARACTERISTICS OF ELECTROACOUSTIC TRANSDUCERS FOR ULTRASONIC WELDING OF THERMOPLASTIC COMPOSITE MATERIALS

N.P. NESTERENKO
The E.O. Paton Electric Welding Institute, NASU, Kyiv, Ukraine

Dependence of electrical and mechanical characteristics of electroacoustic transducers used for ultrasonic welding thermoplastic composite materials on the material of passive elements and position of a piezolayer in the antinode–node system is considered. Comparative analysis is presented for two types of transducers and practical recommendations on optimizing their design are given.

Key words: *ultrasonic welding, thermoplastic composite materials, electroacoustic transducer, optimizing of characteristics*

For the ultrasonic welding (USW) of thermoplastic composite materials (TPCM) the ultrasonic oscillating systems of 0.4–0.6 kW power are widely used. The most important element of these systems is an electromechanical transducer operating in a lower ultrasonic range of frequencies 16–60 kHz. A core-type piezoelectric transducer of Langevin is used as a source of ultrasound [1]. Numerous investigations are devoted to the calculation and designing of the piezotransducers, however, there is no unique approach to the calculation and optimizing their characteristics. This is due to the variety of conditions of operation of transducers and different criteria of evaluation of their effectiveness.

Until recently, the method of equivalent electrical diagrams and method of electrical six terminal networks was the main method of calculation of transducers. The use of these methods limits the feasibility of obtaining information about the distribution of mechanical and temperature parameters of the transducer. However, for the technological processes, in which the loading changes its parameters with time (USW of TPCM items), the need is occurred in a direct evaluation of displacements at the transducer end and stressed state of the piezoceramics. Methods of continuum mechanics give the most complete calculation of a set of thermo- and electromechanial factors. Analysis of transducer behaviour within the scopes of models of continuum mechanics is based to a great extent on using analytical and numerous methods. The main aim of these calculations is to optimize the transducer design, providing the realization of a number of technical requirements, such as efficiency factor, electromechanical and heat conditions, etc.

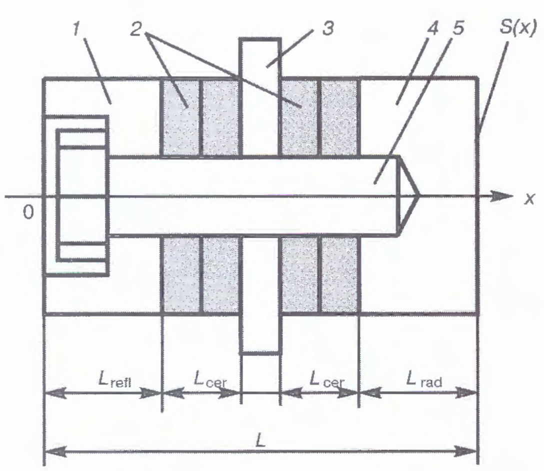

Figure 1. Design of transducer with an intermediate insert (for designations *1*–*5* see the text)

The present article gives results of calculation of two types of piezotransducers using the method of an orthogonal running and also recommendations on optimizing their characteristics depending on the material of cover plates used and position of a piezoactive layer in the antinode–node system.

Figure 1 shows a half-wave transducer with an intermediate metallic insert which is used as a source of mechanical vibrations in USW of TPCM items. It consists of two pairs of piezoceramic rings *2*, an intermediate insert *3*, reflecting *1* and radiating *4* cover plates, which can have a general variable section area $S(x)$. The integrity of a pack, acoustic contact between the elements and the fatigue strength of the piezoceramics are provided by a tightening bolt *5*. St.45, aluminium D16T and titanium VT3-1 alloys and were used as a material of passive elements.

Investigation of resonance (natural) frequencies and shapes of the transducer considered were performed within the scope of a bar theory, taking into account that materials of its elements are linearly-viscoelastic and the ratio $\max_x \sqrt{S(x)} << L$ is fulfilled. The problem statement included the assignment of equations of vibrations for each element of the transducer, determining equations for piezoactive material and material of cover plates, equation of statics and also corresponding mechanical and electrical boundary conditions [2].

The obtained system of differential equations with boundary conditions was solved by a numerical method of orthogonal running. For each variant, defined by the position of a piezoactive material of a constant thickness ($24 \cdot 10^{-3}$ m) and working frequency 20 kHz, the problem for determination of a geometric configuration of the transducer, electroviscoelasticity with allowance for mechanical and dielectric losses in all elements of the transducer was solved. In addition, four variants of transducers made of the following materials were considered depending on the type of passive elements:

1) reflecting cover plate, intermediate insert and radiator of St.45 (below St–St–St);

2) reflecting cover plate of St.45, intermediate insert and radiator of alloy D16T (St–D16T–D16T);

3) all passive elements of alloy D16T (D16T–D16T–D16T);

4) all passive elements of alloy VT3-1 (VT3-1–VT3-1–VT3-1).

The calculations showed that characteristics of the transducer depend on sizes, arrangement and materials of design elements. Thus, the maximum displacement at the working end of the transducer is attained in case of using a reflecting cover plate with a natural acoustic impedance, being higher than the acoustic impedances of ceramics, intermediate insert and radiator (Figure 2). The use of the intermediate insert can change the longitudinal sizes of reflecting and radiating cover plates within the wide ranges. However, in this design the layers of ceramics arranged on different sides of the intermediate insert undergo different mechanical stresses that leads to non-similar temperature conditions of their operation and, as a consequence, to instable operation of all the system. The use of intermediate insert from D16T or VT3-1 of thickness $(3-6) \cdot 10^{-3}$ mm in symmetrical transducers ($L_{refl} = L_{rad}$ and similar material of cover plates) can stabilize their operation due to decrease in dynamic stresses in a piezoactive layer and additional heat removal by this insert.

The design of a high-amplitude transducer with a variable cross-section area $S(x)$ of radiating cover plate and absence of an intermediate insert is more optimum. Depending on the law of changing $S(x)$ at the working end of such transducer the amplitudes of oscillations 5–10 μm are reached. The use of these transducers is especially effective in USW of composite materials on polyvynilchloride matrix [3]. For them, the effect of position of a piezoactive layer on the following parameters was studied: active component of electrical resistance at resonance frequency R; value of amplitude of mechanical displacement at the end of the radiating cover plate u_{max}; consumed electrical power P; coefficient of efficiency of transducer χ; rated amplitude of mechanical stress in a piezoceramic layer σ_{rad}; coefficient of amplification by displacement k_{rad}; dynamic coefficient of electromechanical coupling K_f.

The results of calculations showed that depending on the type of polymer or polymeric matrix of the composite a differentiated approach is required to the design of transducers. Thus, for example, in USW of artificial leathers, items of polyamid, etc. it is rational to arrange the piezoceramic elements closer to the end of a reflecting cover plate, as in this case the growth of amplitude of displacement of end of radiating cover plate and coefficient of exciting effectiveness, decrease in amplitude of a dynamic stress in a piezoceramic layer and consumed electric power are observed. Figure 3 shows that the consumed power for all the variants of transducers is increased with increase in coordinate of ceramics ξ_k ($\xi_k = x/L$). This is explained by the fact that at a constant voltage of the power source the power is increased with a decrease in active electrical resistance of the transducer. It follows from the comparison of Figures 3 and 4 that variant D16T–D16T is advantageous (at absence of intermediate insert) providing a maximum displacement of the end of radiating cover plate at minimum dissipating power. The drawback of this design is decrease in coefficient of electromechanical coupling.

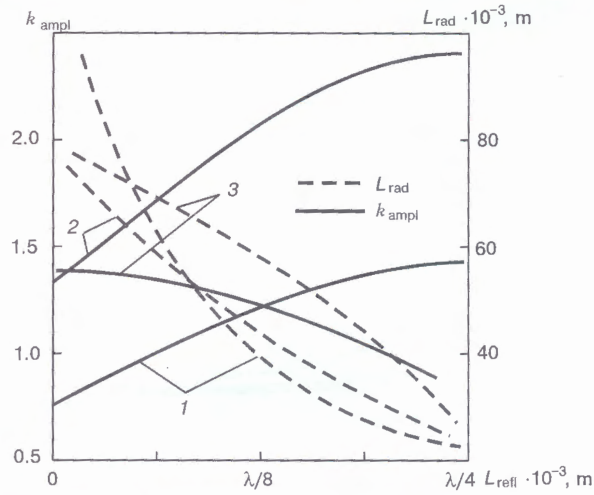

Figure 2. Dependence of coefficient of amplification k_{ampl} (solid curves) and length of radiating cover plate L_{rad} (dashed curves) on the length of reflecting cover plate L_{refl} for cases: *1* — St–St–St; *2* — St–D16T–D16T; *3* — D16T–D16T–D16T

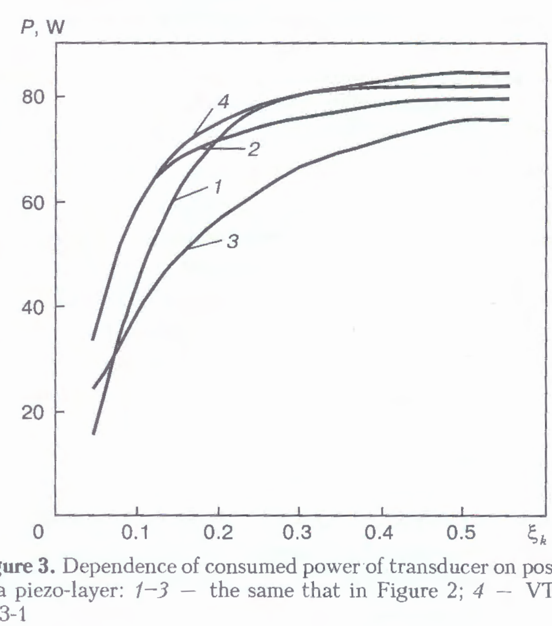

Figure 3. Dependence of consumed power of transducer on position of a piezo-layer: *1–3* — the same that in Figure 2; *4* — VT3-1–VT3-1

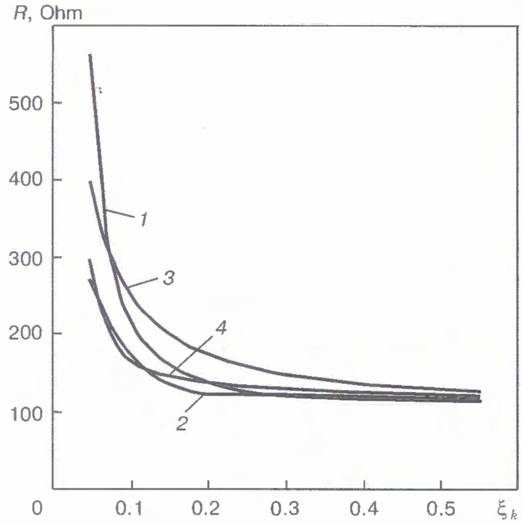

Figure 4. Dependence of value of active electrical resistance on position of a piezo-layer (*1*–*4* — the same that in Figure 3)

It is rational to displace the piezoceramic layer from the end of the reflecting cover plate to the transducer middle for the power transducers in USW of items from polymethylmetacrylate or polystyrene. The positive factors of this design is the increase in coefficient of the electromechanical coupling and also the decrease in electric resistance. Figure 4 shows that the bar-type transducer is typical of a monotonously reducing dependence of resistance on coordinate ξ_k. Moreover, the rate of reducing resistance for variant St–St–St is much higher than in the rest variants. At $\xi_k \geq 0.3$ all the variants are approximately equal from the point of view of electrical resistance.

Material of cover plates greatly influences the characteristics of the high-amplitude transducer. In particular, it is rational to use the combination St–D16T or D16T–D16T for producing high amplitudes of displacement of end of the radiating cover plate. Here, the minimum dynamic loading on a piezoactive layer and effectiveness of transducer exciting are provided using the cover plates from alloy D16T.

The results obtained make it possible to have a more grounded approach to the selection of design of the transducer with allowance for properties of the parts welded and peculiarities of the technological process.

1. Kikuchi, E. (1972) *Ultrasonic transducers*. Moscow: Mir.
2. Nesterenko, M.P., Senchenkov, I.K., Tantsyura, T.P. (2001) Investigation of characteristics of bar-type electromechanical transducers for ultrasonic treatment of materials. *Visnyk Kyiv Univ.*, Series Phys.-Math. Sciences, Issue 4.
3. Volkov, S.S., Chernyak, B.Ya. (1986) *Welding of plastics by ultrasound*. Moscow: Khimiya.

TRIBOLOGICAL CHARACTERISTICS OF COMPOSITE CARBIDE COATINGS

Yu.S. BORISOV[1], **V.S. SYCHEV**[1], **E.N. SHAVLOVSKY**[1], **V.F. LABUNETS**[2] and **E.P. ZOLOTAREVA**[2]
[1]The E.O. Paton Electric Welding Institute, NASU, Kyiv, Ukraine
[2]National Aviation University, Kyiv, Ukraine

Tribological properties of composite carbide coatings, produced on steel 45 by a combination of thermo-chemical treatment and pretreatment by spark alloying have been studied. It is shown that the composite carbide coatings have high tribological characteristics under the conditions of boundary friction.

Key words: *composite vanadium-carbide coatings, tribological characteristics, testing medium, lubricating ability, adhesion, wear resistance, friction factor, spark alloying, thermo-chemical treatment*

Improvement of the reliability and fatigue life of wearing parts of machines and mechanisms is the priority trend of the progress of science and technology. This problem is solved by applying protective coatings.

Boride [1] and carbide [2–4] coatings, produced by various methods, are characterised by a high friction wear resistance under different conditions in service.

One of the methods for formation of wear-resistant carbide coatings on the surface of steel parts is thermo-chemical treatment (TCT) in salt melts, containing carbide forming elements [5]. However, production of carbide coatings is limited by the possibility of strengthening of low- and medium-alloyed steels (carbon content of not less than 0.65 %), this making it difficult to apply local coatings on limited sections of working surfaces.

A solution of this problem can be the application of combined processes of producing composite coatings by the method of TCT with pretreatment by spark alloying (SA). SA allows producing the surface layers with the changed composition, strongly adhering to the substrate. The coatings can be applied on individual sections of the part being treated of strictly limited size. Composition and properties of the produced surface layers are determined by the composition of the alloying electrode, power parameters, specific alloying time, inter-electrode medium and material of the part being processed [6, 7].

This work presents the results of studying the tribological properties of the composite coatings, pro-

Table 1. Tribological characteristics of friction pairs of St.45–St.45 and St.45–protective coating in different lubricating media

Lubricating medium	*Friction pair*				
	St.45–St.45	*St.45–coating No.1*	*St.45–coating No.2*	*St.45–coating No.3*	*St.45–coating No.4*
AMG-10 (used)	τ = 3 s	τ = 20 min, h = 0.1412 μm, f = 0.72–0.60	τ = 6 s	τ = 3 s	τ = 25 min, h = 0.0588 μm, f = 1.12–0.72
Ethylene glycol	τ = 4 s	τ = 8 s	τ = 10 s	τ = 4 s	τ = 15 min, h = 0.0588 μm, f = 0.9–0.6
AMG-10 (as-delivered)	τ = 8 s, tearing out of metal particles	τ = 25 min, h = 0.0588 μm, f = 0.88–0.60	τ = 30 min, h = 0.0588 μm, f = 1–0.556	τ = 2 s	τ = 20 min, h = 0.0588 μm, f = 0.76–0.64
VLP-20	τ = 1.5 min	τ = 20 min, h = 0.0765 μm, f = 0.512–0.492	τ = 25 min, h = 0.0588 μm, f = 0.41–0.48	τ = 20 min, h = 0.0235 μm, f = 0.48–0.42	τ = 25 min, h = 0.0588 μm, f = 0.56–0.50
Mineral oil I-20	τ = 3 s	τ = 25 min, h = 0.0588 μm, f = 0.60–0.56	τ = 30 s	τ = 10 s	τ = 20 min, h = 0.0588 μm, f = 0.64–0.56
Synthetic oil B-3V	τ = 8 min	τ = 20 min, h = 0.0588 μm, f = 0.64–0.60	τ = 20 min, h = 0.0235 μm, f = 0.72–0.56	τ = 20 min, h = 0.0588 μm, f = 0.53–0.46	τ = 20 min, h = 0.0588 μm, f = 0.640–0.592

Note. τ — time of formation of the steady-state value of the lubrication layer thickness or adhesion; h — steady-state value of lubrication layer thickness; f — friction factor.

duced by combining TCT and pretreatment by SA in various lubricating media. The used samples of St.45 had the shape of rings with the inner diameter of 20 mm, outer diameter of 50 mm and height of 10 mm.

Spark alloying in EILV-8A unit in air was used to create in individual sections of the sample the surface layers with a higher (more than 0.65 %) content of carbon. Alloying electrodes were plates in the form of a rectangular prism of 25 to 40 mm cross-section and 20 mm length, made of materials with a high content of carbon: SCh-18-36 cast iron (coating No.1), EG-2 graphite (coating No.2), VK-6 hard alloy (coating No.3), VH-20 hard alloy (coating No.4). Proceeding from the requirements to coating thickness and roughness of the formed surface (δ = 30 μm, R_a < < 3.2 μm) the following SA parameters were selected: reservoir capacitor capacitance — 150 μF, discharge current of reservoir capacitor — 0.9–1.0 A, vibration frequency of vibrator electrode — 450 Hz, specific alloying time — 3 min/cm^2, finish treatment was performed at discharge current of 0.5–0.6 A for 2 min/cm^2. In order to create vanadium-carbide layers TCT was conducted by the technology, developed by the E.O. Paton Electric Welding Institute: sample soaking in borax-based salt melts with addition of the carbide-forming element at the temperature of 950–970 °C for 3 h [5].

Evaluation of the lubricating ability of oils and water-glycol fluids (WGF) in friction of samples with carbide coatings was performed in MI-1M machine under the conditions of sliding friction. Frequency n of sample rotation was 200 rpm, Hertz contact stress σ_s was 200 MPa, surface roughness before testing R_a ≈ ≈ 1.25 μm. Fitting of the strengthened surfaces was conducted by standard procedures [8].

A number of oils and WGF were used during investigations, namely hydraulic oil AMG-10 (used), ethylene glycol, VLP-20, mineral oil I-20, synthetic oil B-3V. Used lubricants met the requirements of 17th class of cleanliness (number of particles of 5 to 10 μm size did not exceed 500 to 1000 per 100 cm^3 of liquid). Lubrication effectiveness is characterised by the thickness of lubrication layer h (measured by the method of voltage drop in the glowing discharge mode [9]) and friction factor f.

At metallographic analysis of samples, processed by SA and subsequent vanadium-carbide plating, etching in Murakami reagent reveals a carbide layer 5 to 7 μm thick, below which is a lower etchability zone up to 30 μm thick. X-ray phase analysis shows mostly the presence of VC and a small amount of α-Fe in the surface layers (10–15 μm). X-ray microprobe analysis demonstrated that the carbide layer on

Table 2. Summary linear wear of friction pairs

Lubricating medium	*Friction pair*		
	St.45–St.45	*St.45–coating No.1*	*St.45–coating No.2*
AMG-10 (used)	0.300	0.100	0.080
Ethylene glycol	0.160	0.040	0.040
AMG-10 (as-delivered)	0.260	0.040	0.010
VLP-20	0.260	0.080	0.020
Mineral oil I-20	0.040	0.020	0.020
Synthetic oil B-3V	0.280	0.040	0.012

the surface is close to the stoichiometric composition of vanadium carbide. During scanning the increase of iron content in the carbide layer is observed. Surface layer microhardness was 20,000–25,000 MPa.

Tables 1 and 2 present the data of investigations of the lubricating ability of oils, WGF and anti-friction ability of friction pairs of St.45–St.45 (*HRC* 56–58) and St.45–protective coating in different media. The least satisfactory results, as can be seen from Table 1, were obtained in investigation of St.45–St.45 friction pair. In all the lubricating media, used in the experiments, this pair practically did not function, as adhesion occurred after a relatively short time (up to 8 min). Adhesion sites are clearly visible on the sample surface, the depth of material tearing out reaching 0.5–2.0 mm on average along a normal to the surface.

Unsatisfactory results when studying the lubricating ability, anti-wear and anti-friction properties of the protective coatings were obtained for ethylene glycol. In this medium satisfactory results were demonstrated by the friction pair of St.45–protective coating No.4: coefficient of friction was 0.9–0.6, time to achieve a stable value of the lubrication layer thickness was 15 min.

The best results of studying the lubricating ability were obtained for protective coatings, tested in such media as WGF — ethylene glycol, VLP-20 and synthetic oil B-3V. This is related to formation of secondary structures on the surface as a result of oxidation-polymerisation processes, proceeding in local contact of the friction pairs. Wear of contacting surfaces with protective coatings in WGF, VLP-20 and synthetic oil B-3V is practically not observed, but their smoothing takes pace. The time to achieve the steady-state value of the lubricating layer thickness in the contact zone was 20 to 25 min, and the thickness was 0.0235–0.0765 μm for different protective coatings.

Thus, adhesion takes place on the working surfaces of the friction pair of St.45–St.45 without coating in all the lubricating media for the given testing conditions.

Tribological properties of composite vanadium-carbide coatings are manifested differently in different testing media. The highest performance is offered by composite coatings, produced by SA with cast iron, graphite and a hard alloy and subsequent vanadium-carbide plating, when exposed to the medium of VLP-20 and synthetic oil B-3V.

Total linear wear of the friction pairs of St.45–St.45 with coating No.1 and No.2 is 2 to 7 times smaller than that of the pair of St.45–St.45 without coating in all the studied media, the minimal total linear wear being found for the composite coating, produced by SA with graphite and subsequent vanadium-carbide plating (coating No.2).

1. Labunets, V.F., Voroshnin, L.G., Kindrachuk, M.V. (1989) *Wear-resistant boride coatings*. Kyiv: Tekhnika.
2. Borisenok, G.V., Vasiliev, L.A., Voroshnin, L.G. et al. (1981) *Thermo-chemical treatment of metals and alloys*. Reference book. Moscow: Metallurgia.
3. Labunets, V.F., Borisov, Yu.S., Shavlovsky, E.N. (1996) Influence of thermo-chemical treatment on resistance of steel 45 to fretting corrosion. *Avtomatich. Svarka*, **11**, 37–39, 47.
4. Labunets, V.F., Shavlovsky, E.N., Teslya, V.F. (1989) Influence of vanadium-carbide plating of structural steels on their wear resistance in MS-20 oil. In: *Investigation of the processes of preparation, application and control of quality of aviation CLM and special liquids*. Kyiv: KIIGA.
5. Borisov, Yu.S., Yushchenko, K.A., Shavlovsky, E.N. et al. (1990) Wear-resistant vanadium-carbide coatings on steels, deposited from borax-based melts. *Zashchitn. Pokrytiya na Metallakh*, **24**, 40–43.
6. Samsonov, G.B., Verkhoturov, A.D., Bovkun, G.A. et al. (1976) *Spark alloying of metallic surfaces*. Kyiv: Naukova Dumka.
7. Verkhoturov, A.D., Mukha, I.M. (1982) *Technology of spark alloying of metal surfaces*. Kyiv: Tekhnika.
8. Karasik, I.I. (1978) *Running-in of materials for slide bearings*. Moscow: Nauka.
9. Rajko, M.V., Kadomsky, V.P. (1971) Investigation of hard films on the friction surface by the electrical conductivity method. *Fiz.-Khim. Mekhanika Materialov*, **1**, 18–23.